

# Topological order in symmetric blockade structures

Tobias F. Maier, Hans Peter Büchler, and Nicolai Lang\*

*Institute for Theoretical Physics III and Center for Integrated Quantum Science and Technology,  
University of Stuttgart, 70550 Stuttgart, Germany*

(Dated: March 24, 2025)

The bottom-up design of strongly interacting quantum materials with prescribed ground state properties is a highly nontrivial task, especially if only simple constituents with realistic two-body interactions are available on the microscopic level. Here we study two- and three-dimensional structures of two-level systems that interact via a simple blockade potential in the presence of a coherent coupling between the two states. For such strongly interacting quantum many-body systems, we introduce the concept of *blockade graph automorphisms* to construct symmetric blockade structures with strong quantum fluctuations that lead to equal-weight superpositions of tailored states. Drawing from these results, we design a quasi-two-dimensional periodic quantum system that – as we show rigorously – features a topological  $\mathbb{Z}_2$  spin liquid as its ground state. Our construction is based on the implementation of a local symmetry on the microscopic level in a system with only two-body interactions.

## I. INTRODUCTION

Condensed matter physics is concerned with the explanation and prediction of emergent phenomena on large scales from systems of many interacting, microscopic degrees of freedom, using a sophisticated arsenal of experimental, theoretical, and numerical techniques. Motivated by tremendous progress in the preparation and control of many quantum degrees of freedom on the atomic scale [1, 2], the “inverse problem” has recently come into focus (Fig. 1): Given a “toolbox” of microscopic constituents (like atoms) that can be controlled precisely and correlated via simple, tunable interactions, is it possible – and if so, how – to robustly engineer a *prescribed* quantum many-body phase? A better understanding of this bottom-up design of quantum materials opens an alternative route to study emergent phenomena in quantum many-body physics. This is emphasized by the pivotal role played by exactly solvable, though often experimentally unrealistic models such as the toric code [3], more general string net models [4], and other parent Hamiltonians [5, 6] like the famous AKLT construction [7] or resonating valence bond states [8, 9]. The “inverse problem” is distinguished (and complicated) by its restriction to a specific type of simple, experimentally accessible interaction on the microscopic level that can be used for the construction of a prescribed phase of matter. Solving this problem is of particular interest for quantum phases with topological order [10] due to potential applications as quantum memories [11] and for topological quantum computing [12].

This paper is a contribution to tackle the “inverse problem” in a particular setting, with focus on the construction of topologically ordered states of matter. We consider a toolbox of elementary two-level systems that interact via a simple blockade potential; such systems can be viewed as spin systems with a strong Ising-type interaction in the

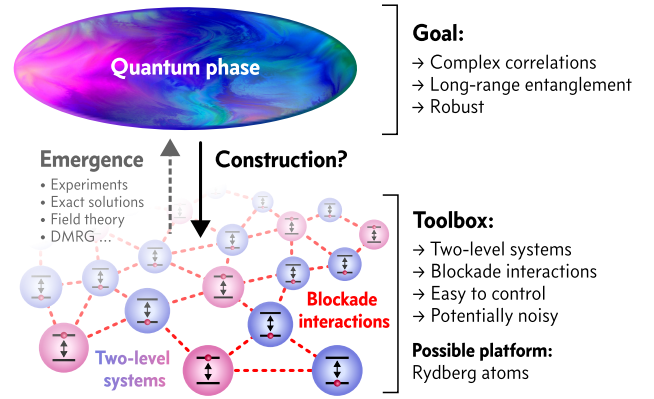


Figure 1. *Rationale.* The “inverse problem” of condensed matter physics studies the construction of prescribed, robust quantum phases from a given set of simple, microscopic constituents. Here we consider a toolbox motivated by (but not specific to) the Rydberg platform: two-level systems can be placed freely in two and three dimensions and interact via a simple blockade mechanism. Our contribution is an extension of the theoretical foundations of this toolbox to construct interesting quantum phases.

presence of transversal and longitudinal magnetic fields. We extend this framework by a versatile concept of symmetry, and leverage this novel tool for the construction of a topological  $\mathbb{Z}_2$  spin liquid. To comply with the rationale of engineered quantum matter, none of these results rely on numerical techniques or perturbative arguments.

Our focus on this particular toolbox is motivated by the significant progress that neutral atom platforms have seen in recent years [2], both on the experimental and the theoretical front: Control on the single-atom level is facilitated by optical lattices and tweezers which allow for the design of arbitrary spatial structures in two and three dimensions comprising hundreds of atoms [13, 14]. The internal states of atoms can be controlled by lasers, microwaves, and electromagnetic fields with high fidelity, both uniformly and with single-site addressability [15, 16],

\* nicolai.lang@itp3.uni-stuttgart.de

while dipole-dipole and/or van der Waals interactions allow for controllable, strong interactions [17]. Van der Waals interactions give rise to the famous *Rydberg blockade mechanism*, where a single excited atom prevents further excitations within a tunable blockade radius [18–22]. The simplicity of this strong interaction, combined with the high level of spatial control over hundreds of atoms, makes the Rydberg platform a prime candidate for quantum simulation [23–31] and the design of artificial quantum matter. Recently, various two-dimensional structures of Rydberg atoms were put forward and studied numerically, with the goal to artificially design interesting quantum phases such as topological spin liquids [32–37], dimer models [38–40], fractonic phases [41–43], lattice gauge theories [44–51] and glassy phases [52]; these studies were complemented by experimental results for systems of several hundred atoms [30, 53, 54]. The same methods used for the design of artificial quantum matter can also be applied to solve optimization problems by encoding them into the geometry of tailored blockade structures, a procedure called “geometric programming” [55–67]; experimental implementations of small problem instances have been reported as well [68–76].

While the neutral atom platform certainly is the most advanced in regard to theory development and experimental sophistication, there are other platforms that allow for tailored blockade interactions in the quantum regime, like superconducting qubit architectures [77] and Rydberg excitons in solid state systems [78].

The fact that the same type of microscopic interactions can be realized on different experimental platforms suggests the development of a “platform agnostic” toolbox for the design of artificial quantum matter. This toolbox provides abstract two-level systems that interact via a simple blockade potential; the pattern and layout of these interactions is then central part of the design process for a particular quantum phase. Recently, first steps towards such a toolbox have been reported [79–82]. While these results explain how the frustration of generic blockade structures can be leveraged to prepare nontrivial, *classical* ground state manifolds, a systematic understanding of the effect of *quantum fluctuations* on these strongly interacting systems is lacking.

In this paper, we take a first step to incorporate quantum fluctuations systematically into the design process of blockade structures to engineer artificial quantum materials. While our focus on this particular toolbox is motivated by the Rydberg platform, all our results are platform agnostic. Our main contribution is the design of a quasi-two-dimensional periodic array of two-level systems that – by construction – stabilizes an equal-weight superposition of loop states when exposed to uniform quantum fluctuations. This feature makes the ground state of this strongly interacting quantum many-body system topologically ordered (in the universality class of the toric code), while using only physically realistic, local, two-body interactions. It is remarkable, and in line with the rationale of engineered quantum matter advertised

above, that these results can be established rigorously, without relying on numerics – and despite the fact that the constructed model is not a renormalization fixed point (as compared to string net models [4] like the toric code Hamiltonian [3]).

To achieve this feat, we extend the toolbox of blockade structures by the concept of *blockade graph automorphisms*, a – not necessarily geometric – symmetry of strong blockade interactions. We show that particularly symmetric (dubbed *fully-symmetric*) blockade structures stabilize equal-weight superpositions of their classical ground states when subject to uniform quantum fluctuations. In combination with the known blueprints for the design of blockade structures with prescribed classical ground state manifolds (studied previously in Refs. [79–82]), this provides a powerful tool for the design of strongly fluctuating quantum systems with nontrivial correlations and entanglement patterns.

The remainder of this paper is structured as follows. In Section II, we introduce the systems under consideration, define the relevant notation, and specify our goal. To make this paper self-contained, we provide in Section III a brief review of prior results on the construction of blockade structures. The discussion of new results starts in Section IV with two motivating examples that lead to the concept of fully-symmetric structures defined in Section V. In Section VI, we introduce and discuss a crucial example for this concept, the fully-symmetric universal gate, which is the basis for the construction detailed in the second half of the paper: First, in Section VII, we discuss general features and constraints that periodic (tessellated) fully-symmetric blockade structures must satisfy. Our main result is then detailed in Section VIII. We start in Section VIII A with a brief review of the toric code, followed by a discussion of fundamental problems in Section VIII B that must be overcome to realize its topological order with a fully-symmetric blockade structure. These insights are used in Section VIII C to engineer a periodic, quasi-two-dimensional system that stabilizes an equal-weight superposition of loop states by construction. We study the symmetries responsible for this feature in Section VIII D, and comment on the geometric embedding of the model in Section VIII E. We complete our discussion of this strongly interacting quantum many-body system in Section VIII F with a study of its many-body spectrum (Section VIII F 1), a rigorous proof of its ground state topological order (Section VIII F 2), and comments on its bulk gap (Section VIII F 3). We close in Section IX with comments on open questions and conclude in Section X.

## II. SETTING & OBJECTIVE

We start with a characterization of the systems we consider in this paper, their formal description, and introduce the required mathematical notation. With these foundations, we can formulate our objective precisely.

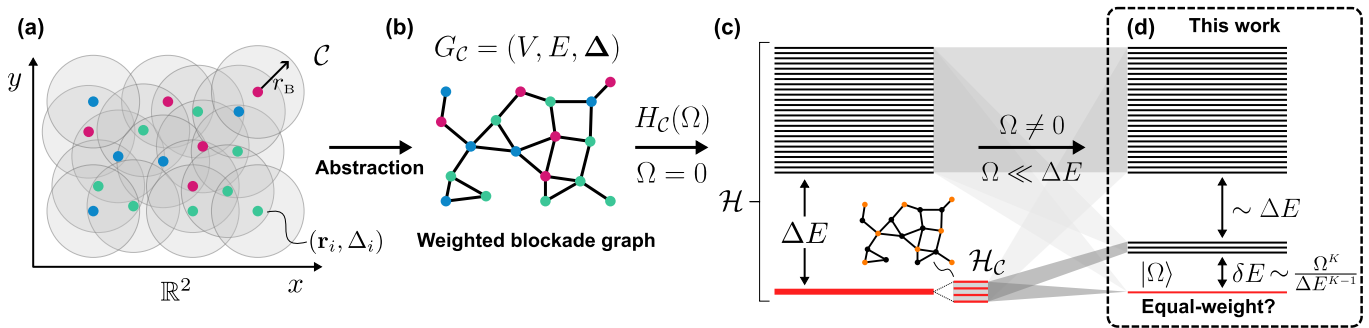


Figure 2. *Setting & Objective.* (a) A two-dimensional arrangement  $\mathcal{C} = (\mathbf{r}_i, \Delta_i)_{i \in V}$  of atoms  $i \in V$  with position  $\mathbf{r}_i$  and detuning  $\Delta_i$  is governed by the Hamiltonian  $H_{\mathcal{C}}$  that describes a blockade interaction with radius  $r_B$ . The detunings are encoded by colors. (b) Interactions and detunings are conveniently represented by a vertex-weighted blockade graph  $G_{\mathcal{C}} = (V, E, \Delta)$ . (c) For  $\Omega = 0$ , the Hamiltonian gives rise to a degenerate low-energy eigenspace  $\mathcal{H}_{\mathcal{C}} < \mathcal{H}$ , separated from the excited states by a gap  $\Delta E$ . The ground states correspond to maximum-weight independent sets of the blockade graph. (d) Our objective is to design blockade structures in which quantum fluctuations  $\Omega \neq 0$  stabilize a ground state that is an equal-weight superpositions of the states in  $\mathcal{H}_{\mathcal{C}}$ .

In this work, we focus on two- and three-dimensional arrangements of two-level systems that interact via a blockade potential

$$U(r) := \begin{cases} 0 & \text{for } r > r_B \\ \infty & \text{for } r \leq r_B \end{cases} \quad (1)$$

with *blockade radius*  $r_B$ ; the latter defines the only length scale of the system and can be set to unity. The two-level systems can be realized by electronic states of atoms, internal spin states, cavity modes, etc. For simplicity, we refer to these systems as “atoms” throughout the paper, although they are not necessarily realized as such. Every atom is assigned an index  $i \in V = \{1 \dots N\}$ , placed at position  $\mathbf{r}_i \in \mathbb{R}^3$ , and described by the state  $|n\rangle_i$  with  $n \in \{0, 1\}$ , where we identify  $|0\rangle_i$  as *ground state* and  $|1\rangle_i$  as *excited state*.

The quantum dynamics of atoms is achieved by coupling the ground state to the excited state with strength  $\Omega_i$ , to which we refer as (*quantum*) *fluctuations*. In addition, each atom can be detuned by  $\Delta_i \geq 0$ . The Hamiltonian that describes such systems is then

$$H_{\mathcal{C}}(\Omega) = \sum_{i < j} U(r_{ij}) n_i n_j + \sum_i (\Omega_i \sigma_i^x - \Delta_i n_i) \quad (2)$$

with  $r_{ij} := |\mathbf{r}_i - \mathbf{r}_j|$  the distance between atoms  $i$  and  $j$ . This Hamiltonian acts on the full Hilbert space  $\mathcal{H} = (\mathbb{C}^2)^{\otimes N}$  with representations  $n_i = |1\rangle\langle 1|_i$  and  $\sigma_i^x = |0\rangle\langle 1|_i + |1\rangle\langle 0|_i$ . Note that detunings  $\Delta_i$  and fluctuations  $\Omega_i$  can in principle be site-dependent; in the following, we assume uniform fluctuations  $\Omega_i \equiv \Omega$  (for simplicity) but allow for non-uniform detunings  $\Delta_i$ . The Hamiltonian (2), together with the blockade interaction (1), is closely related to so called *PXP models* studied on the Rydberg platform [33, 83].

Many-body quantum systems of this form are completely specified by the data  $\mathcal{C} \equiv (\mathbf{r}_i, \Delta_i)_{i \in V}$ , to which we refer as (*blockade*) *structure*, Fig. 2 (a), together with

the uniform quantum fluctuations  $\Omega$ . We refer to structures with  $\Omega = 0$  as *classical*, for then all operators in (2) commute and eigenstates are given by products of the  $\{|0\rangle, |1\rangle\}$ -basis. The purpose of this paper is to deepen our understanding of the effects of quantum fluctuations  $\Omega \neq 0$  on such classical blockade structures.

Because of Eq. (1), the interactions of blockade structures translate to kinematic constraints that can be encoded by a *vertex-weighted blockade graph*  $G_{\mathcal{C}} = (V, E, \Delta)$ , where an edge  $e = (i, j) \in E$  between atoms  $i, j \in V$  indicates that they are in blockade, i.e., their distance  $r_{ij}$  is smaller than the blockade radius  $r_B$ ; the detunings  $\Delta := \{\Delta_i\}_{i \in V}$  are interpreted as weights of the vertices. An abstract graph that can be realized in this way is called a *unit disk (ball) graph* in two (three) dimensions. Conversely, a layout of vertices that realizes a prescribed graph as its blockade graph is a *unit disk (ball) embedding* of this graph (where the “unit” is the blockade radius  $r_B$ ). Throughout the paper, blockade graphs are drawn by solid edges connecting atoms that are in blockade, while the colors of vertices encode their detuning, Fig. 2 (b).

Provided a classical blockade structure  $\mathcal{C}$  ( $\Omega = 0$ ), its ground state manifold  $\mathcal{H}_{\mathcal{C}} \equiv \text{span}\{|\mathbf{n}\rangle \mid \mathbf{n} \in L_{\mathcal{C}}\}$  is spanned by perfectly degenerate product states  $|\mathbf{n}\rangle = |n_1 \dots n_N\rangle$  that are characterized by a subset of excitation patterns  $L_{\mathcal{C}} \subseteq \mathbb{Z}_2^N$ . This manifold is separated by a gap  $\Delta E$  from the excited states  $|\mathbf{n}\rangle$  with patterns  $\mathbf{n} \notin L_{\mathcal{C}}$  (typically  $\Delta E \sim \min_i \Delta_i$ ), Fig. 2 (c). The patterns in  $L_{\mathcal{C}}$  are the *maximum-weight independent sets* (MWIS) of the vertex-weighted blockade graph  $G_{\mathcal{C}}$ . An independent set of a graph is a subset of vertices such that no two vertices are connected by an edge (this accounts for the blockade). A *maximum-weight* independent set is an independent set that maximizes the total weight of vertices [which minimizes the energy contribution of the  $-\Delta_i n_i$  terms in (2)]. Clearly, MWIS correspond to the ground states of  $H_{\mathcal{C}}(\Omega = 0)$ . Finding the maximum-weight independent sets  $L_{\mathcal{C}}$  for a given blockade graph  $G_{\mathcal{C}}$  is known to be NP-

hard [84] (even for the subclass of unit disk graphs [85]) and therefore essentially intractable for larger structures.

Fortunately, this intractability is of no concern to us, since we are *not* interested in deriving the ground state pattern  $L_C$  for a given structure  $\mathcal{C}$ . On the contrary, here (and in our previous work [81]) we are interested in the *inverse problem* of engineering a suitable structure  $\mathcal{C}$  for a given set of ground state patterns  $L_C$ . Usually, these patterns are chosen such that they obey nontrivial logical constraints to implement the solution of optimization problems [55, 59, 61, 70, 73, 80, 82, 86, 87], or enforce local constraints necessary for topologically ordered quantum phases [32–37, 81]. In this context, the set of bit strings  $L_C \subseteq \mathbb{Z}_2^N$  is referred to as the *language* of the structure [88], and the states  $|\mathbf{n}\rangle$  with  $\mathbf{n} \in L_C$  as its *logical states* (we often use patterns  $\mathbf{n}$  and states  $|\mathbf{n}\rangle$  interchangeably). The purpose of the structure  $\mathcal{C}$  is therefore to isolate a prescribed subset of excitation patterns  $L_C$  (realized by the spectral gap  $\Delta E > 0$ ), while remaining agnostic to the differences between patterns within  $L_C$  (realized by the perfect degeneracy of  $H_C$ ). How this inverse problem can be tackled systematically has been studied previously [80–82] and is not our main focus here. However, to make this paper self-contained, we provide a brief review in Section III below.

So let us assume henceforth that we are given a structure  $\mathcal{C}$  that realizes some prescribed language  $L_C$  of logical states as its classical ground state manifold  $\mathcal{H}_C$ . In this paper, we are interested in the effect of weak quantum fluctuations  $|\Omega| \ll \Delta E \sim \Delta_i$  on the low-energy physics of  $H_C(\Omega \neq 0)$ . Most importantly, we are interested in the new ground state(s) of this strongly interacting quantum many-body system, Fig. 2 (d). Without loss of generality, we can expect these to be of the form

$$|\Omega\rangle = \sum_{\mathbf{n} \in L_C} \lambda_{\mathbf{n}}(\Omega) |\mathbf{n}\rangle + \sum_{d \geq 1} \left(\frac{\Omega}{\Delta E}\right)^d \sum_{\mathbf{n} \in L_C^d} \eta_{\mathbf{n}}(\Omega) |\mathbf{n}\rangle \quad (3)$$

with amplitudes  $\lambda_{\mathbf{n}}, \eta_{\mathbf{n}} \in \mathcal{O}(1)$ . Here we introduced the sets of excitation patterns  $L_C^d$  which have Hamming distance  $d$  from  $L_C^0 \equiv L_C$ , i.e.,  $\mathbf{n} \in L_C^d$  means that  $d$  is the minimum number of bits to flip such that  $\mathbf{n}$  becomes a valid logical state in  $L_C$ . For  $\Omega = 0$ , the amplitudes  $\lambda_{\mathbf{n}}$  are clearly arbitrary, but once fluctuations set in, this is no longer the case in general. Presumably, there is a unique ground state characterized by some particular superposition  $\{\lambda_{\mathbf{n}}\}$  of logical patterns from  $L_C$ , dressed by patterns  $\mathbf{n} \in L_C^d$  that violate the constraints of  $L_C$ . To quantify this dressing, we define  $\Lambda^2 := \sum_{\mathbf{n} \in L_C} |\lambda_{\mathbf{n}}|^2$  as the *logical weight* of  $|\Omega\rangle$ .

Since the classical structure  $\mathcal{C}$  is designed to single out – but otherwise not distinguish – the patterns  $\mathbf{n} \in L_C$ , it is reasonable to demand the same in the presence of quantum fluctuations. This means that we are interested in structures where  $\lambda_{\mathbf{n}} \equiv \lambda = \text{const}$  for all  $\mathbf{n} \in L_C$  in Eq. (3) even for  $\Omega \neq 0$ . Thus we seek blockade structures that stabilize *equal-weight superpositions* of logical states in the presence of quantum fluctuations.

This is a reasonable objective, as we would like the classical set of configurations  $L_C$  to “fluctuate as strongly as possible” in the presence of a uniform quantum fluctuations. For example, when blockade structures based on Rydberg atoms are employed to solve optimization problems, the hope is that quantum fluctuations between all allowed logical states in  $L_C$  single out the classical solution – a rationale similar to adiabatic quantum computing [89]. Here we do not focus on optimization problems, but are interested in the preparation of interesting quantum many-body phases. For instance, Anderson’s famous resonating valence bond states [8] and the related dimer states [90] can be idealized as equal-weight superpositions of an extensive set of constrained product states [9]. Similarly, the topological quantum phase of the paradigmatic toric code model [3] is characterized by an equal-weight superposition of “loop states” (see Section VIII A below).

In the first part of this paper, we therefore develop methods to characterize and construct generic blockade structures that stabilize equal-weight superpositions (Sections IV to VI). Subsequently, we apply these methods to construct a periodic blockade structure that actually prepares an equal-weight loop condensate in its ground state (Section VIII C), and lastly, we show that the loss of logical weight  $\Lambda^2 < 1$  due to “non-loop states” does not destroy the topological order (Section VIII F). All central results that follow are constructive and/or analytically rigorous, without resorting to numerical or approximate techniques.

### III. REVIEW: BLOCKADE STRUCTURES

To make this paper self-contained, we continue with a brief review of previous results on *classical* blockade structures, i.e., without quantum fluctuations ( $\Omega = 0$ ). Readers familiar with Ref. [81] can skip this section and continue with Section IV.

As emphasized above, the overarching goal is the *construction* of a blockade structure  $\mathcal{C}$  for a given language  $L$  (= set of bit strings) such that the ground state patterns of  $H_C(\Omega = 0)$  realize this language:  $L_C = L$ . To this end, a versatile class of languages  $L$  to consider are the *rows* of truth tables of Boolean functions. This is so, because any set  $L \subseteq \mathbb{Z}_2^n$  of bit strings  $\mathbf{x} = (x_1, \dots, x_n)$  of uniform length  $n$  can be encoded as solution to a constraint of the form  $f(x_1, \dots, x_n) = 1$  for some Boolean function  $f$ . It is therefore convenient to introduce the class of languages

$$L_f := \{(\mathbf{x}, f(\mathbf{x})) \mid \mathbf{x} \in \mathbb{Z}_2^n\} \quad (4)$$

which contain all  $2^n$  rows of the truth table of the Boolean function  $f$ . If one finds a structure  $\mathcal{C}_f$  such that  $L_{\mathcal{C}_f} = L_f$ , one can simply add an additional detuning to the atom that encodes the value  $f(\mathbf{x})$  to produce a new structure  $\mathcal{C}_{f=1}$  which realizes the language

$$L_{f=1} := \{\mathbf{x} \mid f(\mathbf{x}) = 1, \mathbf{x} \in \mathbb{Z}_2^n\}. \quad (5)$$

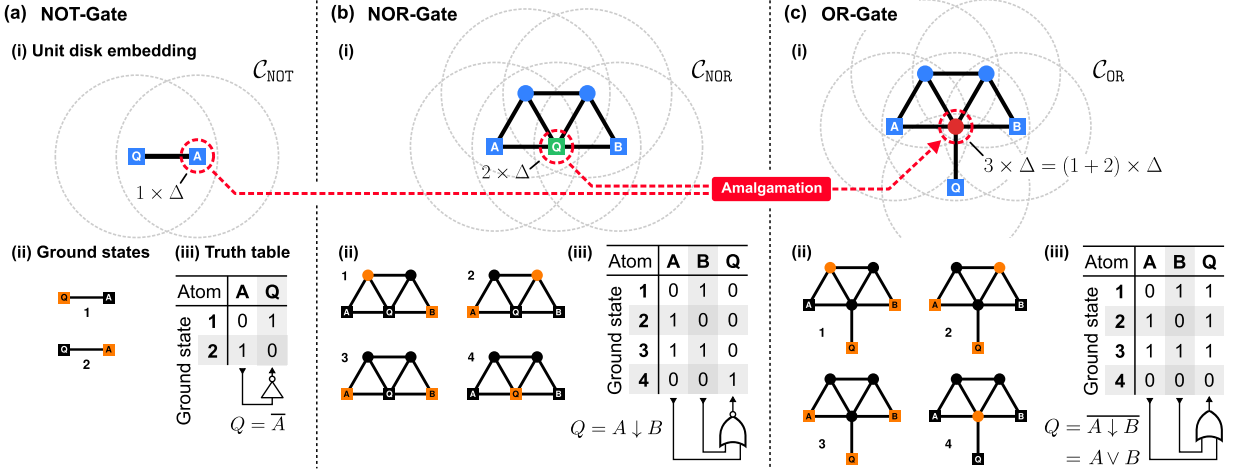


Figure 3. *Review of blockade structures.* (a) The simplest blockade structure  $C_{\text{NOT}}$  consists of two equally detuned atoms in blockade (i). Its degenerate ground state manifold  $\mathcal{H}_{C_{\text{NOT}}}$  is spanned by the two states  $|01\rangle$  and  $|10\rangle$  (ii). It therefore realizes the language  $L_{\text{NOT}} = \{01, 10\}$ , which contains bit strings that correspond to the rows of the truth table of the NOT-gate (iii). (b) The five-atom structure  $C_{\text{NOR}}$  consists of three ports (squares) and two ancillas (disks) (i). It has a four-fold degenerate ground state manifold (ii). If one ignores the ancillas and labels the ground states by the excitation patterns of the ports, one finds the language  $L_{\text{NOR}} = \{001, 010, 100, 110\}$  which corresponds to the truth table of the universal NOR-gate (Not-OR) (iii). (c) The NOT-structure  $C_{\text{NOT}}$  can be “glued” to the output port of the NOR-structure  $C_{\text{NOR}}$  by identifying this port atom with an input port atom of  $C_{\text{NOT}}$ , thereby adding up their detunings (i). This procedure is called *amalgamation* and results in an OR-structure, as can be seen from the ground state patterns (ii) that realize the truth table (iii) of an OR-gate. The existence of the NOR-structure and the possibility of amalgamation make the toolbox of blockade structures functionally complete.

It is therefore paramount to understand the construction of structures that realize the language  $L_f$  for a given Boolean function  $f$ . For example, the simplest such function is the NOT-gate

$$\text{NOT}(x) := \bar{x}, \quad (6)$$

and the language derived from its truth table is simply

$$L_{\text{NOT}} = \{01, 10\}. \quad (7)$$

Our task is to construct a blockade structure  $C_{\text{NOT}}$  such that  $L_{C_{\text{NOT}}} = L_{\text{NOT}}$ , i.e.,  $\mathcal{H}_{C_{\text{NOT}}}$  should have the logical ground state manifold  $\mathcal{H}_{\text{NOT}} = \text{span}\{|01\rangle, |10\rangle\}$ . This is of course realized by a single blockade between two equally detuned atoms, see Fig. 3 (a).  $C_{\text{NOT}}$  is the most elementary, nontrivial blockade structure.

A less trivial Boolean function is the NOR-gate (Not-OR)

$$\text{NOR}(x, y) \equiv x \downarrow y := \overline{x \vee y} \quad (8)$$

with associated language

$$L_{\text{NOR}} = \{001, 010, 100, 110\}, \quad (9)$$

where the last bit encodes the result of the NOR-gate applied to the first two bits. One can show that no structure with three atoms can realize this language [81]. However, if one allows for additional *ancilla* atoms, it becomes possible with the *five-atom* structure  $C_{\text{NOR}}$  depicted in Fig. 3 (b). The three atoms of  $C_{\text{NOR}}$  with states that map one-to-one to bit patterns of  $L_{\text{NOR}}$  are called *ports*. The

remaining two atoms do not contribute additional degrees of freedom to the ground state manifold and are referred to as *ancillas*. The excitation patterns of both ports and ancillas in the ground state manifold of this structure realize the language

$$L_{C_{\text{NOR}}} = \{00100, 01001, 10010, 11000\}, \quad (10)$$

where the ports are printed black and the two ancillas gray. If one ignores the ancilla states (which carry redundant information), this is equivalent to the NOR-language (9). When referring to ground states, we often omit the ancilla states altogether and simply identify  $L_{C_{\text{NOR}}}$  with  $L_{\text{NOR}}$ .

What makes the existence of  $C_{\text{NOR}}$  remarkable is the well-known fact that NOR-gates are *universal*: Any Boolean function  $f(x_1, \dots, x_n)$  can be written as a Boolean circuit built only with NOR-gates [91, 92]. This suggests that one can construct a blockade structure for *any* language  $L_f$ , if there is a systematic way to implement such circuit decompositions by “gluing” several NOR-structures together. This is made possible by a construction called *amalgamation*; the rules are very simple: Two structures that realize Boolean gates can be joined by identifying the atoms that correspond to the in- and output ports to be connected (in the circuit sense), and *adding up* the detunings that the two structures assign to the identified atoms. One easily verifies that the new structure implements the truth table of the Boolean function that the two connected gates define.

This procedure is exemplified in Fig. 3 (c), where the NOT-structure  $C_{\text{NOT}}$  from Fig. 3 (a) is “glued” to the output port of the NOR-structure  $C_{\text{NOR}}$  from Fig. 3 (b), producing

an OR-structure  $\mathcal{C}_{\text{OR}}$ . It is straightforward to check that the ground state manifold of this amalgamation implements the truth table of an OR-gate:

$$L_{\text{OR}} = \{000, 011, 101, 111\}. \quad (11)$$

One can even show that this particular six-atom structure is minimal in the number of atoms [81], although amalgamations typically produce non-minimal structures.

In summary, the existence of a NOR-structure, and the possibility to combine structures via amalgamation, essentially proves that any language  $L$  of length- $n$  bit strings can be realized by some blockade structure  $\mathcal{C}$  with  $N \geq n$  atoms in the sense that  $L_{\mathcal{C}} = L$  if one ignores ancillas. A rigorous derivation, including some technicalities, is presented in Ref. [81]. We stress that this proof works in strictly two dimensions and is constructive, so that  $\mathcal{C}$  can be engineered efficiently in principle. However, the structures derived in this way are typically very convoluted, and numerical optimization techniques must be used to identify functionally equivalent structures with fewer atoms (preferably as few as possible). In Ref. [81] we compiled an exhaustive list of such minimal structures that realize all elementary Boolean gates (AND, OR, XOR, ...).

This result makes the blockade toolbox functionally complete and serves as foundation for the present paper: Given an arbitrary Language  $L$ , we can always assume the existence of a classical blockade structure  $\mathcal{C}$  with degenerate ground state manifold  $\mathcal{H}_{\mathcal{C}}$ , spanned by states with excitation patterns in  $L$ .

#### IV. MOTIVATION: LOGIC PRIMITIVES

We now turn to structures with quantum fluctuations ( $\Omega \neq 0$ ). To illustrate the concepts introduced in Section II, we consider two simple examples: one with and one without an equal-weight superposition of logical states as ground state. These discussions motivate subsequent generalizations, which then facilitate the main results of the paper.

We start with the blockade structure  $\mathcal{C}_{\text{NOR}}$  for a NOR-gate introduced in Ref. [81] and reproduced in Fig. 4 (a-i). As reviewed in Section III, classically it has four degenerate ground states

$$L_{\text{NOR}} = \{00100, 01001, 10010, 11000\} \quad (12)$$

that are easily identified as the rows of the truth table of a Boolean NOR-gate, Fig. 4 (a-ii) and (a-iii). The black bits denote the *ports* and identify the ground states uniquely. By contrast, the gray bits carry redundant information and play the role of *ancillas* (which we can omit when referring to ground states).

When switching on quantum fluctuations  $\Omega$ , the degeneracy of the ground state manifold is lifted with a gap  $\delta E \sim \Omega^2/\Delta E$  and produces a unique ground state  $|\Omega\rangle$ , Fig. 4 (a-v). The exponent of  $\Omega$  follows from the leading

order perturbation, which corresponds to the smallest Hamming distance between ground state configurations in Fig. 4 (a-ii). Exact diagonalization reveals the relative weights  $\{\lambda_{001}, \lambda_{010}, \lambda_{100}, \lambda_{110}\}$  of the four logical states in  $L_{\text{NOR}}$ , and the logical weight  $\Lambda^2 = \lambda_{001}^2 + \lambda_{010}^2 + \lambda_{100}^2 + \lambda_{110}^2$  in the logical space  $\mathcal{H}_{\text{NOR}}$ , see Fig. 4 (a-iv). We find that  $\lambda_{001} = \lambda_{010} \neq \lambda_{100} \neq \lambda_{110}$ , i.e., the new ground state is *not* equal-weight and the quantum fluctuations discriminate between the four logic states. Straightforward numerics reveals that this problem affects the complete family of Boolean gates introduced in Ref. [81]. This suggests that, unsurprisingly, equal-weight superpositions are not typical.

Next, we consider the 8-atom blockade structure  $\mathcal{C}_{\text{ICRS}}$  introduced in Refs. [80, 81]. It has four degenerate ground states, labeled by the configurations of four ports

$$L_{\text{ICRS}} = \{0101, 0110, 1001, 1010\}, \quad (13)$$

which can be interpreted as copying two independent bits and inverting them. Geometrically, the structure realizes an (inverted) crossing of two Boolean wires, a crucial primitive to realize arbitrary Boolean circuits in the plane [80, 81]. An analogous analysis of  $\mathcal{C}_{\text{ICRS}}$  for  $\Omega \neq 0$  reveals that  $\lambda_{0101} = \lambda_{0110} = \lambda_{1001} = \lambda_{1010}$ , i.e., the inverted crossing already achieves our goal and stabilizes a ground state with maximal fluctuations between the four logic states, Fig. 4 (b).

A quick comparison of the geometries and degeneracies in Fig. 4 suggests a relation between *symmetries* of the structure and equal-weight superpositions in the ground state. The NOR-structure  $\mathcal{C}_{\text{NOR}}$  features a single mirror symmetry about its central in-plane axis. This symmetry acts on the excitation patterns in  $L_{\text{NOR}}$  and induces *three* distinct orbits:  $O_1 = \{010, 100\}$ ,  $O_2 = \{001\}$ , and  $O_3 = \{110\}$ , matching the three values of ground state amplitudes in Fig. 4 (a-iv). By contrast, the ICRS-structure features the full dihedral group  $D_4$  as symmetry group. Its action on  $L_{\text{ICRS}}$  produces a single orbit  $O_1 = \{0101, 0110, 1001, 1010\}$  which (presumably) enforces the equal weights of logical amplitudes in the ground state of  $\mathcal{C}_{\text{ICRS}}$ , Fig. 4 (b-iv).

#### V. SYMMETRIC BLOCKADE STRUCTURES

Our next goal is to formalize this notion of *symmetry* of a blockade structure, and make its relation to equal-weight superpositions rigorous. To this end, we need some concepts from graph theory:

**Definition 1** (Graph automorphism). *Given a vertex-weighted graph  $G = (V, E, \Delta)$ . An automorphism  $\phi$  of  $G$  is a one-to-one map  $\phi : V \rightarrow V$  such that  $\Delta_i = \Delta_{\phi(i)}$ , and  $(\phi(i), \phi(j)) \in E$  if and only if  $(i, j) \in E$ . The set of all automorphisms of  $G$  forms the automorphism group  $\text{Aut}(G)$ .*

Pictorially, an automorphism can be thought of as a permutation of vertices (dragging edges along) after which

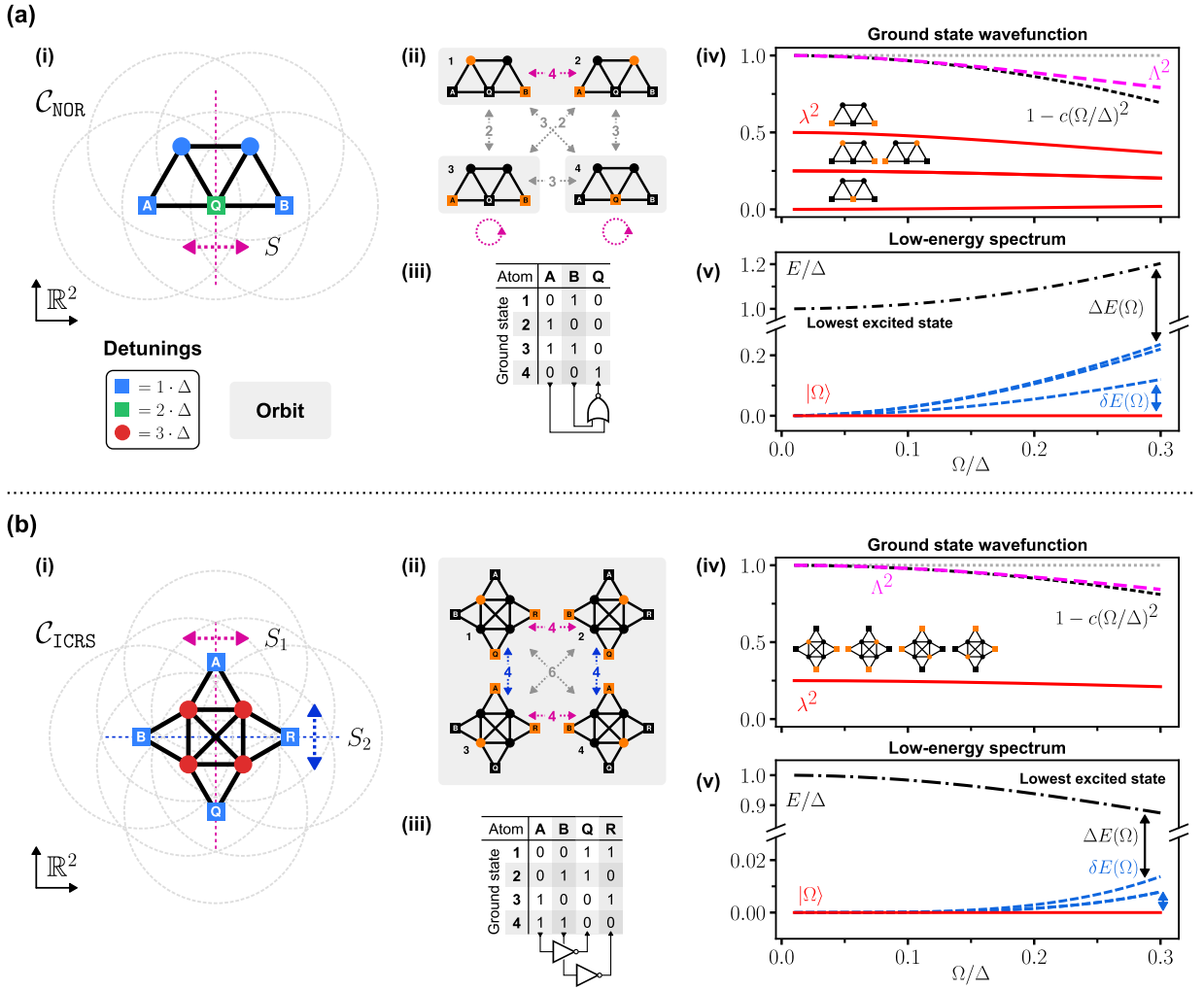


Figure 4. *Motivation: Logic gates.* (a) (i) The NOR-gate introduced in Ref. [81]. It is related to a triangle-based family of primitives that exhaust all fundamental logic gates. (ii) The structure has four degenerate ground states that realize the truth table of a NOR-gate (iii). The numbers at arrows in (ii) denote Hamming distances between excitation patterns. The gray boxes indicate the orbits in which the excitation patterns transform under the symmetry  $S$  highlighted in (i). (iv-v) With quantum fluctuations, the ground state of  $\mathcal{C}_{\text{NOR}}$  is *not* equal-weight, but favors one logic configuration above all others. (b) By contrast, the (inverted) crossing  $\mathcal{C}_{\text{ICRS}}$  has an equal-weight ground state for  $\Omega \neq 0$  (iv-v). It is also highly symmetric (i-ii): The symmetries  $S_1$  and  $S_2$  generate graph automorphisms that transform all ground state patterns into each other [gray box in (ii)].

the graph “looks the same” if one ignores the vertex labels and allows edges to pass through each other; it is the natural notion of a *symmetry* of a graph.

The automorphisms  $\mathcal{A}_C := \text{Aut}(G_C)$  of blockade graphs act naturally on excitation patterns  $\mathbf{n} \in \mathbb{Z}_2^N$  via  $\phi \cdot (n_1 \dots n_N) := (n_{\phi(1)} \dots n_{\phi(N)})$ ; for a pattern  $\mathbf{n}$ , the set  $\mathcal{A}_C \cdot \mathbf{n} := \{\phi \cdot \mathbf{n} \mid \phi \in \mathcal{A}_C\}$  is called the *orbit* of  $\mathbf{n}$ . This group action on excitation patterns then induces a unitary representation  $U_\phi$  on the atom Hilbert space  $\mathcal{H}$  via  $U_\phi |\mathbf{n}\rangle := |\phi \cdot \mathbf{n}\rangle$  (and linear extension).

With these concepts at hand, we can make two immediate observations. First, the unitary representation  $U_\phi$  is a *symmetry* of the blockade Hamiltonian (2) for arbitrary uniform  $\Omega$ :

$$U_\phi H_C U_\phi^\dagger = H_C \quad \forall \phi \in \mathcal{A}_C, \quad (14)$$

and second, this implies that the set of ground state patterns  $L_C$  is *invariant* under the group action of automorphisms:  $\mathcal{A}_C \cdot L_C = L_C$  (for details see Appendix A 1).

Clearly, every orbit of a group action is an invariant set, but the converse it not true in general: invariant sets are the *disjoint union* of orbits. Hence the set of logical patterns can be written as

$$L_C = \bigsqcup_k O_k, \quad (15)$$

where each orbit  $O_k$  is invariant under the action of blockade graph automorphisms separately. We saw this happen for the NOR-gate in Fig. 4 (a-ii).

By contrast, the ICRS-structure has the peculiar property that  $L_C$  is *identical* to an orbit (= is transitive), see Fig. 4 (b-ii). This motivates the following definition:

**Definition 2** (Fully-symmetric blockade structure). A blockade structure  $\mathcal{C}$  is called fully-symmetric if  $\mathcal{A}_{\mathcal{C}} \cdot \mathbf{n} = L_{\mathcal{C}}$  for  $\mathbf{n} \in L_{\mathcal{C}}$ , i.e.,  $L_{\mathcal{C}}$  is an orbit under the action of  $\mathcal{A}_{\mathcal{C}}$ .

With this definition, we can finally generalize our observation that the fully-symmetric ICRS-structure features an equal-weight ground state as follows:

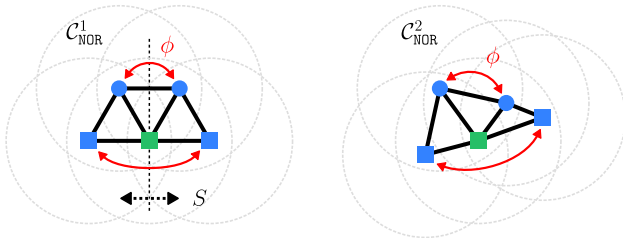
**Proposition 1.** Let  $\mathcal{C}$  be a fully-symmetric blockade structure. Then the ground state  $|\Omega\rangle$  of  $H_{\mathcal{C}}(\Omega)$  is unique for  $\Omega \neq 0$  and has the form

$$|\Omega\rangle = \lambda(\Omega) \sum_{\mathbf{n} \in L_{\mathcal{C}}} |\mathbf{n}\rangle + \sum_{d \geq 1} \left(\frac{\Omega}{\Delta E}\right)^d \sum_{\mathbf{n} \in L_{\mathcal{C}}^d} \eta_{\mathbf{n}}(\Omega) |\mathbf{n}\rangle. \quad (16)$$

In particular, this state satisfies  $U_{\phi} |\Omega\rangle = |\Omega\rangle$  for every blockade graph automorphism  $\phi \in \mathcal{A}_{\mathcal{C}}$ .

We note that, in contrast to the equal-weight property, the uniqueness of the ground state is not a consequence of the symmetry, but rather a generic property of the blockade Hamiltonian (2). A detailed proof of Proposition 1 is given in Appendix A 2. In a nutshell: The uniqueness follows from the form of Eq. (2) via the Perron-Frobenius theorem. Consequently, the ground state forms a one-dimensional (possibly nontrivial) representation of  $U_{\phi}$ , which then requires  $\lambda_{\mathbf{n}} = \lambda = \text{const}$  for all  $\mathbf{n} \in L_{\mathcal{C}}$  due to  $L_{\mathcal{C}}$  being an orbit.

Before we proceed, it is important to emphasize that for blockade potentials (1), the symmetries  $U_{\phi}$  are *not* geometric (Euclidean) symmetries of the structure  $\mathcal{C}$  (despite the suggestive Fig. 4), but topological features of the blockade graph  $G_{\mathcal{C}}$ . For example, the following geometrically distinct embeddings of the NOR-structure from Fig. 4 (a) have the same blockade graphs  $G_{\mathcal{C}_{\text{NOR}}^1} = G_{\mathcal{C}_{\text{NOR}}^2}$  and therefore the same automorphism groups  $\mathcal{A}_{\mathcal{C}_{\text{NOR}}^1} = \mathcal{A}_{\mathcal{C}_{\text{NOR}}^2}$ :



This demonstrates that blockade graph automorphisms (and thereby symmetry groups of blockade Hamiltonians) are more general than the *geometric* symmetries of a structure, as they need not be reflected in these symmetries! For a generic structure, it is also not true that all blockade graph automorphisms can be realized by the Euclidean symmetries of *some special* unit disk/sphere embedding (as is the case for the example above), see Appendix A 3 for a counterexample.

With that said, Proposition 1 translates our goal from finding blockade structures with strong quantum fluctuations into finding fully-symmetric structures. So far, we only know of the inverted crossing ICRS as an example. The obvious follow-up question is whether there are fully-symmetric realizations of *logic gates* like NOR?

## VI. FULLY-SYMMETRIC UNIVERSAL GATE

We start by noting that all triangle-based logic gates (studied in Ref. [81]) suffer from similar asymmetries as the NOR-gate discussed above, i.e., none of them are fully-symmetric. We show now that – quite surprisingly – the ICRS-structure can be extended such that (1) it remains fully-symmetric and (2) it realizes several logic primitives at once; we call this the *fully-symmetric universal (FSU) gate*  $\mathcal{C}_{\text{FSU}}$ .

The construction is illustrated in Fig. 5 (a): We first embed the ICRS-structure in three dimensions, putting the central four atoms on the corners of a tetrahedron. We then augment the structure by two additional atoms to produce a structure with full tetrahedral symmetry  $\mathcal{A}_{\text{FSU}} \simeq S_4$  ( $S_4$  denotes the permutation group of four elements). The latter has many subgroups; here we focus on the Klein four-group  $V = \{\mathbb{1}, C_{2,x}, C_{2,y}, C_{2,z}\}$  which contains the  $\pi$ -rotations  $C_{2,\alpha}$  about the three symmetry axes through opposite *edges* of the tetrahedron. The ground state patterns  $L_{\text{FSU}}$  are depicted in Fig. 5 (b) and transform as a single orbit under  $V$ , thereby producing an equal-weight superposition for  $\Omega \neq 0$  according to Proposition 1, see Fig. 5 (d). What makes this structure “universal” is the fact that depending on which atoms are interpreted as ports, the structure implements several fundamental Boolean gates at once, Fig. 5 (c), including a NOR-gate (which is a universal gate in Boolean algebra).

An exhaustive search [93] shows that there is no fully-symmetric realization of AND- and NOR-gates with less than 8 atoms. That this bound is tight follows from the 8-atom ICRS-structure in Fig. 4 (b) which has 8 atoms and realizes these two gates by reinterpreting certain ancillas as output ports. We also found that fully-symmetric XOR- and XNOR-gates cannot be realized with less than 10 atoms; this makes the FSU-structure in Fig. 5 a minimal fully-symmetric realization of these two gates (we did not show that this realization is unique, though). Lastly, we showed that there are no fully-symmetric NAND- and OR-gates with 10 atoms or less (these two gates are not realized by the FSU-structure).

We conclude with two observations: First, using the three atoms on the upper “wings” of Fig. 5 (a) as ports yields a XOR-gate  $\oplus$ , characterized by configurations with an *even* number of excited atoms. And second, the three atoms on the lower “wings” are the Boolean inverse of their opposite (upper) counterparts, and therefore realize an XNOR-gate  $\odot$ . The FSU-structure thus implements the Boolean identities

$$\underbrace{A \oplus B = C}_{\text{Upper “wings”}} \Leftrightarrow \overline{A \oplus B} = \overline{C} \Leftrightarrow \underbrace{\overline{A} \odot \overline{B} = \overline{C}}_{\text{Lower “wings”}} \quad (17)$$

in a fully-symmetric fashion. This feature is crucial for the last part of the paper where we discuss our main result.

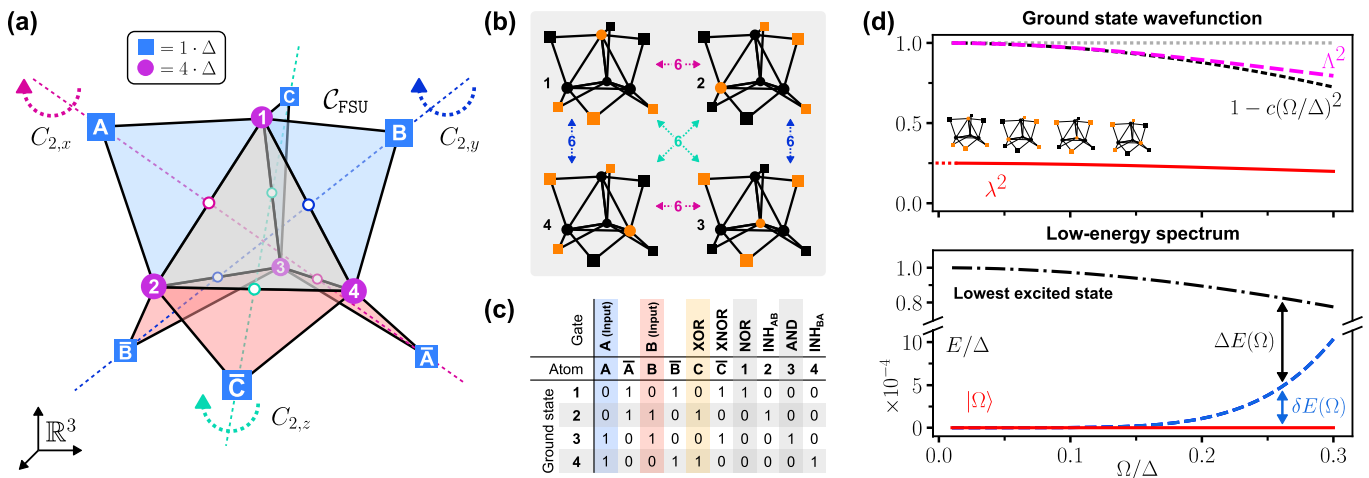


Figure 5. *Fully-symmetric universal (FSU) gate.* (a) The FSU-gate  $C_{\text{FSU}}$  is constructed from the inverted crossing by embedding it in 3D and attaching two additional atoms. The resulting structure has the full tetrahedral symmetry as automorphism group. Here we show the Klein four-group  $V = \{1, C_{2,x}, C_{2,y}, C_{2,z}\}$ , where  $C_{2,\alpha}$  denotes the  $\pi$ -rotation about one of the three symmetry axes  $\alpha = x, y, z$ . (b) The four degenerate ground states form a single orbit under the action of  $V$ , thereby ensuring their equal-weight superposition in the ground state for  $\Omega \neq 0$ . Furthermore, the Hamming distances (numbers on arrows) of all transitions are equal [cf. Fig. 4 (b-ii)]. (c) The gate implements most Boolean primitive gates by choosing different atoms as ports. The six atoms on the “wings” form logically inverted antipodal pairs. We highlight the gate choice for the XOR-gate which becomes important below.  $\text{INH}_{xy} = \neg x \wedge y$  denotes the “inhibition gate” where  $x$  inhibits  $y$ . (d) Weight of the logical states for  $\Omega \neq 0$  and logical overlap in the ground state (upper panel) and low-energy spectrum (lower panel).

## VII. A FIRST VIEW ON TESSELLATIONS

One of the most interesting features of blockade structures is that they can enforce local constraints on translationally invariant systems to prepare non-factorizable low-energy Hilbert spaces (see Refs. [32, 33, 40, 81] for details and examples). Quantum fluctuations within these nontrivial ground state manifolds might then stabilize topologically ordered quantum phases, though this is by no means guaranteed [94–96]. So far, we only considered small structures that realize Boolean logic gates. It is therefore a reasonable next step to ask whether *tessellated* (i.e. scalable and periodic) structures can be fully-symmetric, as this would potentially provide a robust mechanism to stabilize interesting quantum phases.

To understand the necessary requirements, we start by studying a generic condition on the automorphism group of such structures. In group theory, Burnside’s lemma constrains the orbit structure of arbitrary group actions, and thereby imposes a lower bound on the size of the automorphism group of any fully-symmetric (FS) blockade structure (Appendix A 4):

$$\underbrace{|\mathcal{L}_C / \mathcal{A}_C|}_{\# \text{Orbits}} \stackrel{\text{FS}}{=} 1 \stackrel{\text{Burnside}}{\Rightarrow} |\mathcal{A}_C| \geq |\mathcal{L}_C|. \quad (18)$$

That is, fully-symmetric structures must have at least as many automorphisms as ground state configurations. This is very restrictive in the context of quantum phases, where we want to implement nontrivial, *local* degrees of freedom in a scalable system, i.e., asymptotically  $|\mathcal{L}_C| = \dim \mathcal{H}_C \sim$

$d^N$  for some “quantum dimension”  $1 < d < 2$ . This means that the automorphism group of fully-symmetric tessellations must grow *exponentially* with the system size. In particular, the automorphisms inherited from the group of lattice symmetries (point group and translations) cannot be sufficient, as this subgroup is only polynomial in size.

With this knowledge, we can now revisit some of the recently proposed tessellated blockade structures on the Rydberg platform to check whether they are fully-symmetric. Unfortunately, it turns out that neither the structures proposed by Verresen *et al.* [33] (targeting toric code topological order) nor by Zeng *et al.* [40] (targeting quantum dimer models) have automorphism groups large enough to stabilize equal-weight superpositions (Appendices C 1 and C 2). The same is true for the structures proposed by some of us in Ref. [81] to realize the  $\mathbb{Z}_2$ -loop space that underlies the toric code [3, 97] (Appendix C 3). Just as we saw for the logic gates above, fully-symmetric blockade structures seem to be special and hard to come by.

Clearly, the most straightforward path to an exponentially large automorphism group is to construct systems with *local* automorphisms (“gauge automorphisms”). Unfortunately, Eq. (18) is an *implication* and not an equivalence: Even if  $|\mathcal{A}_C| \geq |\mathcal{L}_C|$  is satisfied, the ground state excitation patterns  $\mathcal{L}_C$  can still split in different orbits, and the system fails to be fully-symmetric. This happens, for example, when the local automorphisms act only on ancillas and leave the ports invariant.

In summary, the construction of fully-symmetric tessellated blockade structures has not been achieved yet, and

it is not obvious how to proceed without more specific knowledge about the extensive ground state configurations  $L_C$  to be realized. This is why we focus in the remainder of the paper on a particular problem: the construction of a tessellated blockade structure with  $\mathbb{Z}_2$  toric code topological order.

## VIII. $\mathbb{Z}_2$ TOPOLOGICAL ORDER AND LOCAL AUTOMORPHISMS

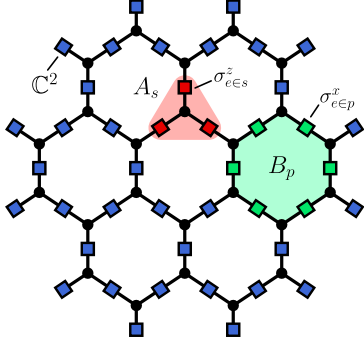
### A. Reminder: Toric code topological order

We start with a brief review of the toric code to set the stage and specify our goal. Readers familiar with the toric code [3] and the results from Ref. [81] can safely skip to Section VIII B.

We consider a honeycomb lattice with one qubit (spin- $\frac{1}{2}$ ) per edge  $e$ , represented by the local Pauli matrices  $\sigma_e^\alpha$  with  $\alpha = x, y, z$ . The toric code Hamiltonian is defined as

$$H_{\text{TC}} = -J_A \sum_{\text{Vertex } s} A_s - J_B \sum_{\text{Faces } p} B_p \quad (19)$$

with  $J_A, J_B > 0$ , *star operators*  $A_s = \prod_{e \in s} \sigma_e^z$  and *plaquette operators*  $B_p = \prod_{e \in p} \sigma_e^x$ . Here  $e \in s$  denotes edges emanating from vertex  $s$  and  $e \in p$  denotes edges bounding face  $p$ :

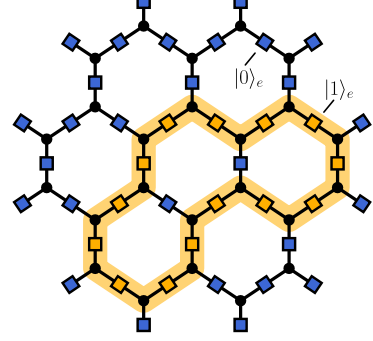


Note that typically the toric code is defined on a square lattice. Here we focus on the honeycomb lattice because its trivalent vertices make the constructions below more natural. (By contracting the vertical edges of the honeycomb lattice one can easily transition to a square lattice afterwards.)

To construct the ground state(s) of (19), one can exploit that all local terms  $A_s$  and  $B_p$  commute pairwise. We can therefore start by setting  $J_B = 0$  and first construct the ground state manifold of the star operators  $A_s$  alone, and subsequently diagonalize the plaquette operators  $B_p$  in this submanifold:

- **Step 1:** The ground state manifold for  $J_B = 0$  is characterized by states with  $+1$  eigenvalues of all star operators  $A_s$  (since  $A_s^2 = \mathbb{1}$ ), i.e., states with an *even* number of excited states  $|1\rangle_e$  adjacent to each vertex. This suggests a “string picture”: we

interpret edges with qubits in state  $|1\rangle_e$  as being occupied by a string ( $\sigma_e^z |1\rangle_e = -|1\rangle_e$ ). Then the constraint imposed by star operators is simply that strings cannot terminate on vertices. The ground state manifold for  $J_B = 0$  is therefore spanned by (exponentially many) *loop* configurations like this:



Note that the boundary conditions determine whether strings are allowed to terminate on the boundary. Above we show a finite patch with “rough” boundaries on which strings can end. By contrast, “smooth” boundaries are obtained by cutting off the dangling edges; on such boundaries strings cannot terminate. For periodic boundaries, strings can also not terminate anywhere. The following discussion is independent of boundary conditions unless noted otherwise.

Let us denote the product states of all qubits by  $|\mathbf{n}\rangle$  and define  $L_{\text{Loop}}$  as the set of all patterns that correspond to valid loop configurations (respecting the chosen boundary conditions); this defines the subspace  $\mathcal{H}_{\text{Loop}} = \text{span}\{|\mathbf{n}\rangle \mid \mathbf{n} \in L_{\text{Loop}}\}$  spanned by these “loop states”.

- **Step 2:** To construct the ground state  $|\Omega\rangle$  of (19), we must also satisfy  $B_p |\Omega\rangle = +1 |\Omega\rangle$  for all faces  $p$  (since  $B_p^2 = \mathbb{1}$ ). It is easy to see that the action of  $B_p$  on a loop state  $|\mathbf{n}\rangle \in \mathcal{H}_{\text{Loop}}$  is to add the elementary loop around face  $p$  (modulo-2) to  $\mathbf{n} \in L_{\text{Loop}}$ , thereby creating another loop configuration:  $B_p |\mathbf{n}\rangle = |\mathbf{n}'\rangle \in \mathcal{H}_{\text{Loop}}$  with  $\mathbf{n}' \in L_{\text{Loop}}$ . This mapping is a bijection from  $L_{\text{Loop}}$  to itself since  $B_p$  is invertible. It is also not hard to see that for open boundaries (all rough or smooth) one can transform any loop configuration into any other by a sequence of  $B_p$  operators.

It follows that the only state invariant under *all* plaquette operators is the *equal-weight* superposition of all loop states (we omit the normalization):

$$|\Omega_{\text{TC}}\rangle \propto \sum_{\mathbf{n} \in L_{\text{Loop}}} |\mathbf{n}\rangle. \quad (20)$$

Eq. (20) is the (unique) ground state of Eq. (19) and the renormalization fixed point of the  $\mathbb{Z}_2$  toric code topological

order. For other boundary conditions (alternating smooth and rough boundaries or periodic boundaries) there is one independent ground state for each element of the (relative) homology group of the spatial manifold on which the lattice is embedded [98]. This topological degeneracy is not important for the following arguments since (gapped) quantum phases are bulk features and independent of boundary conditions.

As a condensate of extended objects ( $\mathbb{Z}_2$ -loops), the state  $|\Omega_{\text{TC}}\rangle$  features a particular pattern of *long-range entanglement* [99]; this makes (20) the simplest example of a *string net condensate*, a family of many-body quantum states that describe two-dimensional topological orders [4]. The particular (abelian) toric code order in (20) makes it a potential substrate for topological quantum memories [11, 100]. The presence of long-range entanglement can be certified and characterized by a non-vanishing topological entanglement entropy [101, 102] (which is not necessarily universal within a topological phase [103, 104]).

Our goal in the remainder of this paper is to construct a tessellated blockade structure with a many-body ground state  $|\Omega\rangle$  in the same topological quantum phase as  $|\Omega_{\text{TC}}\rangle$ . The return of this endeavor would be the realization of the toric code topological order using only the physically accessible two-body interactions of the blockade Hamiltonian (2), instead of the unrealistic four-body interactions in the toric code Hamiltonian (19).

Before we proceed, it is important to remember that two ground states belong to the same quantum phase if they can be adiabatically connected by a gapped Hamiltonian [99], i.e., the ground state  $|\Omega\rangle$  of the blockade structure (to be constructed) and  $|\Omega_{\text{TC}}\rangle$  are not required to be the *same* state. Nonetheless, the aforementioned criterion ensures that they are characterized by the same pattern of long-range entanglement [99] (recall that phases generally correspond to stable renormalization fixed points [105, 106]).

## B. Warm-up: An instructive failure

To motivate our rather involved construction below, it is advisable to consider a more straightforward construction first. This approach was already suggested by some of us in Ref. [81] and, as already mentioned in Section VII, *fails* to prepare the equal-weight superposition (20). The point of the following discussion is to identify a potential *reason* for this failure, which then inspires our (successful) construction in Section VIII C below.

In order to stabilize a state that is (locally) unitarily equivalent to Eq. (20) using the toolbox of blockade structures, one must solve two problems:

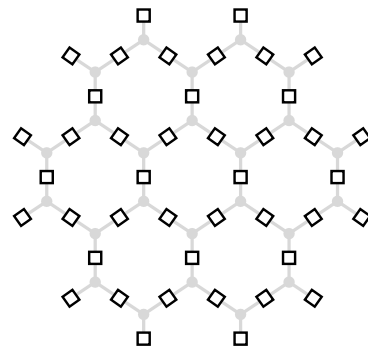
**P1** Construct a structure  $\mathcal{C}_{\text{Loop}}$  such that for  $\Omega = 0$  the ground state manifold  $\mathcal{H}_{\text{Loop}}$  is spanned by degenerate loop configurations  $\mathbf{n} \in L_{\mathcal{C}_{\text{Loop}}} \stackrel{!}{=} L_{\text{Loop}}$ . Note that we can use additional ancilla atoms to achieve this, as long as these atoms do not contribute

degrees of freedom to the ground state manifold. Solving this problem corresponds to the constraint  $A_s = +1$  in the toric code (**Step 1**).

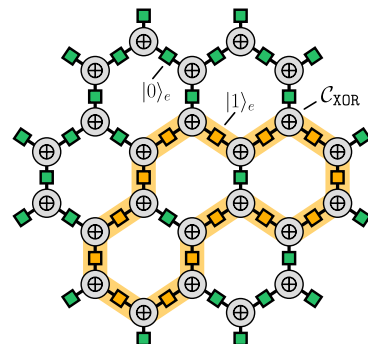
**P2** Ensure that, by switching on uniform quantum fluctuations  $\Omega \neq 0$ , a state  $|\Omega\rangle$  within the same quantum phase as  $|\Omega_{\text{TC}}\rangle$  is stabilized as (unique) ground state of the blockade structure. A promising feature would certainly be an equal-weight superposition of states  $|\mathbf{n}\rangle$  for  $\mathbf{n} \in L_{\mathcal{C}_{\text{Loop}}}$  (potentially with admixtures from other states). Solving this problem corresponds to the constraint  $B_p = +1$  in the toric code (**Step 2**).

Both of these are complicated “inverse problems” that seem hard – if not impossible – to tackle. Fortunately, the solution of **P1** is straightforward using the toolbox from Ref. [81] reviewed in Section III:

It is reasonable to start by placing an atom on each link of the honeycomb lattice. If we set the detunings of all atoms to zero (white boxes), the ground state manifold contains all  $2^N$  excitation patterns and matches the full state space of the conventional toric code (with one spin- $\frac{1}{2}$  per edge):



Next, we must introduce detunings and blockades (and potentially ancillas) such that only loop patterns remain in the ground state manifold. A key insight is that the loop constraint  $A_s = +1$  on a *trivalent* vertex with state  $|x, y, z\rangle$  on its three emanating edges is satisfied if and only if  $x \oplus y = z$ , where  $\oplus$  denotes a XOR-gate (modulo-2 addition). We can therefore pick any blockade structure  $\mathcal{C}_{\text{XOR}}$  that realizes a XOR-gate, put a copy on each vertex of the honeycomb lattice, and then amalgamate the three ports of the gates with the adjacent atoms on the edges:



Note that the constraint  $x \oplus y = z$  is completely symmetric in the three variables; hence it is not important which edges play the role of in- and output ports of the logic gates. The exemplary loop pattern shown clearly satisfies the XOR-constraints on all vertices.

This is the approach to tackle **P1** that has been proposed in Ref. [81], where a specific (minimal) realization for the vertex structure  $\mathcal{C}_{\text{XOR}}$  was given. (We do not repeat this realization here as we do not need it in the following.)

We now turn to **P2**. Since the classical part of the Hamiltonian (2) (blockade interactions and detunings) is fixed by the construction above (and the choice of a particular  $\mathcal{C}_{\text{XOR}}$ ), all we can do is to switch on weak, uniform fluctuations  $\Omega \neq 0$  and hope for the best. Given the general structure of Eq. (2), there is simply no freedom left to tailor the effects of quantum fluctuations to serve our goal. Note that this is the approach of most previous works that proposed realizations of quantum phases by leveraging the Rydberg blockade mechanism [32, 33, 40, 81].

The only tool at our disposal is the concept of *full symmetry* introduced in Section V. Unfortunately, as we rigorously show in Appendix C3, the particular realization of  $\mathcal{C}_{\text{XOR}}$  proposed in Ref. [81] leads to a tessellation that is *not* fully-symmetric due to a lack of automorphisms. While this does not preclude an equal-weight superposition of states in  $\mathcal{H}_{\text{Loop}}$ , it certainly makes it unlikely (as equal-weight superpositions are not typical). To support this claim, we derived a perturbative, low-energy effective Hamiltonian of this particular model [107] and performed numerical simulations using iDMRG [108] to study its ground state properties. While there are quantum fluctuations that induce a certain amount of local entanglement, the results suggest that there is no long-range entanglement (certified by a vanishing topological entanglement entropy). Together, these findings support our suspicion that the many-body ground state of this particular blockade structure is *not* topologically ordered. Furthermore, we take the stance that the only workable path towards solving **P2** is the construction of a fully-symmetric tessellation.

To do so, it is important to understand whether the failure to be fully-symmetric is caused by the particular choice of the vertex structure  $\mathcal{C}_{\text{XOR}}$ , or whether it is rooted in the general architecture suggested above (the proof in Appendix C3 exploits the internal structure of  $\mathcal{C}_{\text{XOR}}$ ). As we show in Appendix B, the architecture is to blame:

**Proposition 2.** *Consider a periodic, tessellated blockade structure on an arbitrary, regular lattice with one port per edge that is shared between adjacent vertex structures; let  $L$  be the set of ground state patterns. Then local automorphisms must leave the ports on edges invariant, and therefore act as the identity on  $L$ .*

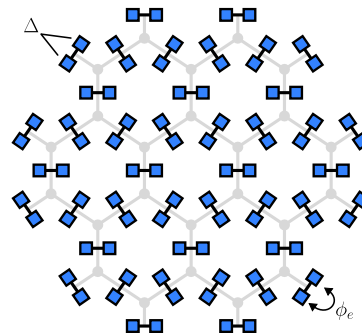
The proof is rather technical; the gist, however, is quite simple: The global topology of the blockade graph is severely restricted by the fact that vertex structures interact only via a single atom (or single link) on the edges.

One can then show that automorphisms must leave ports invariant if they act trivially on ports in the vicinity. In particular, the assumption that an automorphism acts trivially on ports that surround a finite region implies that it acts trivially everywhere. Note that Proposition 2 does not imply that tessellated structures with single ports on edges *cannot* be fully-symmetric; however, it shows that *local* automorphisms cannot be used to establish full symmetry.

In summary, we identified two problems to solve: The  $\mathbb{Z}_2$ -loop constraint (**P1**,  $A_s = +1$ ) can be satisfied on the classical level using the previously developed, versatile toolbox for blockade structures. However, the loop condensation (**P2**,  $B_p = +1$ ) due to uniform quantum fluctuations must be enforced by – preferably local – blockade graph automorphisms that render the structure fully-symmetric. Unfortunately, the most straightforward architecture that solves **P1** necessarily fails to solve **P2**. This insight inspires the construction below and leads to the main result of the paper.

### C. Construction of a fully-symmetric $\mathbb{Z}_2$ -loop blockade structure

In the toric code (Section VIII A), it is the plaquette operators  $B_p$  that act transitively on the space of loop configurations  $L_{\text{Loop}}$  and enforce the equal-weight superposition (20). We therefore should aim for a blockade structure with local “plaquette automorphisms” that do the same. However, Proposition 2 forbids exactly that if we construct the tessellation from vertex structures connected by single links. This makes sense, since automorphisms can only *permute* atoms; but if all atoms on the edges surrounding a face are in state  $|0\rangle_e$ , there is no permutation that can excite them to  $|1\rangle_e$ , i.e., create a fundamental loop. Hence we must encode the fundamental two-dimensional degrees of freedom on edges not in single atoms (as above) but in *pairs* of atoms that are in blockade:



If we detune all atoms by the same amount  $\Delta > 0$  (blue filled boxes), this produces again a degenerate ground state manifold of dimension  $2^N$  (i.e., one qubit per edge), only that now these qubits are encoded in the two states  $|01\rangle_e$  and  $|10\rangle_e$  of the two atoms in blockade. Notably, the structure has a huge automorphism

group; among these are *local* “edge-automorphisms”  $\phi_e$  that permute the two atoms on edge  $e$ . Under these automorphisms, the set of all ground state patterns  $L_N := \{0,1\}^N$  transforms as a single orbit. Hence this structure is fully-symmetric and its ground state for  $\Omega \neq 0$  is the equal-weight superposition of all  $2^N$  bit patterns in  $L_N$ , i.e.,  $|\Omega\rangle \propto \bigotimes_e |+\rangle_e + (\Omega/\Delta E) \sum \dots$  with  $|+\rangle_e = \frac{1}{\sqrt{2}}(|01\rangle_e + |10\rangle_e)$  and where  $\sum \dots$  includes configurations with completely unexcited edges  $|00\rangle_e$ .

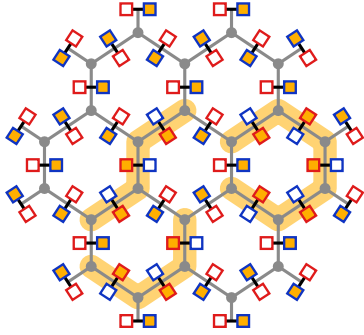
This is not yet what we want, but now that we have enough local automorphisms, we can try to add suitably chosen vertex structures that ...

- (1) enforce the  $\mathbb{Z}_2$ -loop constraint, and
- (2) preserve a local subgroup of “edge-automorphisms” (namely: plaquette automorphisms).

To this end, it is convenient to separate the  $2N$  atoms into two sublattices, with one atom of each per edge (which atom belongs to which sublattice is conventional). In the following, we label the two sublattices by red and blue bounded boxes and blockades. Due to the blockade between the atoms on each edge, it is sufficient to know the ground state pattern of, say, the red sublattice to identify the pattern uniquely. Henceforth we say that an edge is occupied by a string if the red atom is excited:

$$\text{String} \leftrightarrow |10\rangle_e \quad \text{and} \quad \text{Empty} \leftrightarrow |01\rangle_e. \quad (21)$$

In the following, we omit the fill color that indicates the detuning of atoms whenever it is not relevant for the discussion. An exemplary state in the ground state manifold looks like this [orange (white) atoms are (un)excited]:



Note that so far open strings are still part of the ground state manifold. We now turn to the vertex structure that lifts these patterns to excited states and enforces a loop constraint.

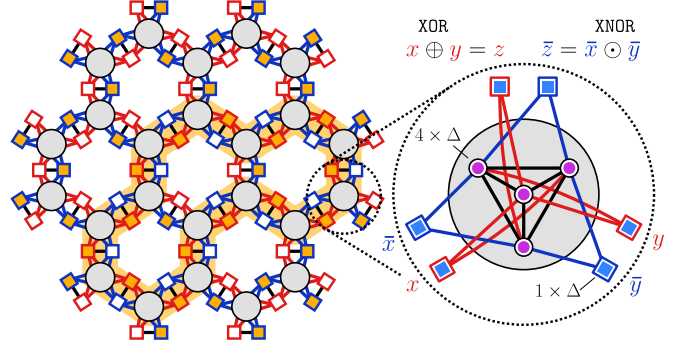
Let us focus on a single vertex with adjacent variables  $(x, \bar{x}, y, \bar{y}, z, \bar{z})$  where  $x, y, z$  denote the string occupations of the three adjacent edges. The  $\mathbb{Z}_2$ -loop constraint, according to our convention (21), is then equivalent to a Boolean XOR-constraint on the red sublattice,

$$x \oplus y \stackrel{!}{=} z \quad \Leftrightarrow \quad \text{All permutations of } x, y, z. \quad (22)$$

The red atoms must therefore be “glued together” by a XOR-structure, just as before. However, consistency requires then for the atoms on the blue sublattice

$$x \oplus y \stackrel{!}{=} z \quad \Leftrightarrow \quad \overline{x \oplus y} \stackrel{!}{=} \bar{z} \quad \Leftrightarrow \quad \bar{x} \odot \bar{y} \stackrel{!}{=} \bar{z} \quad (23)$$

where  $\odot$  denotes a XNOR-gate (exclusive-NOR). To enforce the loop constraint, we therefore need a vertex structure with three inverted *pairs* of ports that realizes both a XOR- and a XNOR-gate in a unified way. This is achieved by the FSU-structure introduced in Section VI; hence we can finalize our construction by placing a copy of  $\mathcal{C}_{\text{FSU}}$  on every vertex and amalgamating their port pairs on the edge atoms:



[Recall Fig. 5 (a) and Eq. (17) and identify red (blue) blockades with the upper (lower) “wings”.]

Note that one needs mirror images of the FSU-structure for one of the two vertices in each unit cell of the honeycomb lattice to ensure that only ports of the same sublattice (= color) are amalgamated. Note also that the FSU-structure automatically enforces that states of atoms of port pairs are inverted. Thus the blockades between pairs of edge atoms (black edges) are actually no longer needed and we can delete them from the tessellation without affecting the loop constraint. For now, we ignore whether this construction can be realized as unit disk or unit ball embedding in two- or three-dimensional space, and simply project the necessary blockades into the plane (the sketch above is not a unit disk embedding!); we return to the question of embeddability in Section VIII E.

By construction, this tessellation only supports closed loop configuration in its ground state manifold; an extended patch, including all ancillas, blockades, and detunings, is depicted in Fig. 6. We refer to this tessellated blockade structure as  $\mathcal{C}_{\text{Loop}}$  in the following.

#### D. Automorphisms of the tessellated blockade structure

We continue with the automorphisms of  $\mathcal{C}_{\text{Loop}}$  to establish its full symmetry. As a preliminary step, we focus on an arbitrary FSU-structure on vertex  $s$ , including its three adjacent edges (but ignoring its three neighboring vertex structures for now). As discussed in Section VI, this structure has a large automorphism group, and we are

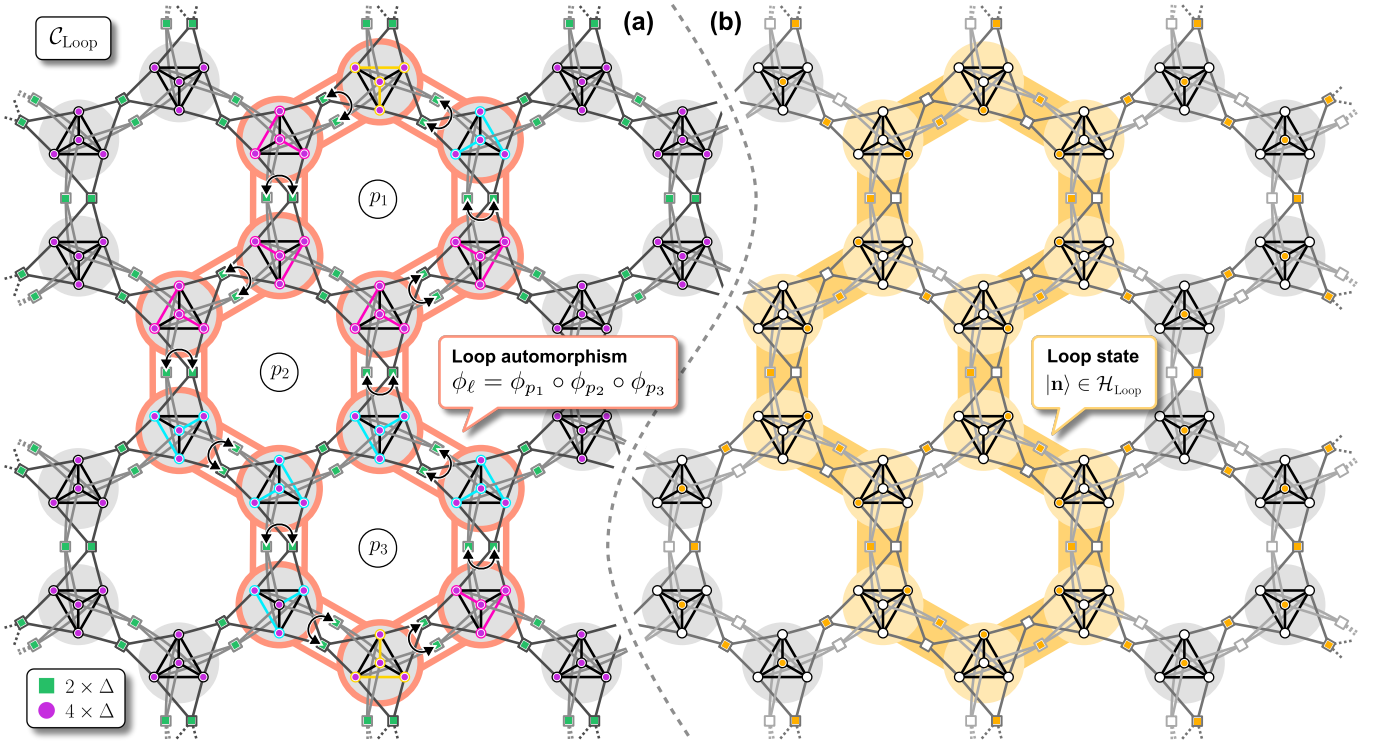


Figure 6. *Tessellated fully-symmetric loop structure*  $\mathcal{C}_{\text{Loop}}$ . Result of the construction discussed in Section VIII C. The tessellation  $\mathcal{C}_{\text{Loop}}$  of FSU-vertices is shown with light gray (formerly red), dark gray (formerly blue) and black blockades. In (a) the fill color of atoms denotes the *detuning* (green:  $2\Delta$ , pink:  $4\Delta$ ), in (b) the *state* of the atom (white: unexcited, orange: excited). (a) Exemplary loop automorphism  $\phi_\ell$  constructed as product of three adjacent plaquette automorphisms  $\phi_{p_1}, \phi_{p_2}, \phi_{p_3}$ . The automorphism decomposes into a chain of vertex- and edge permutations, cf. Fig. 7. Permutations  $\varphi_e$  of edge atoms (squares = ports) are denoted by arrows, permutations  $\varphi_s^\alpha$  of atoms on vertices (circles = ancillas) by colored blockades of the tetrahedra. Note that only atoms with equal detunings are mapped onto each other. It is straightforward to check that the application of  $\phi_\ell$  leaves the complete blockade graph invariant; it therefore corresponds to a loop symmetry  $U_\ell$  of the corresponding blockade Hamiltonian  $H_{\text{Loop}} \equiv H_{\mathcal{C}_{\text{Loop}}}$ . (b) Exemplary excitation pattern  $\mathbf{n} \in L_{\text{Loop}} = L_{\mathcal{C}_{\text{Loop}}}$  that corresponds to a ground state  $|\mathbf{n}\rangle \in \mathcal{H}_{\text{Loop}} \equiv \mathcal{H}_{\mathcal{C}_{\text{Loop}}}$  for  $\Omega = 0$ . Along the yellow loop, the light gray edge atoms are excited (which satisfy XOR-constraints on vertices), whereas everywhere else the dark gray edge atoms are excited (which satisfy XNOR-constraints on vertices). Note that each of the four possible vertex states correlates with one of the four vertex ancillas being excited. It is straightforward to see that the permutations of  $\phi_\ell$  in (a) would act on the pattern in (b) by removing the loop, thereby producing another valid ground state in  $L_{\text{Loop}}$ . This property makes  $H_{\text{Loop}}$  fully-symmetric.

interested in the subgroup that – in a three-dimensional embedding – can be identified with the three rotations about the symmetry axes through opposing edges of the central tetrahedron [recall Fig. 5 (a) and (b)]. We show these automorphisms and their permutations of vertex and edge atoms explicitly in Fig. 7. There we also introduce the decomposition of the three automorphisms

$$\phi_s^\alpha \equiv \varphi_{e_\alpha^1} \circ \varphi_s^\alpha \circ \varphi_{e_\alpha^2}, \quad \alpha \in \{x, y, z\}, \quad (24)$$

into permutations  $\varphi_e$  that act only on atoms on edge  $e$  (ports), and permutations  $\varphi_s^\alpha$  that act only on the tetrahedral atoms (ancillas) on vertex  $s$ . Here  $e_\alpha^1$  and  $e_\alpha^2$  denote the two edges that are singled out by the choice  $\alpha = x, y, z$  (see Fig. 7). Henceforth we denote general *permutations* of atoms by  $\varphi$  to distinguish them from *automorphisms*  $\phi$ . For example, none of the three factors in Eq. (24) is an automorphisms of a single FSU-vertex, only their product is.

Before we continue with the full tessellation  $\mathcal{C}_{\text{Loop}}$ , let us point out that the three automorphisms (24) are reflected in the structure of the truth table of the loop constraints (23). Indeed, from Boolean algebra, we know the identities

$$\begin{array}{ccc} x \oplus y = z & \leftarrow \phi^x \Rightarrow & x \oplus \bar{y} = \bar{z} \\ \updownarrow & \begin{array}{c} \swarrow \phi^z \\ \searrow \phi^y \end{array} & \updownarrow \\ \phi^y & \phi^z = \phi^x \circ \phi^y & \phi^y \\ \downarrow & \begin{array}{c} \swarrow \phi^z \\ \searrow \phi^y \end{array} & \downarrow \\ \bar{x} \oplus y = \bar{z} & \leftarrow \phi^x \Rightarrow & \bar{x} \oplus \bar{y} = z \end{array}$$

and analogous relations for the XNOR-constraint. This demonstrates that the four consistent states on the red sublattice (XOR-constraint) are mapped to each other by the three automorphisms of the FSU-structure – which is the hallmark of its full symmetry.

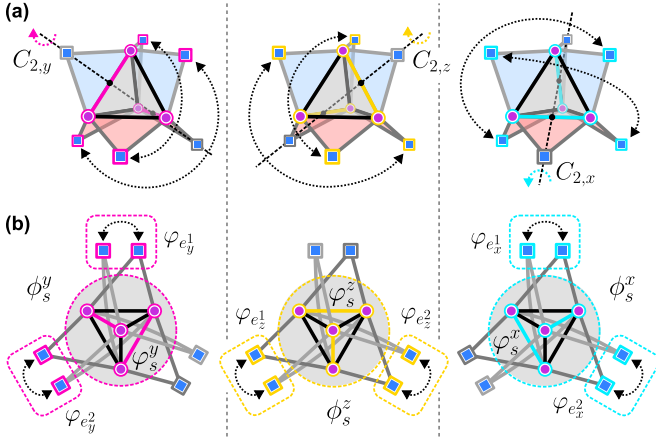


Figure 7. *Automorphisms of an independent FSU-vertex.* (a) The automorphisms  $\phi_s^\alpha$  ( $\alpha = x, y, z$ ) of an independent FSU-structure on vertex  $s$  can be visualized as  $\pi$ -rotations  $C_{2,\alpha}$  of the central tetrahedron about the symmetry axis through opposite edges [recall Fig. 5 (a)]. These symmetries form the Klein four-group  $V$  in which  $(C_{2,\alpha})^2 = 1$  and  $C_{2,x} \cdot C_{2,y} \cdot C_{2,z} = 1$ . (b) In a flattened (not unit disk) representation, each automorphism corresponds to a permutation of ports (squares), indicated by dotted arrows, and of two pairs of ancillas (circles) along the colored blockades of the central tetrahedron. Note that only atoms with the same detunings (fill color) are mapped onto each other, and that always one pair of ports remains invariant (gray ports). Here the blockades to ports are colored light and dark gray instead of red and blue (as in the text). It is convenient to decompose the automorphisms  $\phi_s^\alpha$  into edge and vertex permutations  $\varphi_e$  and  $\varphi_s^\alpha$ , respectively (see text).

The decomposition (24) shows that for each independent FSU-structure on vertex  $s$ , there are three nontrivial automorphisms  $\phi_s^\alpha$  ( $\alpha = x, y, z$ ), each of which affects *two* adjacent edges. Since these edges are *shared* between adjacent vertices in  $\mathcal{C}_{\text{Loop}}$ , applying a vertex automorphism on one vertex necessitates another automorphism on two of its neighbors. Therefore the subgroup  $\mathcal{A}_{\text{Loop}} \subset \mathcal{A}_{\mathcal{C}_{\text{Loop}}}$  of automorphisms of the complete tessellation that is generated by such transformations also obeys a  $\mathbb{Z}_2$ -loop constraint (in addition to the loop constraint on *excitation patterns* in the ground state!). That is, for every closed loop

$$\ell \equiv s_1 \xrightarrow{e_1} s_2 \xrightarrow{e_2} s_3 \dots, \quad (25)$$

given as a sequence of visited vertices  $s_1, s_2, \dots$  and traversed edges  $e_1, e_2, \dots$ , there is a corresponding automorphism  $\phi_\ell \in \mathcal{A}_{\text{Loop}}$  of the form

$$\phi_\ell = \varphi_{s_1}^{\alpha_1} \circ \varphi_{e_1} \circ \varphi_{s_2}^{\alpha_2} \circ \varphi_{e_2} \circ \dots \quad (26)$$

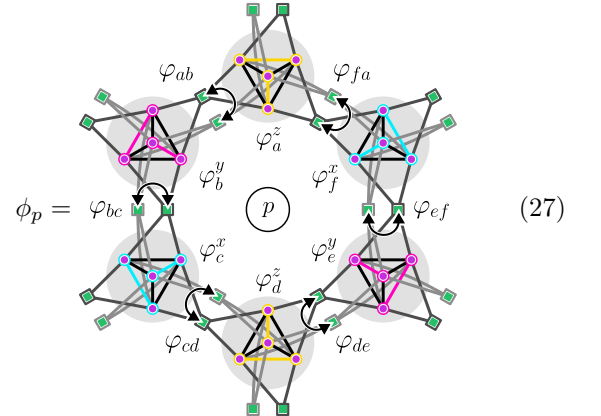
where  $\alpha_i \in \{x, y, z\}$  denotes one of the three possibilities how the loop visits vertex  $s_i$  (recall Fig. 7).

Note that all edge permutations commute trivially:  $\varphi_e \circ \varphi_{\bar{e}} = \varphi_{\bar{e}} \circ \varphi_e$ ; that also all vertex permutations commute  $\varphi_s^\alpha \circ \varphi_s^\beta = \varphi_s^\beta \circ \varphi_s^\alpha$  (even on the same vertex

$s = \bar{s}$ ) follows because the Klein four-group is abelian (Fig. 7). Furthermore, both permutations  $\varphi_e$  and  $\varphi_s^\alpha$  decay into 2-cycles (= transpositions of disjoint pairs of atoms) so that  $(\varphi_e)^2 = 1$  and  $(\varphi_s^\alpha)^2 = 1$  and thereby  $(\phi_\ell)^2 = 1$ . In conclusion,  $\mathcal{A}_{\text{Loop}}$  is an abelian subgroup of the full automorphism group  $\mathcal{A}_{\mathcal{C}_{\text{Loop}}}$ , and can be interpreted as a  $\mathbb{Z}_2$  vector space with the symmetric difference of loops (= composition of automorphisms) as addition (also known as *cycle space* in graph theory [109]).

Pictorially,  $\phi_\ell$  swaps all pairs of inverted ports along  $\ell$  via  $\varphi_e$ , and compensates for these swaps by corresponding vertex permutations  $\varphi_s^\alpha$ . The blockade structure of the FSU-vertex ensures that the result is an isomorphic blockade graph. An example of such a loop automorphism is depicted in Fig. 6 (a). It is important to appreciate that only the *combined* permutations of all tetrahedral vertex atoms and the inverted pairs on edges along the closed loop makes this transformation an automorphism of the blockade graph. In particular, the construction fails if the path of edges does not close!

The smallest of these loop automorphisms are the *plaquette automorphisms* on a hexagon  $p \equiv (abcdef)$ , which can be decomposed into a product of six vertex and six edge permutations:



Multiplication of several such plaquette automorphisms yields loop automorphisms  $\phi_\ell = \prod_{p \in P} \phi_p$ , where  $P$  denotes a set of plaquettes that produce the loop  $\ell = \partial P$  as their boundary  $\partial P$ . Loops  $\ell$  that can be constructed in this way are called *homologically trivial*. For example, the loop automorphism in Fig. 6 (a) can be constructed as product of three elementary plaquette automorphisms.

Note that it is not necessary that  $\ell$  is homologically trivial for  $\phi_\ell$  to be an automorphism. For example, with periodic boundaries, single non-contractible loops around the torus *cannot* be constructed as boundaries of plaquettes, but still give rise to loop automorphisms that satisfy the  $\mathbb{Z}_2$ -loop constraint on every vertex.

The group  $\mathcal{A}_{\text{Loop}}$  of loop automorphisms is therefore generated by plaquette automorphisms and homologically nontrivial loop automorphisms (if any exist), formally:

$$\mathcal{A}_{\text{Loop}} \simeq \langle \{\phi_p \mid \text{Plaquettes } p\} \rangle \oplus H_1(\Sigma). \quad (28)$$

Here,  $H_1(\Sigma)$  denotes the first homology group (over  $\mathbb{Z}_2$ ) of the 2-manifold  $\Sigma$  on which the honeycomb lattice is

embedded. For example, with periodic boundaries it is  $\Sigma = \mathbb{T}$  a torus, and  $H_1(\mathbb{T}) \simeq \mathbb{Z}_2 \times \mathbb{Z}_2 \simeq \{1, \ell_x, \ell_y, \ell_x \oplus \ell_y\}$  where  $\ell_x$  and  $\ell_y$  denote two non-contractible loops around the torus. On lattices with boundaries,  $H_1(\Sigma)$  must be replaced by relative homology groups [98]. Here we are not interested in such details and consider a planar patch of the tessellation with the same type of boundary everywhere; it is then  $H_1(\Sigma) = \{1\}$  as all loops are generated by elementary plaquettes.

With these insights – and our convention (21) to identify strings – it is now evident that  $\varphi_e$  acts on ground state patterns like  $\sigma_e^x$  acts on spins in the toric code: it creates or annihilates a string on edge  $e$ . Loop automorphisms therefore create or annihilate extended loops; in particular, plaquette automorphisms  $\phi_p$  act on ground state patterns by modulo-2 addition of elementary loops; see Fig. 6 (b) for an example. As a consequence, every loop pattern  $\mathbf{n} \in L_{\text{Loop}} \equiv L_{\mathcal{C}_{\text{Loop}}}$  can be constructed from the “no-loop-configuration”  $\mathbf{0}$  by application of some loop automorphism  $\phi \in \mathcal{A}_{\text{Loop}}$ , i.e.,  $L_{\text{Loop}} = \mathcal{A}_{\text{Loop}} \cdot \mathbf{0}$ ; this makes  $\mathcal{C}_{\text{Loop}}$  fully-symmetric, as intended.

As discussed in Section V, every automorphism translates to a unitary symmetry of the blockade Hamiltonian  $H_{\text{Loop}} \equiv H_{\mathcal{C}_{\text{Loop}}}$ . We denote the unitary representation of plaquette automorphisms  $\phi_p$  as  $U_p$ . Since  $\mathcal{A}_{\text{Loop}}$  is abelian, these operators form a local, abelian subgroup of the full symmetry group of the Hamiltonian  $H_{\text{Loop}}$ ,

$$[U_p, U_q] = 0 \quad \text{and} \quad [H_{\text{Loop}}, U_p] = 0, \quad (29)$$

for all plaquettes  $p$  and  $q$ . Note that this remains true for  $\Omega \neq 0$  due to the uniformity of the quantum fluctuations. Since  $\phi_p^2 = \mathbf{1}$ , it follows immediately  $U_p^2 = \mathbf{1}$  and therefore  $U_p^\dagger = U_p$ . It is appropriate to think of these operators as the analogs of the plaquette operators  $B_p$  of the toric code (at least on the ground state manifold). Eq. (29) will be crucial for our study of the many-body ground state in Section VIII F below.

### E. Spatial embedding

Before we turn to the ground state properties of  $H_{\text{Loop}}$ , we briefly discuss potential embeddings of the loop structure  $\mathcal{C}_{\text{Loop}}$ . We stress that an optimized embedding that would bring the structure closer to realization is not (yet) our priority. Here we simply demonstrate that (a slight modification of)  $\mathcal{C}_{\text{Loop}}$  can *in principle* be realized as a quasi-two-dimensional blockade structure of atoms, and leave further improvements to future studies (like reducing the number of atoms and/or increasing the robustness of the blockades).

First, note that a single FSU-vertex can – perhaps surprisingly – be embedded as a *unit disk* graph in two dimensions, see Fig. 8 (a). This embedding, however, is rather tight and not very useful from a practical point of view (where geometrically robust structures are preferable). Another, more problematic downside is that the

inverted pairs of port atoms that belong to *one* edge of  $\mathcal{C}_{\text{Loop}}$  are located *opposite* of each other. It is therefore impossible to tessellate the plane with this embedding (cf. Fig. 6). A *unit ball* embedding in three dimensions is clearly more natural (and more robust), see Fig. 8 (b). The problem of opposite inverted ports remains, though.

A crucial insight to solve this problem is illustrated in Fig. 8 (c): One can “extend” the ports of the FSU-vertex by attaching arbitrarily long *link structures* (see also Ref. [81]) – as long as the length of links that carry inverted signals is equal. It is easy to see that this modification preserves the relevant automorphisms of the structure, so that an extended tessellation  $\mathcal{C}_{\text{Loop}}^{\text{ext}}$  with more atoms (but not more degrees of freedom) per edge can be constructed. While the extension of a single vertex also works with strictly two-dimensional unit disk embeddings, it is unclear whether many vertices can be tessellated and amalgamated without breaking the local automorphisms. The problem that arises in such a planar setup is that the opposing, inverted links must somehow end up on the same edge of the lattice. This can only be achieved by crossing structures [recall Fig. 4 (b)]. However, these crossings “entangle” the blockade graphs of links from *different* edges, and therefore break the plaquette automorphisms. We suspect that a purely two-dimensional construction might be impossible, though we were not able to prove this.

Fortunately, these problems can be circumvented in three dimensions, where links that belong to different edges can simply pass each other without blockades, see Fig. 8 (d). Thus it is indeed possible to realize a suitably extended structure  $\mathcal{C}_{\text{Loop}}^{\text{ext}}$  (which is functionally equivalent to  $\mathcal{C}_{\text{Loop}}$ ) as unit ball graph in three dimensions. Note that the extension of this structure in the third dimension is bounded and does not scale with the lattice size, hence we refer to this embedding as *quasi-two-dimensional*. It seems reasonable to expect that such an extended structure  $\mathcal{C}_{\text{Loop}}^{\text{ext}}$  is not a unit disk graph (and therefore cannot be realized in strictly two dimensions); however, we were not able to prove this rigorously. (Note that deciding whether a given graph is a unit disk graph is NP-hard [110–112]. That is, an efficient proof must exploit the particular structure of the graph.)

In summary, the blockade structure in Fig. 6 (or a slight generalization thereof) *can* be realized as blockade structure in three dimensions. However, finding the simplest, experimentally most accessible realization remains an open question. In the remainder of the paper, we focus again on the unmodified  $\mathcal{C}_{\text{Loop}}$  and ignore its embedding (all results are also valid for embeddable extensions  $\mathcal{C}_{\text{Loop}}^{\text{ext}}$ ).

### F. Ground state properties

In this last section, we study the ground state properties of the blockade Hamiltonian  $H_{\text{Loop}} = H_{\text{Loop}}(\Omega)$  for nonzero quantum fluctuations  $\Omega \neq 0$ . Here we prove our main result, namely that its many-body ground state  $|\Omega\rangle$  is in

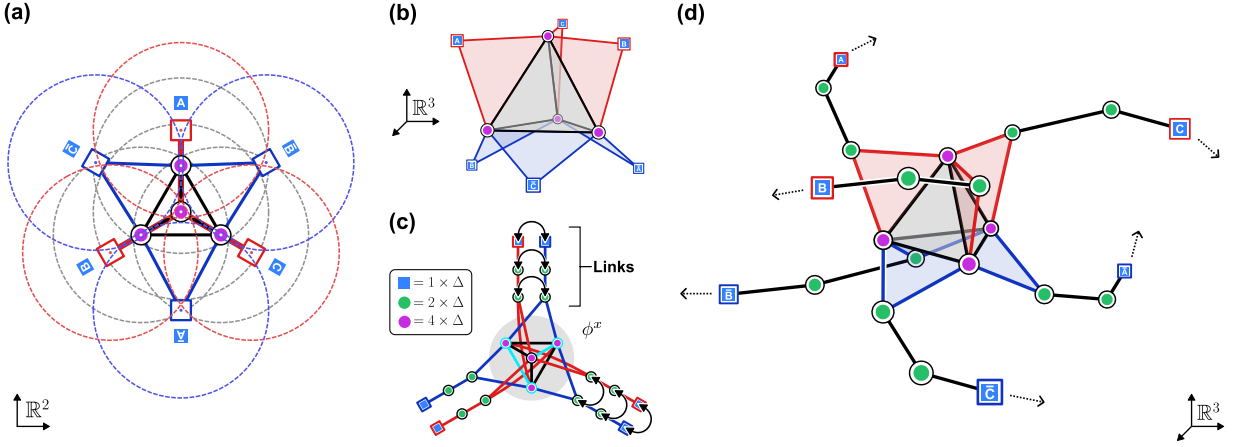


Figure 8. *Embedding of  $\mathcal{C}_{\text{Loop}}$ .* (a) The FSU-vertex alone is a (tight) unit disk graph in  $\mathbb{R}^2$ ; the downside is that the inverted pairs of ports are geometrically opposite to each other. (b) A unit ball embedding in  $\mathbb{R}^3$  is more natural and more robust; it suffers from the same problem, though. (We omit the balls for the sake of clarity, the exact coordinates of atoms are listed in Appendix F.) (c) One can extend the inverted ports of the FSU-vertex by links of *equal length* without breaking its blockade graph automorphisms, as illustrated exemplarily by the (extended) vertex automorphism  $\phi^x$  (cf. Fig. 7). (d) This is useful to “bend” the inverted pairs of ports to one side of the structure, as needed for the tessellated structure  $\mathcal{C}_{\text{Loop}}$ . Indeed, with this trick, one can embed an extended, functionally equivalent, tessellated structure  $\mathcal{C}_{\text{Loop}}^{\text{ext}}$  as a unit ball graph in  $\mathbb{R}^3$ . Note that this embedding is unoptimized (in its number of atoms and robustness of blockades) and therefore quite impractical.

the same quantum phase as the loop condensate  $|\Omega_{\text{TC}}\rangle$  of the toric code. This result is rigorous and does not rely on numerical evidence.

### 1. General features

Let us consider a finite patch of the tessellation  $\mathcal{C}_{\text{Loop}}$  in Fig. 6 with or without periodic boundaries. As detailed in Section VIII D,  $\mathcal{C}_{\text{Loop}}$  is fully-symmetric so that Proposition 1 applies. Namely, it guarantees that the many-body ground state  $|\Omega\rangle$  of  $H_{\text{Loop}}$  for  $\Omega \neq 0$  is unique and given by an equal-weight superposition of loop states from  $\mathcal{H}_{\text{Loop}} \equiv \mathcal{H}_{\mathcal{C}_{\text{Loop}}}$ , dressed by excited states that are suppressed in powers of  $\Omega/\Delta E$ , recall Eq. (16):

$$|\Omega\rangle = \underbrace{\lambda(\Omega) \sum_{\mathbf{n} \in L_{\text{Loop}}} |\mathbf{n}\rangle}_{=: \Lambda|\Omega_0\rangle} + \underbrace{\sum_{d \geq 1} \left(\frac{\Omega}{\Delta E}\right)^d \sum_{\mathbf{n} \in L_{\text{Loop}}^d} \eta_{\mathbf{n}}(\Omega) |\mathbf{n}\rangle}_{=: \sqrt{1-\Lambda^2}|\Omega_\eta\rangle} \quad (30)$$

with  $\langle \Omega_0 | \Omega_\eta \rangle = 0$ .

Note that the form (30) is true for arbitrary  $\Omega \neq 0$ , and not only for small perturbations. This already indicates that one *cannot* deduce from Eq. (30) the presence of topological order – despite the suggestive equal-weight superposition of loop states in  $|\Omega_0\rangle$ ! Furthermore, the *uniqueness* of  $|\Omega\rangle$  is a generic feature of finite-size blockade Hamiltonians like  $H_{\text{Loop}}$  for  $\Omega \neq 0$ ; in particular, it is independent of their boundary conditions. Since we expect  $H_{\text{Loop}}$  to feature topological ground state degeneracies for periodic boundaries, we must conclude that this uniqueness can be due to finite-size gaps that vanish

exponentially fast in the thermodynamic limit. An immediate corollary of Proposition 1 is then that no blockade Hamiltonian of the form (2) can realize the renormalization fixed point (19) of the toric code (as the latter has zero correlation length and therefore perfect topological degeneracy on finite-size systems).

Next, because of Eq. (29) and  $U_p^2 = \mathbb{1}$  and  $U_p^\dagger = U_p$ , we can label the many-body eigenstates of  $H_{\text{Loop}} = H_{\text{Loop}}(\Omega)$ ,

$$H_{\text{Loop}} |E_\Omega^\xi, \xi\rangle = E_\Omega^\xi |E_\Omega^\xi, \xi\rangle, \quad (31)$$

by a sign  $(-1)^{\xi_p} = \pm 1$  per plaquette:

$$U_p |E_\Omega^\xi, \xi\rangle = (-1)^{\xi_p} |E_\Omega^\xi, \xi\rangle. \quad (32)$$

We refer to  $\xi_p \in \{0, 1\}$  as the  $(\mathbb{Z}_2)$ -flux through plaquette  $p$ , in analogy to the toric code. If we set the ground state energy to  $E_\Omega^{\xi^0} = 0$ , we have in particular  $|\Omega\rangle = |0, \xi^0\rangle$ . The flux sector  $\xi^0$  follows from Proposition 1 which states that  $U_p |\Omega\rangle = |\Omega\rangle$  for all plaquette operators  $U_p$ ; together with Eq. (32) this implies  $\xi^0 = \mathbf{0}$ .

In summary, the ground state  $|\Omega\rangle = |0, \mathbf{0}\rangle$  of  $H_{\text{Loop}}$  is in the *flux-free sector*, again in analogy to the toric code where  $B_p |\Omega_{\text{TC}}\rangle = |\Omega_{\text{TC}}\rangle$ . Moreover, due to Eq. (32), the full many-body spectrum of  $H_{\text{Loop}}$  splits into *flux sectors* labeled by flux patterns  $\xi$ . With this knowledge, we turn now to the question of topological order in  $|\Omega\rangle$ .

### 2. Topological order

It is obvious that  $|\Omega_0\rangle$  is in the toric code phase, as it is locally unitary equivalent to the loop condensate (20). (Remember that the additional ancillas on the vertices do

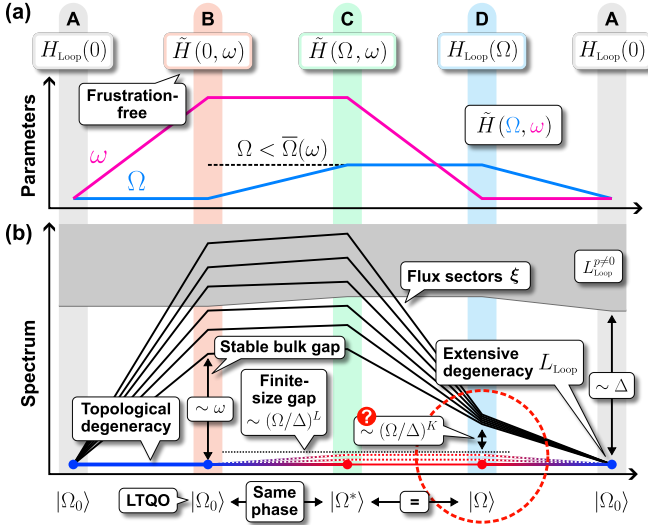


Figure 9. *Spectral properties of  $\tilde{H}(\Omega, \omega)$ .* (a) Family of Hamiltonians  $\tilde{H}(\Omega, \omega)$  parametrized by  $\Omega$  and  $\omega$ . Notably,  $\tilde{H}(0, \omega)$  is frustration-free, an important ingredient for gap stability. (b) Schematic spectrum of  $\tilde{H}(\Omega, \omega)$  along this path. For  $\Omega = 0 = \omega$  (A),  $\tilde{H}(0, 0) = H_{\text{Loop}}(0)$  is purely classical with exponentially degenerate ground state space  $\mathcal{H}_{\text{Loop}}$ . For  $\Omega = 0 < \omega$  (B),  $\tilde{H}(0, \omega)$  is frustration-free and has a fixed point ground state  $|\Omega_0\rangle$  with local topological quantum order (LTQO). Depending on boundary conditions, there can be a (non-extensive) topological ground state degeneracy. The bulk gap of this Hamiltonian is stable against arbitrary, weak, local perturbations, so that for  $0 < |\Omega| < \bar{\Omega}(\omega)$  (C),  $\tilde{H}(\Omega, \omega)$  is still gapped, with a new ground state  $|\Omega^*\rangle$  in the same quantum phase. Switching off  $\omega \searrow 0$  (D) leads to  $H_{\text{Loop}}(\Omega)$  with the ground state  $|\Omega\rangle$ . Due to symmetry, it is  $|\Omega^*\rangle = |\Omega\rangle$ , which allows us to characterize the quantum phase of  $|\Omega\rangle$ . We are ultimately interested in the physics marked by the dashed circle. The question mark indicates that the bulk gap at D remains unproven.

not contribute degrees of freedom to the states in  $\mathcal{H}_{\text{Loop}}$ .) What remains to be shown is that this order is stable under the addition of  $|\Omega_\eta\rangle$  for small but finite fluctuations  $\Omega \neq 0$ .

Since we do not know how to solve  $H_{\text{Loop}}$  exactly, we must take a detour to solve this problem. To this end, we introduce the auxiliary Hamiltonian

$$\tilde{H}(\Omega, \omega) := H_{\text{Loop}}(\Omega) + \frac{\omega}{2} \sum_p (\mathbb{1} - U_p), \quad (33)$$

where we artificially add (experimentally unrealistic) plaquette fluctuations of loops with strength  $\omega$ . We stress that such fluctuations are already *perturbatively* present in  $H_{\text{Loop}}(\Omega)$  alone, although of much weaker, unknown strength. The new term in Eq. (33) penalizes each flux ( $\xi_p = 1$ ) by an additional energy  $\omega$ . Our goal is to use  $\tilde{H}(\Omega, \omega)$  to find a parametric path from a system with exactly known, topologically ordered ground state to  $H_{\text{Loop}}(\Omega) = \tilde{H}(\Omega, 0)$  with ground state  $|\Omega\rangle = |\Omega_0\rangle + |\Omega_\eta\rangle$ , such that the gap remains open along the path (for finite

but sufficiently small  $\Omega$ ); this would establish the topological order of  $|\Omega\rangle$  and demonstrate that  $|\Omega_\eta\rangle$  does not modify the pattern of long-range entanglement [99].

To do so, we proceed along the three steps sketched in Fig. 9 (for mathematical details see Appendix D):

### • Step 1: A $\rightarrow$ B

We start with the classical Hamiltonian  $H_{\text{Loop}}(0) = \tilde{H}(0, 0)$  (A). By construction, this Hamiltonian has an extensively degenerate ground state manifold  $\mathcal{H}_{\text{Loop}}$  spanned by the loop configurations  $L_{\text{Loop}}$ ; its gap  $\sim \Delta$  is given by the detunings.

We now ramp up the artificial plaquette fluctuations  $0 < \omega < \Delta$  (with  $\omega \sim \Delta$ ) while keeping  $\Omega = 0$ . Since  $[U_p, \tilde{H}(0, \omega)] = 0$ , the spectrum of  $\tilde{H}(0, \omega)$  also decomposes into flux sectors. In particular, ground state(s) belong to the zero-flux sector within  $\mathcal{H}_{\text{Loop}}$ . Their construction is analogous to the toric code (Section VIII A), and for open, uniform boundaries one obtains the equal-weight loop condensate

$$|\Omega_0\rangle \propto \sum_{\mathbf{n} \in L_{\text{Loop}}} |\mathbf{n}\rangle. \quad (34)$$

For homologically nontrivial boundaries (like periodic boundaries), there is one independent equal-weight superposition for each element of  $H_1(\Sigma)$  and these are perfectly degenerate. (On the torus, for example, there would be four perfectly degenerate ground states.)

The ground state manifold of  $\tilde{H}(0, \omega)$  is therefore no longer extensively degenerate and within the topologically ordered toric code phase. The gap of  $\tilde{H}(0, \omega)$  is of order  $\omega$  and determines the energy of elementary flux excitations (B).

### • Step 2: B $\rightarrow$ C

Next, we would like to switch on  $\Omega \neq 0$  to reach  $\tilde{H}(\Omega, \omega)$ . In general, this will modify the spectrum, eigenstates and degeneracy of the ground state manifold. In particular, the ground state itself changes,

$$\text{B } |\Omega_0\rangle \xrightarrow[\omega > 0]{\Omega=0 \rightarrow \Omega \neq 0} |\Omega^*\rangle \text{ C} \quad (35)$$

in an unknown way [as we can no longer diagonalize  $\tilde{H}(\Omega, \omega)$ ]. The crucial insight is that, as long as we can guarantee that the gap of  $\tilde{H}(0, \omega)$  does not close when going to  $\tilde{H}(\Omega, \omega)$ , we can conclude that the new ground state  $|\Omega^*\rangle$  belongs to the same quantum phase as  $|\Omega_0\rangle$  [99], i.e., is still in the toric code phase.

Thus the problem reduces to the stability of the gap of  $\tilde{H}(0, \omega)$  under weak local fluctuations  $0 < |\Omega| \ll \omega$ . We stress that in general, bulk gaps are *not* stable under arbitrary local perturbations – even if the latter are small compared to the gap [113].

Fortunately, it can be shown rigorously [114] that a gap *is* stable under arbitrary local, weak perturbations, given the unperturbed Hamiltonian [here:  $\tilde{H}(0, \omega)$ ] is *frustration-free*, and its ground state(s) [here:  $|\Omega_0\rangle$ ] are *topologically ordered*. (More precisely, they must satisfy a condition called *local topological quantum order* [LTQO] [113–115].) In Appendix D we show explicitly that  $\tilde{H}(0, \omega)$  and  $|\Omega_0\rangle$  indeed satisfy these conditions. Note that in the perturbed system  $\tilde{H}(\Omega, \omega)$ , ground state degeneracies can be lifted, but these are provably finite-size and vanish exponentially with system size [114]. In conclusion, we can switch on weak quantum fluctuations  $0 < |\Omega| < \tilde{\Omega}(\omega)$  without closing the bulk gap. Here,  $\tilde{\Omega}(\omega)$  denotes some  $\omega$ -dependent upper bound that guarantees the stability of the gap [114]. This leads us to the new Hamiltonian  $\tilde{H}(\Omega, \omega)$  that is provably in the same gapped quantum phase as the toric code – though with a new, no longer exactly known ground state  $|\Omega^*\rangle$ .

### • Step 3: C $\rightarrow$ D

In the last step, we would like to switch off the auxiliary fluctuations to transition from  $\tilde{H}(\Omega, \omega)$  to  $\tilde{H}(\Omega, 0) = H_{\text{Loop}}(\Omega)$ . Generally, we would again expect a modification of the ground state:

$$\mathbf{C} \quad |\Omega^*\rangle \xrightarrow[\Omega \neq 0]{\omega > 0 \rightarrow \omega = 0} |\Omega\rangle \quad \mathbf{D} \quad (36)$$

The problem is that we cannot consider  $\omega \sim \Delta \gg |\Omega|$  as a small perturbation. Moreover,  $\tilde{H}(\Omega, \omega)$  is *not* frustration-free, so that no gap stability can be inferred. In particular, we cannot conclude that  $H_{\text{Loop}}(\Omega)$  has a bulk gap (see Section VIII F 3 below). This is where the local  $\mathbb{Z}_2$  symmetries of  $H_{\text{Loop}}(\Omega)$  pay off: The eigenbasis  $|E_{\Omega}^{\xi}, \xi\rangle$  of  $H_{\text{Loop}}(\Omega)$  is also an eigenbasis of  $\tilde{H}(\Omega, \omega)$ . Indeed, Eqs. (31) to (33) imply

$$\tilde{H}(\Omega, \omega) |E_{\Omega}^{\xi}, \xi\rangle = (E_{\Omega}^{\xi} + \omega|\xi|) |E_{\Omega}^{\xi}, \xi\rangle \quad (37)$$

with  $|\xi| = \sum_p \xi_p$  the total number of plaquettes with nonzero flux. The only effect of the  $\omega$ -term in Eq. (33) is to shift the eigenenergies of eigenstates in different flux sectors, without modifying the eigenstates themselves.

In Section VIII F 1 we showed that the ground state  $|\Omega\rangle = |0, \mathbf{0}\rangle$  is unique and in the flux-free sector of  $H_{\text{Loop}}(\Omega)$ . Hence Eq. (37) implies  $\tilde{H}(\Omega, \omega) |\Omega\rangle = 0$ , but also that  $\min(E_{\Omega}^{\xi} + \omega|\xi|) \stackrel{\omega \geq 0}{\geq} \min(E_{\Omega}^{\xi}) = 0$ , i.e.,  $|\Omega\rangle$  must be in the ground state manifold of  $\tilde{H}(\Omega, \omega)$ . Since the ground state manifold of  $H_{\text{Loop}}(\Omega)$  is non-degenerate, and eigenenergies can only remain constant or decrease for  $\omega \searrow 0$ , the ground state manifold of  $\tilde{H}(\Omega, \omega)$  must also be non-degenerate. Hence we have shown that actually

$$\mathbf{C} \quad |\Omega^*\rangle = |\Omega\rangle \quad \mathbf{D}, \quad (38)$$

which finally proves that  $|\Omega\rangle$  is in the topologically ordered quantum phase of the toric code.

In conclusion, we managed to transfer our knowledge about the (fixed point) topological order of  $|\Omega_0\rangle$  to the unknown state  $|\Omega\rangle$ ,

$$\overbrace{|\Omega_0\rangle \sim |\Omega^*\rangle}^{\text{Same phase}} = \underbrace{|\Omega\rangle}_{\text{Same state}} = \Lambda |\Omega_0\rangle + \sqrt{1 - \Lambda^2} |\Omega_{\eta}\rangle, \quad (39)$$

where the addition of  $|\Omega_{\eta}\rangle$  perturbs  $|\Omega_0\rangle$  away from the fixed point to  $|\Omega\rangle$ , without leaving the toric codes phase for small but finite, uniform quantum fluctuations  $0 < |\Omega| < \tilde{\Omega}(\omega \sim \Delta)$ . We achieved this by exploiting the gap stability of frustration-free, topologically ordered systems, in conjunction with the local  $\mathbb{Z}_2$  symmetry of the Hamiltonian  $H_{\text{Loop}}$  of the tessellated blockade structure  $\mathcal{C}_{\text{Loop}}$ .

### 3. Bulk gap

We have now rigorously established that the tessellated blockade structure  $\mathcal{C}_{\text{Loop}}$  has a (potentially degenerate) topologically ordered ground state manifold for finite but small fluctuations  $\Omega \neq 0$ . However, we have *not* shown that the system has a finite spectral gap in the thermodynamic limit. Proving the existence or absence of spectral gaps of interacting quantum many-body systems is notoriously difficult [116–118]. Here we conclude our discussion with arguments that might *suggest* (or help to establish) the existence of a bulk gap.

Firstly, one can show (Appendix E) that the large symmetry group  $\mathcal{A}_{\text{Loop}}$  severely restricts the form of the *effective* Hamiltonian on the low-energy subspace  $\mathcal{H}_{\text{Loop}}$ . A Schrieffer-Wolff transformation [119] of  $H_{\text{Loop}}(\Omega)$  yields

$$H_{\text{Loop}}^{\text{eff}} = -J_{\text{eff}} \frac{\Omega^K}{\Delta E^{K-1}} \sum_{\text{Faces } p} U_p + \mathcal{O}\left(\frac{\Omega^{K+2}}{\Delta E^{K+1}}\right), \quad (40)$$

up to a constant shift in energy. The order  $K$  depends on the specific implementation of the structure (e.g., the length of links connecting vertices). The coupling is expected to be positive  $J_{\text{eff}} > 0$ , so that the Hamiltonian (40) is consistent with the zero-flux ground state (30). Most importantly,  $H_{\text{Loop}}^{\text{eff}}$  has a finite gap of order  $J_{\text{eff}} \Omega^K / \Delta E^{K-1}$ . However, this result does not prove a finite gap of  $H_{\text{Loop}}(\Omega)$  because, first, there is no guarantee that the perturbative series converges, and second, the Schrieffer-Wolff transformation implicitly assumes that only the low-energy sector of the unperturbed Hamiltonian  $H_{\text{Loop}}(0)$  is relevant for the perturbed Hamiltonian  $H_{\text{Loop}}(\Omega)$  (which is another unproven assumption).

Secondly, it is well-known that ground states of local, gapped Hamiltonians have only short-range correlations [120]. Conversely, common wisdom associates gapless systems with algebraically decaying correlations.

Our arguments in Section VIII F 2 prove that  $|\Omega\rangle$  is indeed short-range correlated, as it is the ground state of the gapped Hamiltonian  $\tilde{H}(\Omega, \omega)$ . Unfortunately, without additional input, one cannot go the other way and infer the existence of a gap from a short-range correlated ground state, because gapless excitations may not couple to local operators [121, 122].

Lastly, the (presumed) gap induced by the quantum fluctuations  $\Omega$  separates the zero-flux sector of the ground state from higher flux sectors (Fig. 9 D); it therefore corresponds to the “mass” of flux excitations – which are non-dynamical due to the local  $\mathbb{Z}_2$  symmetry. As such, it is analogous to the mass of static charge pairs (mesons) in a pure  $\mathbb{Z}_2$  lattice gauge theory in two dimensions [123–125]. Via well-known duality transformations, the energy gap can then be reinterpreted as the difference between ground state energies of the two-dimensional transverse-field Ising model with and without antiferromagnetic defect lines. This suggests that methods and results from these related fields might provide further insight into the spectral properties of the blockade structure  $\mathcal{C}_{\text{Loop}}$ .

In conclusion, there is anecdotal evidence for a finite bulk gap  $\sim \Omega^K/\Delta^{K-1}$  that separates the zero-flux sector of  $|\Omega\rangle$  from states with flux excitations. However, a rigorous proof of its existence (or absence) is missing.

## IX. OUTLOOK & COMMENTS

There are several loose ends throughout the paper, and a few obvious follow-up questions that need more work:

**Spectral gap.** The question whether our proposed blockade Hamiltonian has a bulk gap remains open. It would be interesting whether any of the (few) known methods to rigorously establish the existence of a bulk gap applies to our system. To strengthen (or debunk) our anecdotal evidence for a gap, one also could resort to numerical techniques like DMRG. However, this approach is complicated by the 36 atoms required to implement a single plaquette of the honeycomb lattice. While the blockade interaction reduces the number of states in the Hilbert space significantly, it hardly compensates for the exponential resource requirements due to the rather large number of atoms in a unit cell.

**Planar tessellations.** It remains unclear whether our proposed tessellated blockade graph necessarily requires three spatial dimensions to be realized as a blockade structure. While it seems unlikely that a functionally equivalent planar embedding exists, we are not aware of a rigorous argument to support this claim. We also showed that none of the previously known tessellations we checked feature local blockade graph automorphisms. Since all these models are realizable as unit disk graphs, one might conjecture that the third dimension is indeed *needed* for fully-symmetric tessellated structure (at least if they implement non-factorizable ground state manifolds). A counterexample to this conjecture would be a strictly

planar, fully-symmetric tessellation that is functionally equivalent to our quasi-two-dimensional model.

**Other XOR/FSU-based tessellations.** In this work, we employed the XOR-constraint – realized by the FSU-structure – to implement a periodic system with local  $\mathbb{Z}_2$ -loop constraints. But XOR-constraints are more versatile than that, as they simply realize a local  $\sigma_i^z \sigma_j^z \sigma_k^z$  interaction. Using a fully-symmetric version of a copy-structure [81], it is possible to connect FSU-structures by double-links (“ladders”) in functionally different ways, without breaking the full symmetry of the tessellation. For instance, it is straightforward to construct a blockade version of the *triangular-plaquette model* (also known as *Newman-Moore model* [126]), where the full symmetry is realized by extensive “fractal” automorphisms on a triangular lattice [127]; the quantum fluctuations then realize (a low-energy version of) the *quantum triangular-plaquette model*, see e.g. Ref. [128] and references therein.

**Fully-symmetric circuits.** It would be interesting to explore how generic the paradigm of fully-symmetric blockade structures actually is. For example, is there a toolbox that allows for the amalgamation of fully-symmetric elementary building blocks and can be used to design fully-symmetric structures for any prescribed set of ground state patterns? This would be potentially useful for applications like geometric programming [79, 80] where optimization problems are encoded in blockade structures and the solution relies on strong fluctuations over a vast search space. For example, one could start with the FSU-gate and use double-links (“ladders”) to relay Boolean variables, and then try to bootstrap a framework akin to *differential signaling* and *balanced circuits* known from electrical engineering.

**Alternative platforms.** As stressed previously, our results apply to any framework with controllable two-level systems that interact via a simple blockade potential. While neutral atom platforms that leverage Rydberg states are currently the most promising candidate for the implementation of such systems, it would be interesting to explore alternative platforms as well [77, 78]. For example, if one could implement blockade graphs *directly* (e.g. using techniques from superconducting circuit QED [129]), one could evade embeddability issues that arise from the geometric nature of the van der Waals interaction between atoms (see next).

**Van der Waals interactions.** In this work, we focused on ideal blockade Hamiltonians that describe abstract two-level systems. Depending on the experimental platform used to implement these models, platform-specific modifications of the Hamiltonian must be taken into account. For instance, the Rydberg blockade only *approximates* a sharply decaying van der Waals interaction. It is nontrivial but crucial for experiments on this platform to study the effects of the long-range tails of these interactions on the proposed blockade structures [96]. For example, such interactions typically break the symmetries provided by blockade graph automorphisms. It is reasonable to expect that these symmetries might survive *if* they

can be realized as Euclidean symmetries of the spatial structure. This makes the design of symmetric blockade structures more involved because geometry enters the stage. We note that Proposition 1 can be readily adapted to van der Waals interactions if blockade graph automorphisms are replaced by isometries (see Appendices A 1 and A 2).

## X. SUMMARY

In this paper, we studied the effect of uniform quantum fluctuations on tailored structures of two-level systems (atoms, spins, cavity modes etc.) that interact via a strong blockade potential (so called *blockade structures*). There are three main results to highlight:

First, we introduced the concept of *blockade graph automorphisms* to describe (not necessarily geometric) symmetries of strongly interacting blockade Hamiltonians with quantum fluctuations. We then defined *fully-symmetric* blockade structures as those, where these symmetries act transitively on the set of excitation patterns in the classical ground state manifold. Our first main contribution is the rigorous proof that uniform quantum fluctuations of fully-symmetric structures stabilize a *unique* ground state with *equal-weight* contributions from each ground state of the classical system. This result provides a versatile tool to engineer blockade structure that experience strong quantum fluctuations by design.

Second, to illustrate these concepts, we constructed the fully-symmetric universal (FSU) gate, a three-dimensional structure of 10 two-level systems that is fully-symmetric and realizes various Boolean gates at once. Among these are XOR- and XNOR-constraints between pairs of two-level systems that are forced into inverted states within the ground state manifold. We then showed step-by-step how this FSU-structure can be used to construct a quasi-two-dimensional periodic tessellation of two-level systems on the honeycomb lattice that enforces a  $\mathbb{Z}_2$  Gauss law on its vertices and features local  $\mathbb{Z}_2$  symmetries on its plaquettes. The action of these symmetries on the “loop

states” (which satisfy the Gauss law) makes this blockade structure fully-symmetric, and therefore stabilizes an equal-weight superposition of loop states as its many-body ground state. This loop condensate is reminiscent of the toric code, and suggest that the proposed tessellation stabilizes topological order. This construction is our second main contribution: It both showcases a highly nontrivial application of the concept of full symmetry, and thereby results in the first known blockade structure that provably stabilizes an equal-weight loop condensate.

Finally, we showed how prior results on the gap stability of topologically ordered systems, in conjunction with the local  $\mathbb{Z}_2$  symmetry of our system, can be exploited to draw conclusions about the topological order of its many-body ground state. In particular, we proved that the ground state of our tessellated blockade structure belongs to the quantum phase of the toric code. This proof is our third main contribution: It showcases a technique that allows access to rigorous results on strongly interacting, tessellated blockade structures – without full knowledge of the eigenstates – to establish the topological order of the ground state. To the best of our knowledge, this is the first system based on two-body blockade interactions where this is known rigorously, without relying on numerical evidence or perturbative techniques.

Combined, these results extend the toolbox for the bottom-up design of tailored quantum matter on platforms that feature simple two-body blockade interactions.

## ACKNOWLEDGMENTS

We acknowledge funding from the Federal Ministry of Education and Research (BMBF) under the grants QRyd-Demo, MUNIQC-Atoms, and the Horizon Europe programme HORIZON-CL4-2021-DIGITAL-EMERGING-01-30 via the project 101070144 (EuRyQa). We thank José Garre Rubio for discussions on potential applications of our toolbox to the quantum Newman-Moore model. TM thanks Malena Bauer for stimulating discussions on graph theory.

- 
- [1] I. Bloch, J. Dalibard and W. Zwerger, *Many-body physics with ultracold gases*, Reviews of Modern Physics **80**(3), 885 (2008), doi:[10.1103/revmodphys.80.885](https://doi.org/10.1103/revmodphys.80.885).
  - [2] A. Browaeys and T. Lahaye, *Many-body physics with individually controlled Rydberg atoms*, Nature Physics **16**(2), 132 (2020), doi:[10.1038/s41567-019-0733-z](https://doi.org/10.1038/s41567-019-0733-z).
  - [3] A. Kitaev, *Fault-tolerant quantum computation by anyons*, Annals of Physics **303**(1), 2 (2003), doi:[10.1016/s0003-4916\(02\)00018-0](https://doi.org/10.1016/s0003-4916(02)00018-0).
  - [4] M. A. Levin and X.-G. Wen, *String-net condensation: A physical mechanism for topological phases*, Physical Review B **71**, 045110 (2005), doi:[10.1103/physrevb.71.045110](https://doi.org/10.1103/physrevb.71.045110).
  - [5] M. Fannes, B. Nachtergaele and R. F. Werner, *Finitely correlated states on quantum spin chains*, Communications in Mathematical Physics **144**(3), 443 (1992), doi:[10.1007/BF02099178](https://doi.org/10.1007/BF02099178).
  - [6] N. Schuch, I. Cirac and D. Pérez-García, *PEPS as ground states: Degeneracy and topology*, Annals of Physics **325**(10), 2153 (2010), doi:[10.1016/j.aop.2010.05.008](https://doi.org/10.1016/j.aop.2010.05.008).
  - [7] I. Affleck, T. Kennedy, E. H. Lieb and H. Tasaki, *Valence bond ground states in isotropic quantum antiferromagnets*, Communications in Mathematical Physics **115**(3), 477 (1988), doi:[10.1007/bf01218021](https://doi.org/10.1007/bf01218021).
  - [8] P. Anderson, *Resonating valence bonds: A new kind of insulator?*, Materials Research Bulletin **8**(2), 153 (1973), doi:[10.1016/0025-5408\(73\)90167-0](https://doi.org/10.1016/0025-5408(73)90167-0).

- [9] N. Schuch, D. Poilblanc, J. I. Cirac and D. Pérez-García, *Resonating valence bond states in the PEPS formalism*, Physical Review B **86**(11), 115108 (2012), doi:[10.1103/physrevb.86.115108](https://doi.org/10.1103/physrevb.86.115108).
- [10] X.-G. Wen, *Colloquium : Zoo of quantum-topological phases of matter*, Reviews of Modern Physics **89**(4), 041004 (2017), doi:[10.1103/revmodphys.89.041004](https://doi.org/10.1103/revmodphys.89.041004).
- [11] E. Dennis, A. Kitaev, A. Landahl and J. Preskill, *Topological quantum memory*, Journal of Mathematical Physics **43**(9), 4452 (2002), doi:[10.1063/1.1499754](https://doi.org/10.1063/1.1499754).
- [12] C. Nayak, S. H. Simon, A. Stern, M. Freedman and S. Das Sarma, *Non-abelian anyons and topological quantum computation*, Reviews of Modern Physics **80**, 1083 (2008), doi:[10.1103/revmodphys.80.1083](https://doi.org/10.1103/revmodphys.80.1083).
- [13] D. Barredo, V. Lienhard, S. de Léséleuc, T. Lahaye and A. Browaeys, *Synthetic three-dimensional atomic structures assembled atom by atom*, Nature **561**(7721), 79 (2018), doi:[10.1038/s41586-018-0450-2](https://doi.org/10.1038/s41586-018-0450-2).
- [14] D. Bluvstein, S. J. Evered, A. A. Geim, S. H. Li, H. Zhou, T. Manovitz, S. Ebadi, M. Cain, M. Kalinowski, D. Hangleiter, J. P. Bonilla Ataides, N. Maskara *et al.*, *Logical quantum processor based on reconfigurable atom arrays*, Nature **626**(7997), 58 (2023), doi:[10.1038/s41586-023-06927-3](https://doi.org/10.1038/s41586-023-06927-3).
- [15] H. Labuhn, S. Ravets, D. Barredo, L. Béguin, F. Nogrette, T. Lahaye and A. Browaeys, *Single-atom addressing in microtraps for quantum-state engineering using Rydberg atoms*, Physical Review A **90**(2), 023415 (2014), doi:[10.1103/PhysRevA.90.023415](https://doi.org/10.1103/PhysRevA.90.023415).
- [16] A. Omran, H. Levine, A. Keesling, G. Semeghini, T. T. Wang, S. Ebadi, H. Bernien, A. S. Zibrov, H. Pichler, S. Choi, J. Cui, M. Rossignolo *et al.*, *Generation and manipulation of Schrödinger cat states in Rydberg atom arrays*, Science **365**(6453), 570 (2019), doi:[10.1126/science.aax9743](https://doi.org/10.1126/science.aax9743).
- [17] N. Sibalic and C. S. Adams, *Rydberg Physics*, IOP Publishing, doi:[10.1088/978-0-7503-1635-4](https://doi.org/10.1088/978-0-7503-1635-4) (2018).
- [18] D. Jaksch, J. I. Cirac, P. Zoller, S. L. Rolston, R. Côté and M. D. Lukin, *Fast quantum gates for neutral atoms*, Physical Review Letters **85**(10), 2208 (2000), doi:[10.1103/physrevlett.85.2208](https://doi.org/10.1103/physrevlett.85.2208).
- [19] D. Tong, S. M. Farooqi, J. Stanojevic, S. Krishnan, Y. P. Zhang, R. Côté, E. E. Eyler and P. L. Gould, *Local blockade of Rydberg excitation in an ultracold gas*, Physical Review Letters **93**(6), 063001 (2004), doi:[10.1103/physrevlett.93.063001](https://doi.org/10.1103/physrevlett.93.063001).
- [20] K. Singer, M. Reetz-Lamour, T. Amthor, L. G. Marcassa and M. Weidemüller, *Suppression of excitation and spectral broadening induced by interactions in a cold gas of Rydberg atoms*, Physical Review Letters **93**(16), 163001 (2004), doi:[10.1103/physrevlett.93.163001](https://doi.org/10.1103/physrevlett.93.163001).
- [21] A. Gaëtan, Y. Miroshnychenko, T. Wilk, A. Chotia, M. Viteau, D. Comparat, P. Pillet, A. Browaeys and P. Grangier, *Observation of collective excitation of two individual atoms in the Rydberg blockade regime*, Nature Physics **5**(2), 115 (2009), doi:[10.1038/nphys1183](https://doi.org/10.1038/nphys1183).
- [22] E. Urban, T. A. Johnson, T. Henage, L. Isenhower, D. D. Yavuz, T. G. Walker and M. Saffman, *Observation of Rydberg blockade between two atoms*, Nature Physics **5**(2), 110 (2009), doi:[10.1038/nphys1178](https://doi.org/10.1038/nphys1178).
- [23] H. Weimer, M. Müller, I. Lesanovsky, P. Zoller and H. P. Büchler, *A Rydberg quantum simulator*, Nature Physics **6**(5), 382 (2010), doi:[10.1038/nphys1614](https://doi.org/10.1038/nphys1614).
- [24] I. Georgescu, S. Ashhab and F. Nori, *Quantum simulation*, Reviews of Modern Physics **86**(1), 153 (2014), doi:[10.1103/revmodphys.86.153](https://doi.org/10.1103/revmodphys.86.153).
- [25] P. Schauß, J. Zeiher, T. Fukuhara, S. Hild, M. Cheneau, T. Macrì, T. Pohl, I. Bloch and C. Gross, *Crystallization in Ising quantum magnets*, Science **347**(6229), 1455 (2015), doi:[10.1126/science.1258351](https://doi.org/10.1126/science.1258351).
- [26] H. Labuhn, D. Barredo, S. Ravets, S. de Léséleuc, T. Macrì, T. Lahaye and A. Browaeys, *Tunable two-dimensional arrays of single Rydberg atoms for realizing quantum Ising models*, Nature **534**(7609), 667 (2016), doi:[10.1038/nature18274](https://doi.org/10.1038/nature18274).
- [27] C. Gross and I. Bloch, *Quantum simulations with ultracold atoms in optical lattices*, Science **357**(6355), 995 (2017), doi:[10.1126/science.aal3837](https://doi.org/10.1126/science.aal3837).
- [28] H. Bernien, S. Schwartz, A. Keesling, H. Levine, A. Omran, H. Pichler, S. Choi, A. S. Zibrov, M. Endres, M. Greiner, V. Vuletić and M. D. Lukin, *Probing many-body dynamics on a 51-atom quantum simulator*, Nature **551**(7682), 579 (2017), doi:[10.1038/nature24622](https://doi.org/10.1038/nature24622).
- [29] E. Altman, K. R. Brown, G. Carleo, L. D. Carr, E. Demler, C. Chin, B. DeMarco, S. E. Economou, M. A. Eriksson, K.-M. C. Fu, M. Greiner, K. R. Hazzard *et al.*, *Quantum simulators: Architectures and opportunities*, PRX Quantum **2**(1), 017003 (2021), doi:[10.1103/prxquantum.2.017003](https://doi.org/10.1103/prxquantum.2.017003).
- [30] G. Semeghini, H. Levine, A. Keesling, S. Ebadi, T. T. Wang, D. Bluvstein, R. Verresen, H. Pichler, M. Kalinowski, R. Samajdar, A. Omran, S. Sachdev *et al.*, *Probing topological spin liquids on a programmable quantum simulator*, Science **374**(6572), 1242 (2021), doi:[10.1126/science.abi8794](https://doi.org/10.1126/science.abi8794).
- [31] P. Scholl, M. Schuler, H. J. Williams, A. A. Eberharter, D. Barredo, K.-N. Schymik, V. Lienhard, L.-P. Henry, T. C. Lang, T. Lahaye, A. M. Läuchli and A. Browaeys, *Quantum simulation of 2D antiferromagnets with hundreds of Rydberg atoms*, Nature **595**(7866), 233 (2021), doi:[10.1038/s41586-021-03585-1](https://doi.org/10.1038/s41586-021-03585-1).
- [32] R. Samajdar, W. W. Ho, H. Pichler, M. D. Lukin and S. Sachdev, *Quantum phases of Rydberg atoms on a Kagome lattice*, Proceedings of the National Academy of Sciences **118**(4), e2015785118 (2021), doi:[10.1073/pnas.2015785118](https://doi.org/10.1073/pnas.2015785118).
- [33] R. Verresen, M. D. Lukin and A. Vishwanath, *Prediction of toric code topological order from Rydberg blockade*, Physical Review X **11**(3), 031005 (2021), doi:[10.1103/physrevx.11.031005](https://doi.org/10.1103/physrevx.11.031005).
- [34] P. Tarabunga, F. Surace, R. Andreoni, A. Angelone and M. Dalmonte, *Gauge-theoretic origin of Rydberg quantum spin liquids*, Physical Review Letters **129**(19), 195301 (2022), doi:[10.1103/PhysRevLett.129.195301](https://doi.org/10.1103/PhysRevLett.129.195301).
- [35] K. Slagle, Y. Liu, D. Aasen, H. Pichler, R. S. K. Mong, X. Chen, M. Endres and J. Alicea, *Quantum spin liquids bootstrapped from Ising criticality in Rydberg arrays*, Physical Review B **106**(11), 115122 (2022), doi:[10.1103/PhysRevB.106.115122](https://doi.org/10.1103/PhysRevB.106.115122).
- [36] A. Maity, Y. Iqbal and R. Samajdar, *Fermionic parton theory of Rydberg  $\mathbb{Z}_2$  quantum spin liquids*, arXiv (2024), doi:[10.48550/arXiv.2409.17219](https://doi.org/10.48550/arXiv.2409.17219).
- [37] Z. Wang and L. Pollet, *Renormalized classical spin liquid on the ruby lattice*, Physical Review Letters **134**(8), 086601 (2025), doi:[10.1103/PhysRevLett.134.086601](https://doi.org/10.1103/PhysRevLett.134.086601).
- [38] Z. Yan, R. Samajdar, Y.-C. Wang, S. Sachdev and Z. Y. Meng, *Triangular lattice quantum dimer model with*

- variable dimer density, *Nature Communications* **13**(1) (2022), doi:[10.1038/s41467-022-33431-5](https://doi.org/10.1038/s41467-022-33431-5).
- [39] Z. Zeybek, R. Mukherjee and P. Schmelcher, *Quantum phases from competing van der Waals and dipole-dipole interactions of Rydberg atoms*, *Physical Review Letters* **131**(20), 203003 (2023), doi:[10.1103/PhysRevLett.131.203003](https://doi.org/10.1103/PhysRevLett.131.203003).
- [40] Z. Zeng, G. Giudici and H. Pichler, *Quantum dimer models with Rydberg gadgets*, *Physical Review Research* **7**(1), 1012006 (2025), doi:[10.1103/physrevresearch.7.1012006](https://doi.org/10.1103/physrevresearch.7.1012006).
- [41] R. Verresen, N. Tantivasadakarn and A. Vishwanath, *Efficiently preparing Schrödinger's cat, fractons and non-Abelian topological order in quantum devices*, arXiv (2021), doi:[10.48550/arXiv.2112.03061](https://doi.org/10.48550/arXiv.2112.03061).
- [42] N. E. Myerson-Jain, S. Yan, D. Weld and C. Xu, *Construction of fractal order and phase transition with Rydberg atoms*, *Physical Review Letters* **128**(1), 017601 (2022), doi:[10.1103/PhysRevLett.128.017601](https://doi.org/10.1103/PhysRevLett.128.017601).
- [43] R. A. Macêdo and R. G. Pereira, *Fractonic criticality in Rydberg atom arrays*, *Physical Review B* **110**(8), 085144 (2024), doi:[10.1103/PhysRevB.110.085144](https://doi.org/10.1103/PhysRevB.110.085144).
- [44] F. M. Surace, P. P. Mazza, G. Giudici, A. Lerose, A. Gambassi and M. Dalmonte, *Lattice gauge theories and string dynamics in Rydberg atom quantum simulators*, *Physical Review X* **10**(2), 021041 (2020), doi:[10.1103/PhysRevX.10.021041](https://doi.org/10.1103/PhysRevX.10.021041).
- [45] A. Celi, B. Vermersch, O. Viyuela, H. Pichler, M. D. Lukin and P. Zoller, *Emerging two-dimensional gauge theories in Rydberg configurable arrays*, *Physical Review X* **10**(2), 021057 (2020), doi:[10.1103/physrevx.10.021057](https://doi.org/10.1103/physrevx.10.021057).
- [46] L. Homeier, A. Bohrdt, S. Linsel, E. Demler, J. C. Halimeh and F. Grusdt, *Realistic scheme for quantum simulation of  $\mathbb{Z}_2$  lattice gauge theories with dynamical matter in  $(2+1)D$* , *Communications Physics* **6**(1) (2023), doi:[10.1038/s42005-023-01237-6](https://doi.org/10.1038/s42005-023-01237-6).
- [47] R. Samajdar, D. G. Joshi, Y. Teng and S. Sachdev, *Emergent  $\mathbb{Z}_2$  gauge theories and topological excitations in Rydberg atom arrays*, *Physical Review Letters* **130**(4), 043601 (2023), doi:[10.1103/PhysRevLett.130.043601](https://doi.org/10.1103/PhysRevLett.130.043601).
- [48] J. Feldmeier, N. Maskara, N. U. Köylüoğlu and M. D. Lukin, *Quantum simulation of dynamical gauge theories in periodically driven Rydberg atom arrays*, arXiv (2024), doi:[10.48550/arXiv.2408.02733](https://doi.org/10.48550/arXiv.2408.02733).
- [49] N. U. Köylüoğlu, N. Maskara, J. Feldmeier and M. D. Lukin, *Floquet engineering of interactions and entanglement in periodically driven Rydberg chains*, arXiv (2024), doi:[10.48550/ARXIV.2408.02741](https://doi.org/10.48550/ARXIV.2408.02741).
- [50] Y. Cheng and H. Zhai, *Emergent  $U(1)$  lattice gauge theory in Rydberg atom arrays*, *Nature Reviews Physics* **6**(9), 566 (2024), doi:[10.1038/s42254-024-00749-6](https://doi.org/10.1038/s42254-024-00749-6).
- [51] J. Shah, G. Nambiar, A. V. Gorshkov and V. Galitski, *Quantum spin ice in three-dimensional Rydberg atom arrays*, *Physical Review X* **15**(1), 011025 (2025), doi:[10.1103/PhysRevX.15.011025](https://doi.org/10.1103/PhysRevX.15.011025).
- [52] Z. Yan, Y.-C. Wang, R. Samajdar, S. Sachdev and Z. Y. Meng, *Emergent glassy behavior in a kagome Rydberg atom array*, *Physical Review Letters* **130**(20), 206501 (2023), doi:[10.1103/PhysRevLett.130.206501](https://doi.org/10.1103/PhysRevLett.130.206501).
- [53] S. Ebadi, T. T. Wang, H. Levine, A. Keesling, G. Semeghini, A. Omran, D. Bluvstein, R. Samajdar, H. Pichler, W. W. Ho, S. Choi, S. Sachdev *et al.*, *Quantum phases of matter on a 256-atom programmable quantum simulator*, *Nature* **595**(7866), 227 (2021), doi:[10.1038/s41586-021-03582-4](https://doi.org/10.1038/s41586-021-03582-4).
- [54] T. Manovitz, S. H. Li, S. Ebadi, R. Samajdar, A. A. Geim, S. J. Evered, D. Bluvstein, H. Zhou, N. U. Köylüoğlu, J. Feldmeier, P. E. Dolgirev, N. Maskara *et al.*, *Quantum coarsening and collective dynamics on a programmable simulator*, *Nature* **638**(8049), 86 (2025), doi:[10.1038/s41586-024-08353-5](https://doi.org/10.1038/s41586-024-08353-5).
- [55] H. Pichler, S.-T. Wang, L. Zhou, S. Choi and M. D. Lukin, *Quantum optimization for maximum independent set using Rydberg atom arrays*, arXiv (2018), doi:[10.48550/arxiv.1808.10816](https://doi.org/10.48550/arxiv.1808.10816).
- [56] L. T. Brady and S. Hadfield, *Iterative quantum algorithms for maximum independent set: A tale of low-depth quantum algorithms*, arXiv (2023), doi:[10.48550/arXiv.2309.13110](https://doi.org/10.48550/arXiv.2309.13110).
- [57] C. Vercellino, G. Vitali, P. Viviani, E. Giusto, A. Scionti, A. Scarabosio, O. Terzo and B. Montrucchio, *BBQ-mIS: A parallel quantum algorithm for graph coloring problems*, IEEE International Conference on Quantum Computing and Engineering pp. 141–147 (2023), doi:[10.1109/QCE57702.2023.10198](https://doi.org/10.1109/QCE57702.2023.10198).
- [58] C. Dalyac, L. Leclerc, L. Vignoli, M. Djellabi, W. d. S. Coelho, B. Ximenez, A. Dareaux, D. Dreon, V. E. Elfving, A. Signoles, L.-P. Henry and L. Henriët, *Graph algorithms with neutral atom quantum processors*, *The European Physical Journal A* **60**(9) (2024), doi:[10.1140/epja/s10050-024-01385-5](https://doi.org/10.1140/epja/s10050-024-01385-5).
- [59] L. Bombieri, Z. Zeng, R. Tricarico, R. Lin, S. Notarnicola, M. Cain, M. D. Lukin and H. Pichler, *Quantum adiabatic optimization with Rydberg arrays: localization phenomena and encoding strategies*, arXiv (2024), doi:[10.48550/ARXIV.2411.04645](https://doi.org/10.48550/ARXIV.2411.04645).
- [60] M. Y. Naghmouchi and W. d. S. Coelho, *Mixed-integer linear programming solver using Benders decomposition assisted by a neutral-atom quantum processor*, *Physical Review A* **110**(1), 012434 (2024), doi:[10.1103/PhysRevA.110.012434](https://doi.org/10.1103/PhysRevA.110.012434).
- [61] M. Lanthaler, K. Ender, C. Dłaska and W. Lechner, *Quantum optimization with globally driven neutral atom arrays*, arXiv (2024), doi:[10.48550/ARXIV.2410.03902](https://doi.org/10.48550/ARXIV.2410.03902).
- [62] A. M. Farouk, I. I. Beterov, P. Xu and I. I. Ryabtsev, *Generation of quantum phases of matter and finding a maximum-weight independent set of unit-disk graphs using Rydberg atoms*, *Physical Review A* **110**(2), 022442 (2024), doi:[10.1103/PhysRevA.110.022442](https://doi.org/10.1103/PhysRevA.110.022442).
- [63] M. Dupont and B. Sundar, *Extending relax-and-round combinatorial optimization solvers with quantum correlations*, *Physical Review A* **109**(1), 012429 (2024), doi:[10.1103/PhysRevA.109.012429](https://doi.org/10.1103/PhysRevA.109.012429).
- [64] B. F. Schiffer, D. S. Wild, N. Maskara, M. Cain, M. D. Lukin and R. Samajdar, *Circumventing superexponential runtimes for hard instances of quantum adiabatic optimization*, *Physical Review Research* **6**(1), 013271 (2024), doi:[10.1103/PhysRevResearch.6.013271](https://doi.org/10.1103/PhysRevResearch.6.013271).
- [65] A. Byun, J. Jung, K. Kim, M. Kim, S. Jeong, H. Jeong and J. Ahn, *Rydberg-atom graphs for quadratic unconstrained binary optimization problems*, *Advanced Quantum Technologies* **7**(8) (2024), doi:[10.1002/qute.202300398](https://doi.org/10.1002/qute.202300398).
- [66] L. Leclerc, C. Dalyac, P. Bendotti, R. Griset, J. Mikael and L. Henriët, *Implementing transferable annealing protocols for combinatorial optimisation on neutral atom quantum processors: a case study on smart-charging of electric vehicles*, arXiv (2024), doi:[10.48550/arXiv.2411.16656](https://doi.org/10.48550/arXiv.2411.16656).

- [67] M. J. A. Schuetz, R. S. Andrist, G. Salton, R. Yalovetzky, R. Raymond, Y. Sun, A. Acharya, S. Chakrabarti, M. Pistoia and H. G. Katzgraber, *Quantum compilation toolkit for Rydberg atom arrays with implications for problem hardness and quantum speedups*, arXiv (2024), doi:[10.48550/arXiv.2412.14976](https://doi.org/10.48550/arXiv.2412.14976).
- [68] A. Byun, M. Kim and J. Ahn, *Finding the maximum independent sets of Platonic graphs using Rydberg atoms*, PRX Quantum **3**(3), 030305 (2022), doi:[10.1103/prxquantum.3.030305](https://doi.org/10.1103/prxquantum.3.030305).
- [69] M. Kim, K. Kim, J. Hwang, E.-G. Moon and J. Ahn, *Rydberg quantum wires for maximum independent set problems*, Nature Physics **18**(7), 755 (2022), doi:[10.1038/s41567-022-01629-5](https://doi.org/10.1038/s41567-022-01629-5).
- [70] S. Ebadi, A. Keesling, M. Cain, T. T. Wang, H. Levine, D. Bluvstein, G. Semeghini, A. Omran, J.-G. Liu, R. Samajdar, X.-Z. Luo, B. Nash *et al.*, *Quantum optimization of maximum independent set using Rydberg atom arrays*, Science **376**(6598), 1209 (2022), doi:[10.1126/science.abo6587](https://doi.org/10.1126/science.abo6587).
- [71] C. Dalyac, L.-P. Henry, M. Kim, J. Ahn and L. Henriët, *Exploring the impact of graph locality for the resolution of MIS with neutral atom devices*, arXiv (2023), doi:[10.48550/arXiv.2306.13373](https://doi.org/10.48550/arXiv.2306.13373).
- [72] S. Jeong, M. Kim, M. Hhan, J. Park and J. Ahn, *Quantum programming of the satisfiability problem with Rydberg atom graphs*, Physical Review Research **5**(4), 043037 (2023), doi:[10.1103/PhysRevResearch.5.043037](https://doi.org/10.1103/PhysRevResearch.5.043037).
- [73] A. Byun, J. Jung, K. Kim, M. Kim, S. Jeong, H. Jeong and J. Ahn, *Rydberg-atom graphs for quadratic unconstrained binary optimization problems*, Advanced Quantum Technologies **7**(8) (2024), doi:[10.1002/qute.202300398](https://doi.org/10.1002/qute.202300398).
- [74] J. Park, S. Jeong, M. Kim, K. Kim, A. Byun, L. Vignoli, L.-P. Henry, L. Henriët and J. Ahn, *Rydberg-atom experiment for the integer factorization problem*, Physical Review Research **6**(2), 023241 (2024), doi:[10.1103/physrevresearch.6.023241](https://doi.org/10.1103/physrevresearch.6.023241).
- [75] P. Cazals, A. François, L. Henriët, L. Leclerc, M. Marin, Y. Naghmouchi, W. d. S. Coelho, F. Sikora, V. Vitale, R. Watrigant, M. W. Garzillo and C. Dalyac, *Identifying hard native instances for the maximum independent set problem on neutral atoms quantum processors*, arXiv (2025), doi:[10.48550/arXiv.2502.04291](https://doi.org/10.48550/arXiv.2502.04291).
- [76] A. G. de Oliveira, E. Diamond-Hitchcock, D. M. Walker, M. T. Wells-Pestell, G. Pelegrí, C. J. Picken, G. P. A. Malcolm, A. J. Daley, J. Bass and J. D. Pritchard, *Demonstration of weighted-graph optimization on a Rydberg-atom array using local light shifts*, PRX Quantum **6**(1), 010301 (2025), doi:[10.1103/PRXQuantum.6.010301](https://doi.org/10.1103/PRXQuantum.6.010301).
- [77] R. Menta, F. Cioni, R. Aiudi, M. Polini and V. Giovannetti, *Globally driven superconducting quantum computing architecture*, Physical Review Research **7**(1), 1012065 (2025), doi:[10.1103/PhysRevResearch.7.L012065](https://doi.org/10.1103/PhysRevResearch.7.L012065).
- [78] J. Heckötter, V. Walther, S. Scheel, M. Bayer, T. Pohl and M. Aßmann, *Asymmetric Rydberg blockade of giant excitons in Cuprous Oxide*, Nature Communications **12**(1) (2021), doi:[10.1038/s41467-021-23852-z](https://doi.org/10.1038/s41467-021-23852-z).
- [79] J. Wurtz, P. L. S. Lopes, N. Gemelke, A. Keesling and S. Wang, *Industry applications of neutral-atom quantum computing solving independent set problems*, arXiv (2022), doi:[10.48550/arxiv.2205.08500](https://doi.org/10.48550/arxiv.2205.08500).
- [80] M.-T. Nguyen, J.-G. Liu, J. Wurtz, M. D. Lukin, S.-T. Wang and H. Pichler, *Quantum optimization with arbitrary connectivity using Rydberg atom arrays*, PRX Quantum **4**, 010316 (2023), doi:[10.1103/PRXQuantum.4.010316](https://doi.org/10.1103/PRXQuantum.4.010316).
- [81] S. Stastny, H. P. Büchler and N. Lang, *Functional completeness of planar Rydberg blockade structures*, Physical Review B **108**(8), 085138 (2023), doi:[10.1103/physrevb.108.085138](https://doi.org/10.1103/physrevb.108.085138).
- [82] M. Lanthaler, C. Dłaska, K. Ender and W. Lechner, *Rydberg-blockade-based parity quantum optimization*, Phys. Rev. Lett. **130**, 220601 (2023), doi:[10.1103/PhysRevLett.130.220601](https://doi.org/10.1103/PhysRevLett.130.220601).
- [83] I. Lesanovsky, *Many-body spin interactions and the ground state of a dense Rydberg lattice gas*, Physical Review Letters **106**(2), 025301 (2011), doi:[10.1103/physrevlett.106.025301](https://doi.org/10.1103/physrevlett.106.025301).
- [84] R. M. Karp, *Reducibility Among Combinatorial Problems*, pp. 219–241, Springer Berlin Heidelberg, ISBN 9783540682790, doi:[10.1007/978-3-540-68279-0\\_8](https://doi.org/10.1007/978-3-540-68279-0_8) (2009).
- [85] B. N. Clark, C. J. Colbourn and D. S. Johnson, *Unit disk graphs*, Discrete Mathematics **86**(1-3), 165 (1990), doi:[10.1016/0012-365x\(90\)90358-o](https://doi.org/10.1016/0012-365x(90)90358-o).
- [86] M. F. Serret, B. Marchand and T. Ayrál, *Solving optimization problems with Rydberg analog quantum computers: Realistic requirements for quantum advantage using noisy simulation and classical benchmarks*, Physical Review A **102**(5), 052617 (2020), doi:[10.1103/PhysRevA.102.052617](https://doi.org/10.1103/PhysRevA.102.052617).
- [87] C. Dłaska, K. Ender, G. B. Mbeng, A. Kruckenhauser, W. Lechner and R. van Bijnen, *Quantum optimization via four-body Rydberg gates*, Physical Review Letters **128**(12), 120503 (2022), doi:[10.1103/physrevlett.128.120503](https://doi.org/10.1103/physrevlett.128.120503).
- [88] In theoretical computer science, a (formal) language  $L$  is any subset  $L \subseteq \Sigma^*$  of finite strings constructed from some set of characters  $\Sigma$  called an *alphabet*; the elements of a formal language are called *words*.  $\Sigma^*$  is called the *Kleene closure* and denotes the set of all finite strings of characters in  $\Sigma$ . In our case  $\Sigma = \{0, 1\}$  and  $\Sigma^*$  denotes the set of all finite bit strings. Note that  $\mathbb{Z}_2^N \subset \Sigma^*$  is the set of bit strings of uniform length  $N$ .
- [89] T. Albash and D. A. Lidar, *Adiabatic quantum computation*, Reviews of Modern Physics **90**(1), 015002 (2018), doi:[10.1103/revmodphys.90.015002](https://doi.org/10.1103/revmodphys.90.015002).
- [90] D. S. Rokhsar and S. A. Kivelson, *Superconductivity and the quantum hard-core dimer gas*, Physical Review Letters **61**(20), 2376 (1988), doi:[10.1103/physrevlett.61.2376](https://doi.org/10.1103/physrevlett.61.2376).
- [91] H. M. Sheffer, *A set of five independent postulates for Boolean algebras, with application to logical constants*, Transactions of the American Mathematical Society **14**(4), 481 (1913), doi:[10.1090/s0002-9947-1913-1500960-1](https://doi.org/10.1090/s0002-9947-1913-1500960-1).
- [92] W. Wernick, *Complete sets of logical functions*, Transactions of the American Mathematical Society **51**(0), 117 (1942), doi:[10.1090/s0002-9947-1942-0005281-2](https://doi.org/10.1090/s0002-9947-1942-0005281-2).
- [93] To generate all possible blockade graphs, we used the tool **geng** which is a part of the package **nauty**. To compute the automorphism groups, we also utilized the package **nauty** [130].
- [94] G. Giudici, M. D. Lukin and H. Pichler, *Dynamical preparation of quantum spin liquids in Rydberg atom*

- arrays, *Physical Review Letters* **129**(9), 090401 (2022), doi:[10.1103/physrevlett.129.090401](https://doi.org/10.1103/physrevlett.129.090401).
- [95] R. Sahay, A. Vishwanath and R. Verresen, *Quantum spin puddles and lakes: NISQ-era spin liquids from non-equilibrium dynamics*, arXiv (2022), doi:[10.48550/arxiv.2211.01381](https://doi.org/10.48550/arxiv.2211.01381).
- [96] M. J. O'Rourke and G. K.-L. Chan, *Entanglement in the quantum phases of an unfrustrated Rydberg atom array*, *Nature Communications* **14**(1) (2023), doi:[10.1038/s41467-023-41166-0](https://doi.org/10.1038/s41467-023-41166-0).
- [97] A. Kitaev, *Anyons in an exactly solved model and beyond*, *Annals of Physics* **321**(1), 2 (2006), doi:[10.1016/j.aop.2005.10.005](https://doi.org/10.1016/j.aop.2005.10.005).
- [98] S. B. Bravyi and A. Y. Kitaev, *Quantum codes on a lattice with boundary*, arXiv (1998), doi:[10.48550/arxiv.quant-ph/9811052](https://doi.org/10.48550/arxiv.quant-ph/9811052).
- [99] X. Chen, Z.-C. Gu and X.-G. Wen, *Local unitary transformation, long-range quantum entanglement, wave function renormalization, and topological order*, *Physical Review B* **82**(15), 155138 (2010), doi:[10.1103/physrevb.82.155138](https://doi.org/10.1103/physrevb.82.155138).
- [100] R. Acharya, D. A. Abanin, L. Aghababae-Beni, I. Aleiner, T. I. Andersen, M. Ansmann, F. Arute, K. Arya, A. Asfaw, N. Astrakhantsev, J. Atalaya, R. Babush *et al.*, *Quantum error correction below the surface code threshold*, *Nature* **638**(8052), 920 (2024), doi:[10.1038/s41586-024-08449-y](https://doi.org/10.1038/s41586-024-08449-y).
- [101] A. Kitaev and J. Preskill, *Topological entanglement entropy*, *Physical Review Letters* **96**, 110404 (2006), doi:[10.1103/physrevlett.96.110404](https://doi.org/10.1103/physrevlett.96.110404).
- [102] M. Levin and X.-G. Wen, *Detecting topological order in a ground state wave function*, *Physical Review Letters* **96**, 110405 (2006), doi:[10.1103/physrevlett.96.110405](https://doi.org/10.1103/physrevlett.96.110405).
- [103] D. J. Williamson, A. Dua and M. Cheng, *Spurious topological entanglement entropy from subsystem symmetries*, *Physical Review Letters* **122**(14), 140506 (2019), doi:[10.1103/physrevlett.122.140506](https://doi.org/10.1103/physrevlett.122.140506).
- [104] I. H. Kim, M. Levin, T.-C. Lin, D. Ranard and B. Shi, *Universal lower bound on topological entanglement entropy*, *Physical Review Letters* **131**(16), 166601 (2023), doi:[10.1103/physrevlett.131.166601](https://doi.org/10.1103/physrevlett.131.166601).
- [105] X.-G. Wen, *Quantum field theory of many-body systems*, Oxford graduate texts. Oxford University Press, Oxford [u.a.], repr edn., ISBN 9780199227259 (2010).
- [106] S. Sachdev, *Quantum phase transitions*, Cambridge University Press, Cambridge, second edition, 5th printing edn., ISBN 0521514681 (2015).
- [107] T. Maier, *Quantum many-body phases with gauge constraints*, Bachelor Thesis, University of Stuttgart (2023).
- [108] J. Hauschild, J. Unfried, S. Anand, B. Andrews, M. Bintz, U. Borla, S. Divic, M. Drescher, J. Geiger, M. Hefel, K. Hémerly, W. Kadow *et al.*, *Tensor network Python (TeNPy) version 1*, *SciPost Phys. Codebases* p. 41 (2024), doi:[10.21468/SciPostPhysCodeb.41](https://doi.org/10.21468/SciPostPhysCodeb.41).
- [109] R. Diestel, *Graph Theory*, Springer Berlin Heidelberg, ISBN 9783662701072, doi:[10.1007/978-3-662-70107-2](https://doi.org/10.1007/978-3-662-70107-2) (2025).
- [110] H. Brey and D. G. Kirkpatrick, *Unit disk graph recognition is NP-hard*, *Computational Geometry* **9**(1-2), 3 (1998), doi:[10.1016/s0925-7721\(97\)00014-x](https://doi.org/10.1016/s0925-7721(97)00014-x).
- [111] F. Kuhn, T. Moscibroda and R. Wattenhofer, *Unit disk graph approximation*, In *Proceedings of the 2004 joint workshop on Foundations of mobile computing - DIALM-POMC '04*. ACM Press, doi:[10.1145/1022630.1022634](https://doi.org/10.1145/1022630.1022634) (2004).
- [112] C. McDiarmid and T. Müller, *Integer realizations of disk and segment graphs*, *Journal of Combinatorial Theory, Series B* **103**(1), 114 (2013), doi:[10.1016/j.jctb.2012.09.004](https://doi.org/10.1016/j.jctb.2012.09.004).
- [113] S. Bravyi, M. B. Hastings and S. Michalakis, *Topological quantum order: Stability under local perturbations*, *Journal of Mathematical Physics* **51**(9) (2010), doi:[10.1063/1.3490195](https://doi.org/10.1063/1.3490195).
- [114] S. Michalakis and J. P. Zwolak, *Stability of frustration-free Hamiltonians*, *Communications in Mathematical Physics* **322**(2), 277 (2013), doi:[10.1007/s00220-013-1762-6](https://doi.org/10.1007/s00220-013-1762-6).
- [115] S. Bravyi and M. B. Hastings, *A short proof of stability of topological order under local perturbations*, *Communications in Mathematical Physics* **307**(3), 609 (2011), doi:[10.1007/s00220-011-1346-2](https://doi.org/10.1007/s00220-011-1346-2).
- [116] E. Lieb, T. Schultz and D. Mattis, *Two soluble models of an antiferromagnetic chain*, *Annals of Physics* **16**(3), 407 (1961), doi:[10.1016/0003-4916\(61\)90115-4](https://doi.org/10.1016/0003-4916(61)90115-4).
- [117] T. S. Cubitt, D. Perez-Garcia and M. M. Wolf, *Undecidability of the spectral gap*, *Nature* **528**(7581), 207 (2015), doi:[10.1038/nature16059](https://doi.org/10.1038/nature16059).
- [118] M. J. Kastoryano and A. Lucia, *Divide and conquer method for proving gaps of frustration free Hamiltonians*, *Journal of Statistical Mechanics: Theory and Experiment* **2018**(3), 033105 (2018), doi:[10.1088/1742-5468/aaa793](https://doi.org/10.1088/1742-5468/aaa793).
- [119] S. Bravyi, D. P. DiVincenzo and D. Loss, *Schrieffer-Wolff transformation for quantum many-body systems*, *Annals of Physics* **326**(10), 2793 (2011), doi:[10.1016/j.aop.2011.06.004](https://doi.org/10.1016/j.aop.2011.06.004).
- [120] M. B. Hastings and T. Koma, *Spectral gap and exponential decay of correlations*, *Communications in Mathematical Physics* **265**(3), 781 (2006), doi:[10.1007/s00220-006-0030-4](https://doi.org/10.1007/s00220-006-0030-4).
- [121] C. Fernández-González, N. Schuch, M. M. Wolf, J. I. Cirac and D. Pérez-García, *Gapless Hamiltonians for the toric code using the projected entangled pair state formalism*, *Physical Review Letters* **109**(26), 260401 (2012), doi:[10.1103/physrevlett.109.260401](https://doi.org/10.1103/physrevlett.109.260401).
- [122] C. Fernández-González, N. Schuch, M. M. Wolf, J. I. Cirac and D. Pérez-García, *Frustration free gapless Hamiltonians for matrix product states*, *Communications in Mathematical Physics* **333**(1), 299 (2014), doi:[10.1007/s00220-014-2173-z](https://doi.org/10.1007/s00220-014-2173-z).
- [123] F. J. Wegner, *Duality in generalized Ising models and phase transitions without local order parameters*, *Journal of Mathematical Physics* **12**(10), 2259 (1971), doi:[10.1063/1.1665530](https://doi.org/10.1063/1.1665530).
- [124] E. Fradkin and L. Susskind, *Order and disorder in gauge systems and magnets*, *Physical Review D* **17**(10), 2637 (1978), doi:[10.1103/physrevd.17.2637](https://doi.org/10.1103/physrevd.17.2637).
- [125] E. Fradkin and S. H. Shenker, *Phase diagrams of lattice gauge theories with Higgs fields*, *Physical Review D* **19**(12), 3682 (1979), doi:[10.1103/physrevd.19.3682](https://doi.org/10.1103/physrevd.19.3682).
- [126] M. E. J. Newman and C. Moore, *Glassy dynamics and aging in an exactly solvable spin model*, *Physical Review E* **60**(5), 5068 (1999), doi:[10.1103/physreve.60.5068](https://doi.org/10.1103/physreve.60.5068).
- [127] T. Devakul, Y. You, F. J. Burnell and S. Sondhi, *Fractal symmetric phases of matter*, *SciPost Physics* **6**(1) (2019), doi:[10.21468/scipostphys.6.1.007](https://doi.org/10.21468/scipostphys.6.1.007).

- [128] K. Sfairopoulos and J. P. Garrahan, *The quantum Newman-Moore model in a longitudinal field*, arXiv (2024), doi:[10.48550/ARXIV.2409.09235](https://doi.org/10.48550/ARXIV.2409.09235).
- [129] I. Carusotto, A. A. Houck, A. J. Kollár, P. Roushan, D. I. Schuster and J. Simon, *Photonic materials in circuit quantum electrodynamics*, *Nature Physics* **16**(3), 268 (2020), doi:[10.1038/s41567-020-0815-y](https://doi.org/10.1038/s41567-020-0815-y).
- [130] B. D. McKay and A. Piperno, *Practical graph isomorphism, II*, *Journal of Symbolic Computation* **60**, 94 (2014), doi:[10.1016/j.jsc.2013.09.003](https://doi.org/10.1016/j.jsc.2013.09.003).
- [131] M. Saffman, T. G. Walker and K. Mølmer, *Quantum information with Rydberg atoms*, *Reviews of Modern Physics* **82**(3), 2313 (2010), doi:[10.1103/RevModPhys.82.2313](https://doi.org/10.1103/RevModPhys.82.2313).
- [132] T. Kato, *A Short Introduction to Perturbation Theory for Linear Operators*, Springer US, ISBN 9781461257004, doi:[10.1007/978-1-4612-5700-4](https://doi.org/10.1007/978-1-4612-5700-4) (1982).
- [133] R. K. Guy, *An olla-podrida of open problems, often oddly posed*, *The American Mathematical Monthly* **90**(3), 196 (1983), doi:[10.2307/2975549](https://doi.org/10.2307/2975549).
- [134] A. Hamma, R. Ionicioiu and P. Zanardi, *Ground state entanglement and geometric entropy in the Kitaev model*, *Physics Letters A* **337**(1–2), 22 (2005), doi:[10.1016/j.physleta.2005.01.060](https://doi.org/10.1016/j.physleta.2005.01.060).
- [135] N. Datta, J. Fröhlich, L. Rey-Bellet and R. Fernández, *Low-temperature phase diagrams of quantum lattice systems. II. Convergent perturbation expansions and stability in systems with infinite degeneracy*, *Helvetica Physica Acta* **69**(5), 752 (1996).

## Appendix A: Miscellaneous proofs & derivations

### 1. Automorphisms as symmetries of blockade Hamiltonians

As already defined in Definition 1, an automorphism  $\phi \in \mathcal{A}_C := \text{Aut}(G_C)$  acts on excitation patterns  $\mathbf{n} \in \mathbb{Z}_2^N$  via  $(\phi \cdot \mathbf{n})_i = n_{\phi(i)}$ . This induces a unitary representation on the full Hilbert space  $\mathcal{H}$  of the blockade structure,

$$U_\phi |\mathbf{n}\rangle := |\phi \cdot \mathbf{n}\rangle. \quad (\text{A1})$$

As  $\phi$  is bijective, it acts as a permutation of the configurations  $\mathbf{n} \in \mathbb{Z}_2^N$ . Thus the matrix representation of  $U_\phi$  in the basis  $|\mathbf{n}\rangle$  is a permutation matrix. In particular, this implies that  $U_\phi$  is unitary.

In the remainder of this section, we show that the operators  $U_\phi$  are symmetries of the blockade Hamiltonian (2). To this end, we first reformulate the problem in terms of the blockade graph  $G_C = (V, E, \Delta)$ , as introduced in Section II.

The natural measure of distance on a graph is the graph metric (cf. Appendix B1). In the following, we denote the distance of vertices  $i, j \in V$  with respect to the graph metric as  $d_{ij}$ . By construction, two vertices  $i, j \in V$  are in blockade iff  $(i, j) \in E$ , which is equivalent to  $d_{ij} = 1$ . Thus we can write the blockade potential in terms of the graph metric as

$$U(d) := \begin{cases} 0, & d > 1 \\ U_0, & d = 1. \end{cases} \quad (\text{A2})$$

In the limit  $U_0 \rightarrow \infty$  we recover the blockade potential as given in Eq. (1). However, it is mathematically more convenient to consider a finite but arbitrary large blockade strength  $U_0$ . Note that this does not change the classical degeneracy of the considered blockade structures if  $U_0$  is large enough. Thus, in the following we consider the generalized blockade Hamiltonian

$$H_C := \sum_{i < j} U(d_{ij}) n_i n_j + \sum_i (\Omega_i \sigma_i^x - \Delta_i n_i), \quad (\text{A3})$$

with  $U$  given by Eq. (A2). The remainder of this section is dedicated to the proof of the following proposition:

**Proposition 3.** *For any  $\phi \in \mathcal{A}_C$ , the generalized blockade Hamiltonian (A3) is invariant under  $U_\phi$ :  $U_\phi^\dagger H_C U_\phi = H_C$ .*

*Proof.* For this proof, we denote the operator  $\hat{n}_i$  with a hat to avoid confusion with its eigenvalues  $n_i$ . We compute the action of  $U_\phi^\dagger \hat{n}_i U_\phi$  and  $U_\phi^\dagger \sigma_i^x U_\phi$  on basis states  $|\mathbf{n}\rangle$ :

For  $\hat{n}_i$ , we obtain

$$U_\phi^\dagger \hat{n}_i U_\phi |\mathbf{n}\rangle = U_\phi^\dagger \hat{n}_i |\phi \cdot \mathbf{n}\rangle \quad (\text{A4a})$$

$$= U_\phi^\dagger (\phi \cdot \mathbf{n})_i |\phi \cdot \mathbf{n}\rangle \quad (\text{A4b})$$

$$= n_{\phi(i)} |\mathbf{n}\rangle \quad (\text{A4c})$$

$$= \hat{n}_{\phi(i)} |\mathbf{n}\rangle. \quad (\text{A4d})$$

The operators  $\sigma_i^x$  flip the state of one atom in an excitation pattern  $|\mathbf{n}\rangle$ . Thus  $\sigma_i^x$  also has a natural action on the excitation patterns

$$(\sigma_i^x \cdot \mathbf{n})_k := \begin{cases} n_k & k \neq i \\ 1 - n_i & k = i. \end{cases} \quad (\text{A5})$$

This is consistent with its usual operator definition, in the sense that  $\sigma_i^x |\mathbf{n}\rangle = |\sigma_i^x \cdot \mathbf{n}\rangle$ . We now show that  $\sigma_i^x \cdot (\phi \cdot \mathbf{n}) = \phi \cdot (\sigma_{\phi(i)} \cdot \mathbf{n})$ . To this end, consider the components of the left expression

$$(\sigma_i^x \cdot (\phi \cdot \mathbf{n}))_k = \begin{cases} (\phi \cdot \mathbf{n})_k & k \neq i \\ 1 - (\phi \cdot \mathbf{n})_i & k = i \end{cases} \quad (\text{A6a})$$

$$= \begin{cases} n_{\phi(k)} & k \neq i \\ 1 - n_{\phi(i)} & k = i. \end{cases} \quad (\text{A6b})$$

On the other hand, we obtain for the components of the right expression

$$(\phi \cdot (\sigma_{\phi(i)} \cdot \mathbf{n}))_k = (\sigma_{\phi(i)} \cdot \mathbf{n})_{\phi(k)} \quad (\text{A7a})$$

$$= \begin{cases} n_{\phi(k)} & \phi(k) \neq \phi(i) \\ 1 - n_{\phi(i)} & \phi(k) = \phi(i) \end{cases} \quad (\text{A7b})$$

$$= \begin{cases} n_{\phi(k)} & k \neq i \\ 1 - n_{\phi(i)} & k = i \end{cases} \quad (\text{A7c})$$

$$= (\sigma_i^x \cdot (\phi \cdot \mathbf{n}))_k. \quad (\text{A7d})$$

Here we used that  $\phi$  is a bijection, hence  $\phi(i) = \phi(k)$  is equivalent to  $i = k$ .

With this preparation, we obtain

$$\begin{aligned} \sigma_i^x U_\phi |\mathbf{n}\rangle &= |\sigma_i^x \cdot (\phi \cdot \mathbf{n})\rangle \\ &= |\phi \cdot (\sigma_{\phi(i)} \cdot \mathbf{n})\rangle = U_\phi \sigma_{\phi(i)}^x |\mathbf{n}\rangle. \end{aligned} \quad (\text{A8})$$

Since the states  $|\mathbf{n}\rangle$  constitute a basis of  $\mathcal{H}$ , it follows that  $U_\phi^\dagger \sigma_i^x U_\phi = \sigma_{\phi(i)}^x$ .

With these preliminary results, we calculate the action of  $U_\phi$  on the Hamiltonian  $H_C$ . We obtain:

$$U_\phi^\dagger H_C U_\phi = \sum_{i < j} U(d_{ij}) n_{\phi(i)} n_{\phi(j)} + \sum_i \left( \Omega \sigma_{\phi(i)}^x - \Delta_i n_{\phi(i)} \right) \quad (\text{A9a})$$

$$= \sum_{k < l} U(d_{\phi^{-1}(k)\phi^{-1}(l)}) n_k n_l + \sum_k \left( \Omega \sigma_k^x - \Delta_{\phi^{-1}(k)} n_k \right) \quad (\text{A9b})$$

$$= \sum_{k < l} U(d_{kl}) n_k n_l + \sum_k \left( \Omega \sigma_k^x - \Delta_k n_k \right) \quad (\text{A9c})$$

$$= H_C \quad (\text{A9d})$$

For the second equality, we reordered the summation, which is possible since  $\phi$  is a bijection. For the third equality, we used that  $\phi$  is an automorphism of the vertex-weighted blockade graph  $G_C$ , which implies  $\Delta_{\phi^{-1}(k)} = \Delta_k$  and  $d_{\phi^{-1}(k)\phi^{-1}(l)} = d_{kl}$ . ■

In most physical realizations of blockade structures, the blockade potential (1) is only an approximation of the true interaction. On the Rydberg platform, the true potential is a van der Waals interaction  $U(r) = C_6/r^6$  [131]. In this case, the Hamiltonian (2) cannot be solely encoded by a blockade graph. However, Proposition 3 can be readily generalized: As the van der Waals potential depends on the actual positions of the atoms, the automorphisms must be replaced by bijective maps on  $V$  that induce *isometries* on the set of atom positions, i.e.,  $|\mathbf{r}_i - \mathbf{r}_j| \stackrel{!}{=} |\mathbf{r}_{\phi(i)} - \mathbf{r}_{\phi(j)}|$ . It is then straightforward to check that with these modifications the proof for Proposition 3 still holds. In this case, the  $U_\phi$  are still symmetries of the Rydberg Hamiltonian, including van der Waals interactions.

## 2. Fully-symmetric blockade structures

Here we provide a detailed proof of Proposition 1. We prove the two parts of the proposition separately: First, we show that the ground state of the Hamiltonian  $H_C$  is unique, as this is independent of the symmetry. Second, we use the symmetries introduced in Appendix A 1 to show the equality of the coefficients  $\lambda_{\mathbf{n}}$ .

**Lemma 1.** *For  $\Omega \neq 0$ , the Hamiltonian  $H_C$  [Eq. (A3)] has a unique ground state  $|\Omega\rangle$ . This ground state can be expanded in the basis of excitation patterns as*

$$|\Omega\rangle = \sum_{\mathbf{n}} C_{\mathbf{n}}(\Omega) |\mathbf{n}\rangle \quad (\text{A10})$$

with coefficients that satisfy  $C_{\mathbf{n}}(\Omega) \neq 0$  for all  $\mathbf{n}$ .

For the proof of Lemma 1 we make use of a classical result from linear algebra, the *Perron-Frobenius theorem*; for reference see [132, chapter I.4]. We shortly summarize the contents of this theorem and its prerequisites:

To any matrix  $M \in \mathbb{R}^{n \times n}$  we can associate a *directed* graph  $G_M^d$ . Its vertex set is given by  $V_M := \{1, \dots, n\}$ ;

the edges of this graph are defined via  $(i, j) \in E_M$  iff  $M_{i,j} \neq 0$ . The matrix  $M$  is called *irreducible* if  $G_M^d$  is *strongly connected* (one can reach every vertex from every other vertex by following the *directed* edges of the graph). This directed graph can be turned into an undirected graph  $G_M^u$  by “forgetting” the directions of the edges. If  $M$  is symmetric, then  $G_M^d$  is strongly connected iff  $G_M^u$  is connected.

Next, a matrix  $M \in \mathbb{R}^{n \times n}$  is called *essentially nonnegative*, if it has nonnegative off-diagonal elements. For a matrix  $M \in \mathbb{R}^{n \times n}$ , its *spectral radius*  $\varrho(M)$  is defined as  $\varrho(M) := \max\{|\lambda| \mid \lambda \in \sigma(M)\} > 0$ . We denote the *spectrum* of  $M$  as  $\sigma(M)$  and the *eigenspace* of  $M$  associated to the eigenvalue  $\lambda \in \sigma(M)$  as  $\text{Eig}(M, \lambda)$ .

With these concepts, we can formulate the following theorem:

**Theorem 1** (Perron-Frobenius). *Let  $M \in \mathbb{R}^{n \times n}$  be a irreducible and essentially nonnegative matrix. Then ...*

1. *The spectral radius  $\varrho(M) > 0$  is an eigenvalue of  $M$ :  $\varrho(M) \in \sigma(M)$ .*
2. *The eigenspace associated to  $\varrho(M)$  is one-dimensional:  $\dim_{\mathbb{C}} \text{Eig}(M, \varrho(M)) = 1$ .*
3.  *$M$  has an eigenvector  $\mathbf{v} = (v_i)_{i=1}^n$  with eigenvalue  $\varrho(M)$  with only positive components:  $v_i > 0$ .*

We emphasize that the first claim is not trivial, even for finite-dimensional systems: It is obvious that there exists an eigenvalue  $\lambda$  with  $|\lambda| = \varrho(M)$ , but Theorem 1 also fixes its phase. In the following, we only apply this theorem to real and symmetric matrices. In this case, all eigenvalues of  $M$  are real, thus it is well-defined to say that  $\varrho(M)$  is the largest eigenvalue of  $M$ .

With these tools at hand, we prove Lemma 1:

*Proof.* First, we consider the case  $\Omega > 0$ . Note that Lemma 1 makes statements about the *ground state* of  $H_C$ , but Theorem 1 only makes claims about the eigenstate with the *largest* eigenvalue. Thus we want to apply Theorem 1 to the operator  $-H_C$  instead. However, for  $\Omega > 0$ , the off-diagonal elements  $\langle \mathbf{n} | (-H_C) | \mathbf{n}' \rangle$  are negative, so that the matrix is *not* essentially nonnegative. To fix this, we must first unitarily transform the operator  $-H_C$ :

To this end, define the transformation

$$Z := \prod_i \sigma_i^z, \quad (\text{A11})$$

where  $\sigma_i^z = |1\rangle\langle 1|_i - |0\rangle\langle 0|_i$  denotes the Pauli- $z$  matrix. As  $(\sigma_i^z)^2 = 1$  and  $\sigma_i^z \sigma_j^z = \sigma_j^z \sigma_i^z$  for  $i \neq j$ ,  $Z$  is an involution, i.e.,  $Z^2 = \mathbb{1}$ . The operators  $\sigma_i^z$  anticommute with  $\sigma_i^x$  and commute with  $\sigma_j^x$  for  $i \neq j$ . So we immediately obtain the identities

$$Z \sigma_i^x Z = -\sigma_i^x \quad \text{and} \quad Z n_i Z = n_i. \quad (\text{A12})$$

Now we can define the auxiliary operator

$$\tilde{H}_C := Z(-H_C)Z = -ZH_CZ \quad (\text{A13})$$

with the explicit form

$$\begin{aligned} \tilde{H}_C &= -Z \left( \sum_{k<l} U(d_{kl}) n_k n_l + \sum_k (\Omega \sigma_k^x - \Delta_k n_k) \right) Z \\ &= -\sum_{k<l} U(d_{kl}) n_k n_l + \sum_k (\Omega \sigma_k^x + \Delta_k n_k). \end{aligned} \quad (\text{A14})$$

Let  $h$  denote the matrix representation of this Hamiltonian in the basis of excitation patterns, i.e., the matrix elements are defined by  $h_{\mathbf{n}, \mathbf{n}'} := \langle \mathbf{n} | \tilde{H}_C | \mathbf{n}' \rangle$ . The off-diagonal elements ( $\mathbf{n} \neq \mathbf{n}'$ ) of this matrix are given by

$$h_{\mathbf{n}, \mathbf{n}'} = \begin{cases} \Omega & \text{if } \langle \mathbf{n} | \sum_k \sigma_k^x | \mathbf{n}' \rangle \neq 0 \\ 0 & \text{otherwise} \end{cases}. \quad (\text{A15})$$

Therefore  $h$  is *essentially nonnegative*.

To apply Theorem 1, we have to show in addition that  $h$  is *irreducible*. To this end, we show that  $\mathbf{n}$  is connected to  $\mathbf{0}$  in  $G_h^u$  for all  $\mathbf{n} \in \mathbb{Z}_2^N$ . Here,  $N$  denotes the number of atoms in  $\mathcal{C}$  and  $\mathbf{0} = (0, \dots, 0)$  is the configuration where no atom is excited. Eq. (A15) shows that  $h_{\mathbf{n}, \mathbf{n}'} > 0$  iff  $\mathbf{n}$  and  $\mathbf{n}'$  differ in exactly one component. Hence a path from  $\mathbf{n}$  to  $\mathbf{0}$  in  $G_h^u$  can be constructed by successively flipping all components in  $\mathbf{n}$  to 0. This implies that  $G_h^u$  is connected and establishes the irreducibility of  $h$ .

Finally, we can apply Theorem 1 to the matrix  $h$ . As spectral properties are independent of the chosen basis, the conclusions also hold for the auxiliary operator  $\tilde{H}_C$ . Furthermore, from  $\tilde{H}_C = -ZH_CZ$  and the invertibility of  $Z$ , it follows that  $\sigma(\tilde{H}_C) = -\sigma(H_C)$  and thus  $\max(\sigma(\tilde{H}_C)) = -\min(\sigma(H_C))$ . Via well-known facts about eigenspaces, we find that

$$\begin{aligned} &\text{Eig}(\tilde{H}_C, \max(\sigma(\tilde{H}_C))) \\ &= \text{Eig}(-ZH_CZ, -\min(\sigma(H_C))) \end{aligned} \quad (\text{A16a})$$

$$= \text{Eig}(ZH_CZ, \min(\sigma(H_C))) \quad (\text{A16b})$$

$$= Z \text{Eig}(H_C, \min(\sigma(H_C))). \quad (\text{A16c})$$

As  $Z$  is invertible, this implies in particular that

$$\begin{aligned} &\dim_{\mathbb{C}} \text{Eig}(H_C, \min(\sigma(H_C))) \\ &= \dim_{\mathbb{C}} \text{Eig}(\tilde{H}_C, \max(\sigma(\tilde{H}_C))) \stackrel{\text{Thm. 1}}{\underset{1. \& 2.}{\cong}} 1, \end{aligned} \quad (\text{A17})$$

i.e., the ground state of  $H_C$  is unique.

The third statement of Theorem 1 implies that any eigenvector  $|\tilde{\Omega}\rangle \in \text{Eig}(\tilde{H}_C, \max(\sigma(\tilde{H}_C)))$  has the form

$$|\tilde{\Omega}\rangle = e^{i\alpha} \sum_{\mathbf{n}} c_{\mathbf{n}} |\mathbf{n}\rangle, \quad (\text{A18})$$

where  $e^{i\alpha}$  is global phase and  $c_{\mathbf{n}} > 0$ ; in the following, we set  $e^{i\alpha} = 1$  without loss of generality.

By Eq. (A16c), the ground state  $|\Omega\rangle$  of  $H_C$  has then the form

$$|\Omega\rangle = Z |\tilde{\Omega}\rangle = \sum_{\mathbf{n}} c_{\mathbf{n}} Z |\mathbf{n}\rangle \quad (\text{A19a})$$

$$= \sum_{\mathbf{n}} (-1)^{\delta(\mathbf{n})} c_{\mathbf{n}} |\mathbf{n}\rangle, \quad (\text{A19b})$$

where we defined

$$\delta(\mathbf{n}) := \sum_i (1 - n_i) \quad (\text{A20})$$

as the number of atoms in  $\mathbf{n}$  that are not excited. This finally proves the claim of Lemma 1 for the case  $\Omega > 0$ .

For completeness, we also sketch the proof for  $\Omega < 0$ . In this case, the off-diagonal elements of  $\langle \mathbf{n} | (-H_C) | \mathbf{n}' \rangle$  are already positive; thus we can simply define  $\tilde{H}_C := -H_C$  as the auxiliary operator. The matrix representation of this operator is then irreducible and essentially nonnegative and we can apply Theorem 1. The remainder of the proof follows analogously with the substitution  $Z \mapsto 1$ .

We stress that this proof remains valid in the strict ‘‘PXP-limit’’ with  $U_0 = \infty$ , where the Hilbert space is restricted to the subspace of excitation patterns that do not violate blockades. ■

Now we prove the second part of Proposition 1, namely that all configurations in  $L_C$  enter with equal weight into the ground state:

*Proof.* From Lemma 1 we know that the ground state has the form

$$|\Omega\rangle = \sum_{\mathbf{n}} C_{\mathbf{n}}(\Omega) |\mathbf{n}\rangle, \quad (\text{A21})$$

where  $C_{\mathbf{n}}(\Omega) := (-1)^{\delta(\mathbf{n})} c_{\mathbf{n}} \neq 0$  (in the case  $\Omega > 0$ , for  $\Omega < 0$  one can replace  $\delta(\mathbf{n}) \mapsto 0$ ). By Proposition 3, the operators  $U_{\phi}$  commute with  $H_C$  and therefore leave the eigenspaces invariant; in particular the ground state manifold is invariant. As the ground state manifold is one-dimensional (again by Lemma 1), and the representation of  $U_{\phi}$  is unitary, the action of  $U_{\phi}$  on the ground state  $|\Omega\rangle$  must have the form

$$U_{\phi} |\Omega\rangle = e^{i\varphi(\phi)} |\Omega\rangle \quad (\text{A22})$$

and it follows

$$U_{\phi} |\Omega\rangle = \sum_{\mathbf{n}} e^{i\varphi(\phi)} C_{\mathbf{n}}(\Omega) |\mathbf{n}\rangle. \quad (\text{A23})$$

On the other hand, we obtain

$$U_\phi |\Omega\rangle = \sum_{\mathbf{n}} C_{\mathbf{n}}(\Omega) U_\phi |\mathbf{n}\rangle \quad (\text{A24a})$$

$$= \sum_{\mathbf{n}} C_{\mathbf{n}}(\Omega) |\phi \cdot \mathbf{n}\rangle \quad (\text{A24b})$$

$$= \sum_{\mathbf{n}} C_{\phi^{-1} \cdot \mathbf{n}}(\Omega) |\mathbf{n}\rangle. \quad (\text{A24c})$$

Comparing Eq. (A23) and Eq. (A24c) implies

$$e^{i\varphi(\phi)} C_{\mathbf{n}}(\Omega) = C_{\phi^{-1} \cdot \mathbf{n}}(\Omega). \quad (\text{A25})$$

Next we show that the phase must be equal to 1. As our Hamiltonian is real, all eigenvectors can be chosen to have real components, thus the only possibilities for the phases are  $e^{i\varphi(\phi)} = \pm 1$ . By the definition of the coefficients  $C_{\mathbf{n}}(\Omega)$ , Eq. (A25) becomes

$$e^{i\varphi(\phi)} (-1)^{\delta(\mathbf{n})} c_{\mathbf{n}} = (-1)^{\delta(\phi^{-1} \cdot \mathbf{n})} c_{\phi^{-1} \cdot \mathbf{n}}. \quad (\text{A26})$$

As  $\phi$  acts as a permutation of atoms, it preserves the number of excited atoms, hence  $\delta(\mathbf{n}) = \delta(\phi^{-1} \cdot \mathbf{n})$ . Thus we obtain

$$e^{i\varphi(\phi)} c_{\mathbf{n}} = c_{\phi^{-1} \cdot \mathbf{n}}. \quad (\text{A27})$$

(The same relation follows for  $\Omega < 0$  where  $\delta(\mathbf{n}) \equiv 0$ .) As the coefficients  $c_{\mathbf{n}}$  are real and positive, the only phase that satisfies this equation is  $e^{i\varphi(\phi)} = 1$  for all  $\phi$ . This shows that if two configurations  $\mathbf{n}, \mathbf{m}$  are part of the same orbit, i.e.,  $\mathbf{m} = \phi \cdot \mathbf{n}$  for some  $\phi \in \mathcal{A}_C$ , then it must be  $C_{\mathbf{n}}(\Omega) = C_{\mathbf{m}}(\Omega)$ .

So far this result holds for arbitrary blockade structures. Now we focus on the fully-symmetric case. For  $\mathbf{n} \in L_C$ , we introduced the nomenclature  $C_{\mathbf{n}}(\Omega) =: \lambda_{\mathbf{n}}(\Omega)$  in Eq. (3). If  $L_C$  is an orbit under the action of  $\mathcal{A}_C$ , then our results above imply that  $\lambda_{\mathbf{n}}(\Omega) = \lambda_{\mathbf{m}}(\Omega)$  for any  $\mathbf{n}, \mathbf{m} \in L_C$ ; that is,  $\lambda_{\mathbf{n}}(\Omega) \equiv \lambda(\Omega)$ , as claimed. ■

We want to note that these methods can also be applied to more general Hamiltonians. Here we briefly sketch some results in that regard:

First, consider the generalized fluctuation term  $\sum_i \Omega_i \sigma_i^x$  with site-dependent  $\Omega_i$ . If  $\Omega_{\phi(i)} = \Omega_i$ , then  $U_\phi$  remains a symmetry for this generalized Hamiltonian. Furthermore, the proof for the uniqueness of the ground state still goes through by choosing the modified transformation  $Z = \prod_{i: \Omega_i > 0} \sigma_i^z$ . It is then straightforward to check that Proposition 1 still holds.

Next, consider the generalized Hamiltonian  $H'_C$  with modified fluctuation term  $\sum_i \Omega_i \sigma_i^x$ , where  $\Omega_i = \pm \Omega$  (with  $\Omega > 0$ ). Define  $W := \prod_{i: \Omega_i < 0} \sigma_i^z$ , then  $WH'_C W$  is in the form of Eq. (A3) with  $\Omega_i \equiv \Omega > 0$ . If  $U_\phi$  is a symmetry of  $WH'_C W$  then  $WU_\phi W$  is a symmetry of  $H'_C$ . As discussed in the last paragraph, the uniqueness of the ground state still holds. Straightforward calculations show that the ground state of  $H'_C$  satisfies  $WU_\phi W |\Omega\rangle = |\Omega\rangle$  which leads to the presence of additional signs in the coefficients  $\lambda_{\mathbf{n}}$ .

It is also possible to add additional terms to the Hamiltonian (A3), as long as they do not break the symmetries and the uniqueness of the ground state. Since the latter is based on the construction of an essentially nonnegative auxiliary matrix (using transformations like  $Z$ ), we are not aware of any general criterion that characterized perturbations where this procedure works. An example for which the uniqueness remains in tact is a hopping term with  $t > 0$ :

$$H' := -t \sum_{\{i,j\} \in E} (\sigma_i^+ \sigma_j^- + \sigma_i^- \sigma_j^+). \quad (\text{A28})$$

It is clearly invariant under  $U_\phi$ . It also does not break the uniqueness proof, as irreducibility still holds and the auxiliary operator  $-ZH'Z$  has nonnegative matrix elements.

Finally, we want to mention that our proof for the uniqueness of the ground state never used any properties of the interaction potential  $U$ . As a consequence (with the modifications described in Appendix A1), Proposition 2 also applies to structures of Rydberg atoms where  $U$  is given by the van der Waals interaction.

### 3. Example: Blockade graph automorphisms not realized by geometric symmetries

Let  $G = (V, E)$  be a finite (simple) graph and  $\rho : V \rightarrow \mathbb{R}^d$  be a unit ball embedding in  $d$  dimensions, i.e. it is injective and  $\{i, j\} \in E$  iff  $d_2(\rho_i, \rho_j) \leq 1$ ; here  $d_2(\cdot, \cdot)$  denotes the Euclidean metric. Any automorphism  $\phi \in \text{Aut}(G)$  induces a map on  $\rho(V)$  by  $f_\phi : \rho(V) \rightarrow \rho(V)$ ,  $\rho_i \mapsto \rho_{\phi(i)}$ . The map  $f_\phi$  is a geometric symmetry of the (embedded) graph, if it is an isometry.

Now consider the complete graph with  $n$  vertices  $G = K_n$ , we set  $V = \{1, \dots, n\}$ . The automorphism group of this graph is  $\text{Aut}(K_n) = S_n$  where  $S_n$  denotes the symmetric group. For any two pairs of vertices  $\{i, j\}, \{k, l\} \in E$ , there exists an automorphism  $\sigma \in S_n$  such that  $\{i, j\} = \{\sigma(k), \sigma(l)\}$ . Suppose all graph automorphisms of  $K_n$  induce geometric symmetries, then it follows

$$d_2(\rho_i, \rho_j) = d_2(\rho_{\sigma(k)}, \rho_{\sigma(l)}) \quad (\text{A29a})$$

$$= d_2(f_\sigma(\rho_k), f_\sigma(\rho_l)) = d_2(\rho_k, \rho_l). \quad (\text{A29b})$$

Thus all points in  $\rho(V)$  have equal distance.

The maximum number of points that are pairwise equidistant is known as the *equilateral dimension*. It is a well-known fact [133] that the equilateral dimension of the Euclidean space  $\mathbb{R}^d$  is  $d + 1$ . Hence we must have  $n = |V| = |\rho(V)| \leq d + 1$  for a unit ball embedding of  $K_n$  that implements all automorphisms as geometric symmetries.

For example, the complete graph  $K_n$  can only be symmetrically unit disk embedded in  $d = 2$  if  $n \leq 3$ . In particular  $K_4$  cannot be embedded in  $\mathbb{R}^2$  such that all its automorphisms are realized by geometric symmetries.

This could be achieved in  $\mathbb{R}^3$  though, where all automorphisms can be realized as symmetries of the tetrahedron.

#### 4. Lower bound on the automorphism group size

Burnside's lemma yields a lower bound for the number of orbits in  $L_C$ :

$$\underbrace{|L_C / \mathcal{A}_C|}_{\text{Number of orbits}} \stackrel{\text{Burnside}}{=} \frac{1}{|\mathcal{A}_C|} \sum_{\phi \in \mathcal{A}_C} |L_C^\phi| \geq \frac{|L_C|}{|\mathcal{A}_C|} \quad (\text{A30})$$

where  $L_C^\phi$  denotes the set of elements in  $L_C$  that are invariant under  $\phi$  and we used that  $\mathbb{1} \in \mathcal{A}_C$  and  $L_C^\mathbb{1} = L_C$ . This implies in particular for a fully-symmetric structure:

$$1 \stackrel{!}{=} |L_C / \mathcal{A}_C| \Rightarrow |\mathcal{A}_C| \geq |L_C|. \quad (\text{A31})$$

### Appendix B: No-Go theorem for fully-symmetric tessellated blockade structures

Here we provide details on the proof of Proposition 2.

#### 1. Basic results from graph theory

In this section we introduce some terminology and nomenclature from graph theory, that we will need in the following sections, for reference see e.g. [109]. In the following we only consider finite simple graphs  $G = (V, E)$ , with vertex set  $V$  and edge set  $E$ . We denote edges as  $\{u, v\} \in E$  for vertices  $u, v \in V$ . If the edge set is clear then we also write  $u \sim v$  iff  $\{u, v\} \in E$ , in this case we say  $u$  and  $v$  are adjacent. The *degree* of a vertex  $v$  is defined as the number of vertices adjacent to  $v$ , it is denoted  $\deg(v)$ . For any subset  $W \subseteq V$ , its *induced subgraph* is defined as the graph with vertex set  $W$  and edge set  $E_W := \{\{u, v\} \in E \mid u, v \in W\}$ .

A *path* in  $G$  is an ordered list vertices  $\gamma = (v_0, \dots, v_n)$ , where  $v_0, \dots, v_n \in V$  and  $\{v_i, v_j\} \in E$  for all iff  $j = i \pm 1$ . We denote the length of this list as  $|\gamma|$ . The *graph metric*  $d_G(u, v)$  on  $G$  is defined as the length of the shortest path between the vertices  $u$  and  $v$  in  $G$  minus one, i.e.,

$$d_G(u, v) := \min\{|\gamma| - 1 \mid \text{paths } \gamma \text{ from } u \text{ to } v\}. \quad (\text{B1})$$

The graph metric allows to define the *k-neighborhood* of a vertex  $v \in V$  as

$$B_k(v) = \{v' \in V \mid d_G(v, v') \leq k\} \quad (\text{B2})$$

and the *k-sphere* as

$$\partial B_k(v) = \{v' \in V \mid d_G(v, v') = k\}. \quad (\text{B3})$$

A graph  $G$  is called *connected*, if there is a path between any two vertices in  $V$ . A maximal subset of  $V$  that

is connected, is called a *connected component*. A vertex  $v \in V$  is called a *cut-vertex*, if the induced subgraph of  $V \setminus \{v\}$  has more connected components than  $G$ .

The graph metric is invariant under automorphisms of  $G$ , i.e.,

$$d_G(v, w) = d_G(\phi(v), \phi(w)), \quad (\text{B4})$$

for  $u, v \in V$  and  $\phi \in \text{Aut}(G)$ . Thus also the *k-neighborhood* and the *k-sphere* are compatible with automorphisms in the sense that

$$\phi(B_k(v)) = B_k(\phi(v)). \quad (\text{B5})$$

and

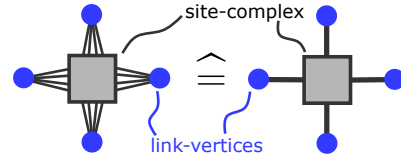
$$\phi(\partial B_k(v)) = \partial B_k(\phi(v)). \quad (\text{B6})$$

As a special case of Eq. (B6), the degree of a vertex is invariant under automorphisms, i.e.,  $\deg(v) = \deg(\phi(v))$  for  $v \in V$ .

Furthermore, let  $\gamma$  is a path from  $u$  to  $v$ . Then  $\phi(\gamma)$  is a path from  $\phi(u)$  to  $\phi(v)$ . This implies that, if  $S$  is a connected induced subgraph of  $G$ , then  $\phi(S)$  is also a connected induced subgraph of  $G$ . Thus, if  $v$  is a cut-vertex, then  $\phi(v)$  must also be a cut-vertex.

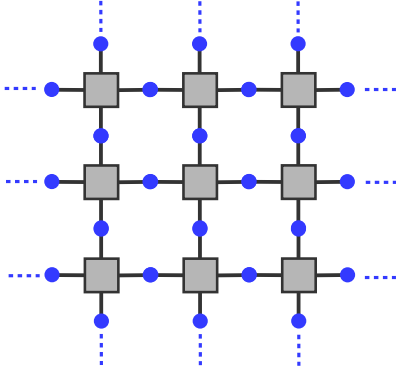
#### 2. Proof of the No-Go theorem

The setup of our No-Go theorem is the following. The building block of the tessellated graph  $G$  is an unknown *site-structure*, that is connected to four *link-vertices*. These link-vertices can be connected to an arbitrary number of vertices in the site-structures. For the sake of comprehensibility in the illustrations, we indicate these multiple edges by a single (thick) line, however it is important to keep in mind that a link-vertex can have multiple connections into the site-structure.



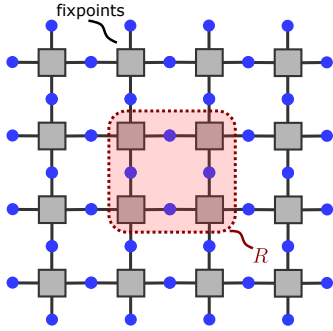
We refer to this graph as  $G_{\text{sing}}$ , furthermore we assume that it is connected. We refer to the graph metric on  $G_{\text{sing}}$  as  $d_{\text{sing}}(\cdot, \cdot)$ . The illustration may suggest, that the problem is highly symmetric. However, we do *not* assume any symmetries (rotation/reflections) of the site-structure, thus the illustrations have to be treated carefully.

The tessellated graph is then build by copying and translating  $G_{\text{sing}}$  and identifying the overlapping link-vertices.



We call a graph  $G$  that can be build in this way a *single-link tessellated graph*. We also consider periodic boundary conditions, here the link-vertices on opposing boundaries of the graph are identified. The main result of this section is the proof of the following theorem, which essentially states, that a single-link tessellated graph does not admit nontrivial local automorphisms.

**Theorem 2.** *Let  $G$  be a single-link tessellated graph together with a weight function  $\Delta$ , such that the link-vertices are interpreted as ports in the sense of Section III. Let  $\phi \in \text{Aut}(G)$ , such that any vertex outside of a rectangular region is fixed, e.g.*



Then  $\phi$  acts trivially on the maximum-weight independent sets of  $G$ .

As a first step, we argue, that we only have to consider the rectangular region and the link-vertices that are directly connected to it.

**Lemma 2.** *Let  $\tilde{V} \subseteq V$  be the vertex set that consists of the vertices in the rectangular region and the link-vertices connected to them. Let  $\tilde{G}$  be the induced subgraph of  $\tilde{V}$ . If all vertices outside of the rectangular region are fixed by an automorphism  $\phi \in \text{Aut}(G)$ , then we can restrict it to an automorphism on  $\tilde{G}$ , that we denote the same symbol. This automorphism fixes all link-vertices on the border of  $\tilde{G}$ .*

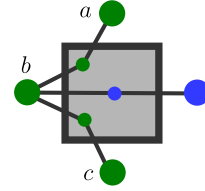
With this in mind, the idea for the proof of Theorem 2 is, to show that the topology of the graph implies that the link-vertices in  $\tilde{G}$ , that are closest to the boundary, are also fixed. To this end, we use the invariance of the graph metric under graph automorphisms. However

the relation between the graph metrics  $d_{\text{sing}}$  and  $d_{\tilde{G}}$  are a priori nontrivial. So the first step is to establish a connection.

The graph metric  $d_{\text{sing}}$  is the length of the shortest path between two link-vertices, sharing the same site-structure  $U$ , that is contained in this site-structure. Thus for a fixed sequence of link-vertices  $(v_1, \dots, v_n)$  for  $n \in \mathbb{N}$ , the length of the shortest path in  $\tilde{G}$ , that has crosses between two site-structures in exactly the vertices  $v_1, \dots, v_n$ , is given by

$$L((v_1, \dots, v_n)) := \sum_{i=1}^{n-1} d_{\text{sing}}(v_i, v_{i+1}). \quad (\text{B7})$$

This precise phrasing is actually crucial here, as the path may contain other link-vertices than  $v_1, \dots, v_n$ , if the path returns to the same site-structure it originated from. This case cannot be excluded, for example in the site-structure



the shortest path between the link-vertices  $a$  and  $c$  contains the link-vertex  $b$ . However, this is fully incorporated into the graph metric  $d_{\text{sing}}$ , so we do not have to keep track of link-vertices where the path does not cross between site-structures. This helps a lot with the notation. This makes the notation much more convenient.

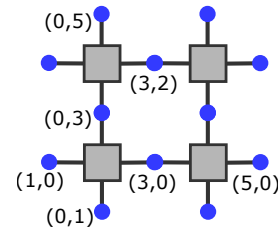
For the expression (B7) to be well-defined we can set  $d_{\text{sing}}(v_i, v_{i+1}) = \infty$ , if  $v_i$  and  $v_{i+1}$  do not share a site-structure. Consequently, for link-vertices  $v, w \in L$ ,  $d_{\tilde{G}}(v, w)$  is given by the minimum of  $L((v, v_1, \dots, v_n, w))$  over all sequences of link-vertices  $(v, v_1, \dots, v_n, w)$ .

We can exclude certain sequences, that cannot be minimal. If  $v_{i-1}, v_i$  and  $v_{i+1}$  all are part of one graph  $G_{\text{sing}}$ . Then by the triangle inequality we find

$$d_{\text{sing}}(v_{i-1}, v_i) + d_{\text{sing}}(v_i, v_{i+1}) \geq d_{\text{sing}}(v_{i-1}, v_{i+1}). \quad (\text{B8})$$

Thus to find the path of minimal length, it is sufficient to consider paths with the property that three successive vertices cannot belong to the same graph  $G_{\text{sing}}$ . Furthermore the only path where two successive link-vertices are part of one graph  $G_{\text{sing}}$  have finite length. We will refer to such paths as *candidate-paths*.

To formalize arguments about the path of minimal length, we introduce a labeling of the link-vertices by tuples  $(n_x, n_y) \in \mathbb{Z}^2$  where  $n_x$  and  $n_y$  have different parity.

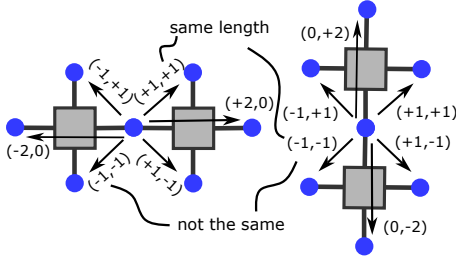


A sequence of link-vertices is now represented as a sequence of tuples  $((n_x^{(i)}, n_y^{(i)})_{i=1}^n$ . We denote the difference of two successive tuples as  $(\delta_x^{(i)}, \delta_y^{(i)}) := (n_x^{(i+1)}, n_y^{(i+1)}) - (n_x^{(i)}, n_y^{(i)})$ , we refer to such a tuple as a *move*. The sequence of labels can be reconstructed from the sequence of differences and the start point via

$$(n_x^{(n)}, n_y^{(n)}) = (n_x^{(1)}, n_y^{(1)}) + \sum_{i=1}^{n-1} (\delta_x^{(i)}, \delta_y^{(i)}). \quad (\text{B9})$$

Conversely, to construct a sequence from  $(n_x^{(1)}, n_y^{(1)})$  to  $(n_x^{(n)}, n_y^{(n)})$ , we have to find a sequence  $(\delta_x^{(i)}, \delta_y^{(i)})$ , such that Eq. (B9) holds.

However not any such sequence can be realized by an actual sequence of link-vertices. As discussed above, two successive link-vertices must share a site-structure directly connected to them. Thus the set of moves is restricted to  $(\pm 1, \pm 1)$  and depending on the parity of the vertex,  $(0, \pm 2)$  or  $(\pm 2, 0)$ . Also note, that the same move can represent different lengths, depending on the parity of the start vertex of the move. Likewise, if a move can be transferred into another move by revering its direction, the same length is associated to the two moves.



For candidate-paths, the restrictions translate directly to rules which moves can come in immediate succession.

previous move	parity	possible next move
(+1, -1)	(even, odd)	(+1, +1), (+1, -1), (+2, 0)
(+1, -1)	(odd, even)	(+1, -1), (-1, -1), (0, -2)
(+1, +1)	(even, odd)	(+1, +1), (+1, -1), (+2, 0)
(+1, +1)	(odd, even)	(-1, +1), (+1, +1), (0, +2)
(-1, +1)	(even, odd)	(-1, +1), (-1, -1), (-2, 0)
(-1, +1)	(odd, even)	(-1, +1), (+1, +1), (0, +2)
(-1, -1)	(even, odd)	(-1, +1), (-1, -1), (-2, 0)
(-1, -1)	(odd, even)	(+1, -1), (-1, -1), (0, -2)
(+2, 0)	-	(+1, +1), (+1, -1), (+2, 0)
(-2, 0)	-	(-1, +1), (-1, -1), (-2, 0)
(0, +2)	-	(-1, +1), (+1, +1), (0, +2)
(0, -2)	-	(+1, -1), (-1, -1), (0, -2)

Suppose we are given a sequence of moves that contains a move, that changes only one coordinate, e.g.,  $(0, +2)$ . Removing this move from the sequence creates another valid path, as this type of move does not change the possible next moves. By Eq. (B9) the endpoint of this reduced sequences is  $(n_x^{(n)}, n_y^{(n)}) - (\delta_x^{(i)}, \delta_y^{(i)})$ , where  $(n_x^{(n)}, n_y^{(n)})$

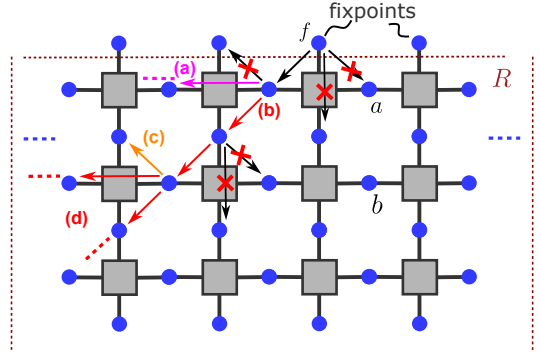


Figure 10. *Visualizations for Lemma 3.* Shown is the positioning of the vertices used in Lemma 3. The arrows indicate possible candidate-paths from  $f$  to  $b$ , we search for such a path that is shorter than all possible paths from  $f$  to  $a$ . Moves that can be immediately excluded are crossed out. (a) A path containing only moves  $(-2, 0)$  cannot reach the vertex  $b$ . (b) To reach  $b$  the path must contain  $(-1, -1)$ , the only allowed follow-up is  $(-1, -1)$ . (c) This path would contain three distinct diagonal move and thus can be excluded via the triangle inequality. (d) The only remaining path is a descent to the bottom left boundary. Thus this path can never reach  $b$ .

was the endpoint of the original sequence. As each move is associated with a strictly positive distance, the length path to the new endpoint is strictly less than the original path.

Equipped with these tools, we can prove the following lemma.

**Lemma 3.** *The distances of vertices  $f, a, b \in \tilde{G}$ , positioned as shown in Fig. 10, satisfy  $d_{\tilde{G}}(f, b) > d_{\tilde{G}}(f, a)$ .*

This may look trivial, but the possible asymmetry of the site-structures makes the proof rather technical. However, the gist is quiet simple to summarize: To go to the right one either has to go to the right or three times to the left. Both paths make the path from  $f$  to  $b$  longer than the path from  $f$  to  $a$ .

*Proof.* We show, that for any path from  $f$  to  $b$ , there is a path from  $f$  to  $a$  with strictly smaller length.

For a path from  $f$  to  $a$  the sum of the moves must equal  $(+1, -1)$ , for a path from  $f$  to  $b$  the sum of the moves must equal  $(+1, -3)$  (cf. Eq. (B9)). The difference between the vertices  $a$  and  $b$  is exactly  $(0, -2)$ . Consequently, if a path from  $f$  to  $b$  contains the move  $(0, -2)$ , it can be removed, which creates a path from  $f$  to  $a$ , with strictly smaller length (as discussed above).

In similar fashion, there is a path from  $f$  to  $a$  consisting of this singular move  $(+1, -1)$ . Thus if a path from  $f$  to  $b$  contains this move, then there is a path from  $f$  to  $a$  with strictly smaller length (i.e., the path consisting of only the move  $(+1, -1)$ ).

Thus, if there is a path from  $f$  to  $b$ , that is shorter than every path from  $f$  to  $a$  it, cannot contain the moves  $(0, -2)$  and  $(+1, -1)$ . So in the following we only have to consider paths that do not contain these moves.

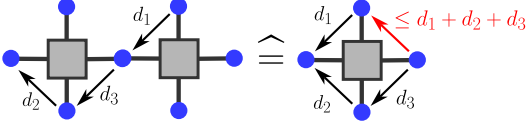
For any candidate-path from  $f$  to  $b$ , there are three possible moves from the start point, i.e.,  $(-1, -1)$ ,  $(+1, -1)$  and  $(0, -2)$ . As we already excluded the latter two moves, the only possibility is the move  $(-1, -1)$  (cf. Fig. 10). The vertex  $f$  is in a (even, odd) position, thus, as the first move is  $(-1, -1)$ , the next vertex in the candidate-path is in a (odd, even) position. Thus, the next possible moves are  $(-1, +1)$ ,  $(-1, -1)$ ,  $(-2, 0)$ .

The move  $(-1, +1)$  leads to a link-vertex, that is only connected to one site-structure, hence there are no possible further moves (as we are interested in candidate-paths, cf. Fig. 10).

The move  $(-2, 0)$  does not change the next possible moves. Moreover, repeating the move  $(-2, 0)$  over and over, the only decreases the  $x$ -component of the label and the path eventually hits the boundary on the left (cf. Fig. 10 (a)). Thus to reach the vertex  $b$ , the path must eventually include the move  $(-1, -1)$  (cf. Fig. 10 (b)).

After the move  $(-1, -1)$  the path is in an (even, odd) position, as was the vertex  $f$ . As discussed before, we only have to further examine paths where the next move is  $(-1, -1)$ . Then the new endpoint is in an (odd, even) position and the next possible moves are  $(-1, +1)$ ,  $(-1, -1)$ ,  $(-2, 0)$ .

Now the move  $(-1, +1)$  is available, however then the path contains tree different diagonal moves, i.e.,  $(-1, -1)$  starting from an (even, odd) and an (odd, even) position and  $(-1, +1)$ . Thus by the triangle inequality, this path has length strictly larger than then the length associated to  $(+1, -1)$ , a path from  $f$  to  $a$  (cf. Fig. 10 (c)).



However excluding the move  $(-1, +1)$ , the path can only contain the moves  $(-1, -1)$  and  $(0, -2)$  (if it is available), hence the  $x$ -component is only ever decreased along the path. Hence the path cannot reach  $b$  (cf. Fig. 10 (d)).

We remark, that this proof can easily be extended to all vertices in  $\tilde{G}$ , such that their label has a difference of  $(0, -2k)$ ,  $k \in \mathbb{N}$  from  $a$ . Furthermore, Lemma 3 also holds in the mirrored or rotated situation, as the argument are symmetric under rotations and reflections.

We proceed to prove the first main ingredient for Theorem 2.

**Lemma 4.** *Let  $f_1, f_2 \in \tilde{G}$  be two link-vertices at the boundary, attached to neighboring site-structures  $U_1, U_2$  and  $a \in \tilde{G}$  the link-vertex between  $U_1$  and  $U_2$  (cf. Fig. 11), then  $\phi(a) = a$ .*

*Proof.* We focus on one spacial orientation, as the argument is the same in all cases.

Let  $d_1 := d_{\tilde{G}}(f_1, a)$ , then  $B_{d_1}(f_1)$  cannot contain vertices right of the vertical through  $a$ , as shown in Fig. 11. Any path  $\gamma$  from  $f_1$  to the right of the vertical must

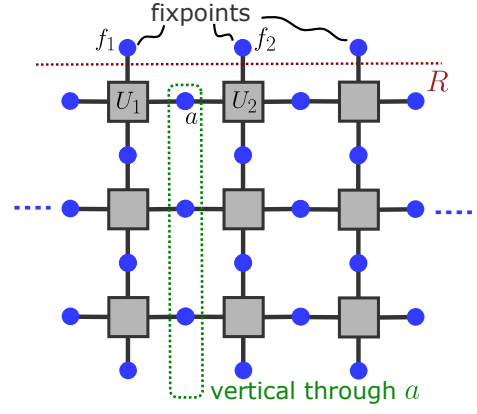


Figure 11. Visualizations for Lemma 4. Shown is the positioning of the vertices used in Lemma 4. In addition, the vertical of link-vertices through  $a$  is shown. For  $d_1 := d_{\tilde{G}}(f_1, a)$ , the set  $B_{d_1}(f_1)$  cannot contain vertices right of this vertical, analogous for  $d_2 := d_{\tilde{G}}(f_2, a)$ , the set  $B_{d_2}(f_2)$  cannot contain vertices left of this vertical.

contain one of the link-vertices on this vertical. Thus  $\gamma = (f_1, \dots, l, \dots, w)$ , where  $l$  is a link-vertex on the vertical and  $w$  is the final vertex. However by Lemma 3,

$$|(f_1, \dots, l)| - 1 \geq d_{\tilde{G}}(f_1, l) \geq d_{\tilde{G}}(f_1, a). \quad (\text{B10})$$

As the remaining part of the path contains at least one vertex  $|(\dots, w)| \geq 1$ , we find that  $|\gamma| - 1 > d_{\tilde{G}}(f_1, a)$ . As this is true for any path from  $a$  to  $w$ , we have that  $w \notin B_{d_1}(f_1)$ .

In addition, Lemma 3 shows that the only link-vertex on the vertical, that can be part of  $B_{d_1}(f_1)$ , is  $a$ .

As the argument is symmetric, we also know that  $B_{d_2}(f_2)$  cannot contain vertices left of the vertical through  $a$ , where  $d_2 = d_{\tilde{G}}(f_2, a)$ . Furthermore, the only vertex on the vertical that can be part of  $B_{d_2}(f_2)$  is  $a$ .

This shows that  $B_{d_1}(f_1) \cap B_{d_2}(f_2) = \{a\}$ . For the image under  $\phi$ , we find

$$\{\phi(a)\} = \phi(B_{d_1}(f_1)) \cap \phi(B_{d_2}(f_2)) \quad (\text{B11a})$$

$$= B_{d_1}(\phi(f_1)) \cap B_{d_2}(\phi(f_2)) \quad (\text{B11b})$$

$$= B_{d_1}(f_1) \cap B_{d_2}(f_2) = \{a\}. \quad (\text{B11c})$$

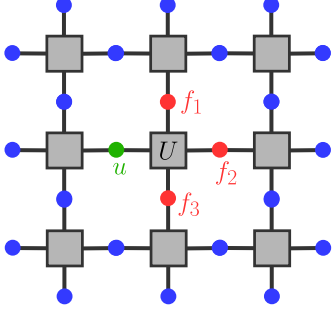
Hence  $\phi(a) = a$ .

Note, that for the setup shown in Fig. 11, despite the suggestive appearance, it is in principle impossible to find a similar bound for  $B_{d_1}(f_1)$  to the left side. The reason is, the site-structure can be arbitrarily asymmetric.

Repeated application of this lemma leads to site-structures with tree fixed link-vertices. To proceed we proof another lemma.

**Lemma 5.** *Let  $\phi \in \text{Aut}(G)$  and  $f_1, f_2, f_3, u$  be the link-vertices attached to some site-structure  $U \subseteq G$ . Suppose that three of the four link-vertices  $f_1, f_2, f_3$  are fixed by  $\phi$ . Further assume, that the graph does not end with  $u$  (i.e.,*

there is a site-structure different from  $U$  adjacent to  $u$ ) and that  $|U| < |U^C|$ . Then also the fourth link-vertex  $x$  is fixed and  $\phi(U) = U$ .



*Proof.* We remove  $f_1, f_2, f_3$  from the graph, to create the vertex set  $V'$  which induces the subgraph  $G'$ . Note, that this graph  $G'$  is still connected. Furthermore, by construction the vertex  $u$  is a cut-vertex in  $G'$ . Under removal of  $u$ ,  $G'$  decomposes in the connected components  $U$  and  $U^C := V \setminus U$ .

The restriction of  $\phi$  onto  $V'$  is a well-defined automorphism, that we denote with the same symbol. The vertex  $u$  being a cut-vertex in  $G'$ , implies that  $\phi(u)$  is also a cut-vertex in  $G'$  (cf. Appendix B 1). Thus the removal of  $\phi(u)$  splits  $G'$  into the components  $\phi(U)$  and  $\phi(U^C)$ .

Now we assume that  $\phi(u) \neq u$  and show that this leads to a contradiction.

- **Case 1:**  $\phi(u) \in U$ . We know,  $U^C \cup \{u\}$  is connected in  $G'$ . As  $\phi(u)$  does not lie in this component, its connectivity cannot be influenced by the removal of  $\phi(u)$ . So  $U^C \cup \{u\}$  must be part of *one* connected component, i.e., either  $U^C \cup \{u\} \subseteq \phi(U^C)$  or  $U^C \cup \{u\} \subseteq \phi(U)$ . As the set on the left is in both cases larger than the set on the right, this is a contradiction.
- **Case 2:**  $\phi(u) \in U^C$ . We know,  $U \cup \{u\}$  is connected in  $G'$ . As  $\phi(u)$  does not lie in this component, its connectivity cannot be influenced by the removal of  $\phi(u)$ . So  $U \cup \{u\}$  must be part of *one* connected component, i.e., either  $U \cup \{u\} \subseteq \phi(U^C)$  or  $U \cup \{u\} \subseteq \phi(U)$ . As  $|\phi(U)| = |U| < |U \cup \{u\}|$ , the only possibility is  $U \cup \{u\} \subseteq \phi(U^C)$ . Furthermore, this implies

$$\phi(U) = V' \setminus \phi(U^C) \subseteq U^C \setminus \{u\}. \quad (\text{B12})$$

- **Case 2.1:**  $\phi(u)$  is a link-vertex. As  $\phi(u) \neq u$ , none of the adjacent site-structures can be  $U$ , we denote these adjacent site-structures as  $U_1, U_2$ . Both of these site-structures remain connected if  $\phi(u)$  is removed, so both of them are subset of  $\phi(U)$  or  $\phi(U^C)$  respectively. They cannot both lie in the same component, as  $\phi(u)$  must be connected to both components and is only connected to  $U_1$  and  $U_2$ . Let *w.l.o.g.*  $U_1 \subseteq \phi(U)$ .

The site-structure  $U_1$  must have at least one link-vertex in  $G'$  other than  $\phi(u)$ . We denote this link-vertex as  $c$ . The reason for this is, that in  $G$  each site-structure has four link-vertices. We removed three link-vertices, which only share the site-structure  $U$ . Therefore, all other site-structures have at least three link-vertices left in  $G'$ .

By construction,  $U_1 \cup \{c\}$  is connected, thus also  $U_1 \cup \{c\} \subseteq \phi(U)$ . However the left side is larger than the right side as  $|U_1| = |U|$ . So we have reached a contradiction.

- **Case 2.2:**  $\phi(u)$  is not a link-vertex. Suppose that there is a link-vertex  $x \in \phi(U)$ , let  $U_1, U_2$  its adjacent unit cells. Let *w.l.o.g.*  $\phi(u) \in U_1$ , then as  $U_2 \cup \{x\}$  is connected, thus  $U_2 \cup \{x\} \subseteq \phi(U)$ . Which is a contradiction.

The only remaining possibility is, that no link-vertex is in  $\phi(U)$ . Let  $U'$  be the unit cell with  $\phi(u) \in U'$ . Then we have  $\phi(U) \subseteq U' \setminus \{\phi(u)\}$ , as connections to other unit cells would contain a link-vertex. However this is a contradiction, as the right side is smaller than the left side.

Therefore we have proven, that  $\phi(u) = u$ . This creates the connected components  $U$  and  $U^C$ . As we assume that  $|U| < |U^C|$  and  $\phi$  is bijective, the only possibility is  $\phi(U) = U$ . ■

By combining Lemma 4 and Lemma 5 we can "grow" the boundary be one site-structure to the inside. However, we cannot immediately repeat this procedure, as we only know that the link-vertices are fixed and not the site-structures. Moreover, we cannot prove this from our assumptions. If every site-structure would contain a disconnected NOT-gate, then there is a graph automorphism that exchanges the two atoms of the NOT-gate and leaves all other vertices invariant. To obtain a connected counterexample, connect the two vertices of the NOT-gate to one arbitrary vertex.

However in the end, we care about the maximum-weight independent sets of the graph. If we interpret the link-vertices as ports, then such an automorphism inside the site-structures cannot change the ports and thus the maximum-weight independent sets. So these single site-structure automorphisms "do not matter."

To formalize this idea, we prove that we can factorize the automorphism into a trivial part and a nontrivial part, where we can apply Lemma 4 and Lemma 5 again.

In the following we will not need to multiply two automorphisms, so we denote the composition by juxtaposition  $\phi_1 \phi_2 := \phi_1 \circ \phi_2$ . Likewise we use  $\coprod$  to denote the composition of multiple automorphisms.

**Lemma 6.** *If all link-vertices of a site-structure  $U$  are fixed by an automorphism  $\phi \in \text{Aut}(G)$ . Then  $\phi$  factors*

as

$$\phi = \phi_A \phi_B \quad (\text{B13})$$

with  $\phi_A, \phi_B \in \text{Aut}(G)$  and

$$\phi_A|_U = \text{id}_U \quad \phi_B|_{U^C} = \text{id}_{U^C}. \quad (\text{B14})$$

In particular, as  $\phi_A$  and  $\phi_B$  have disjoint support, they commute.

In addition, if  $\Delta$  is a weight function for  $G$  which is invariant under  $\phi$ , then it is also invariant under  $\phi_A$  and  $\phi_B$ .

*Proof.* We define the functions

$$\phi_A(v) := \begin{cases} \phi(v), & v \in U \\ v & v \notin U \end{cases} \quad (\text{B15a})$$

$$\phi_B(v) := \begin{cases} \phi(v), & v \notin U \\ v, & v \in U. \end{cases} \quad (\text{B15b})$$

By construction, these fulfill the desired requirements. Now we show, that  $\phi_A$  and  $\phi_B$  are indeed automorphisms. First note, that by Lemma 5 we have  $\phi(U) = U$ .

1. For injectivity the cases  $u, v \in U$  and  $u, v \notin U$  are clear. So let  $u \in U, v \in U^C$ . Therefore  $\phi_A(u) = \phi(u) \in U$  and  $\phi_A(v) = v \in U^C$ . Therefore  $\phi_A(u) \neq \phi_A(v)$ .
2. For surjectivity let  $u \in V$ . If  $u \in U^C$ , then  $\phi_A(u) = u$ . If  $u \in U$ , then the required preimage is  $u = \phi^{-1}(u) \in U$ .
3. For edge transitivity, let  $v, w \in V$ , such that  $\{v, w\} \in E$ . The cases  $u, v \in U$  and  $u, v \in U^C$  are clear. So let  $u \in U, v \in U^C$ . This implies, that  $v$  is one of the link-vertices of  $U$  and according to requirement  $\phi(v) = v\phi_A(v)$ . Therefore we have

$$\{\phi_A(u), \phi_A(v)\} = \{\phi(u), \phi(v)\} \in E. \quad (\text{B16})$$

This shows that  $\phi_A \in \text{Aut}(G)$ . The proof is analogous for  $\phi_B$ .

The addition follows directly from the fact, that  $\Delta$  is invariant under  $\phi$  and the identity. ■

Now we formalize the idea of growing the boundary to the inside.

**Lemma 7.** *Let  $G$  be a single-link tessellated graph and  $\phi \in \text{Aut}(G)$  an automorphism, that fixes every vertex outside of a rectangular region  $R$ . Then  $\phi$  factors as*

$$\phi = \prod_i \phi_{U_i}, \quad (\text{B17})$$

where the index  $i$  labels the site-structures in  $R$ , such that for the  $i$ -th site-structure  $U_i$ ,

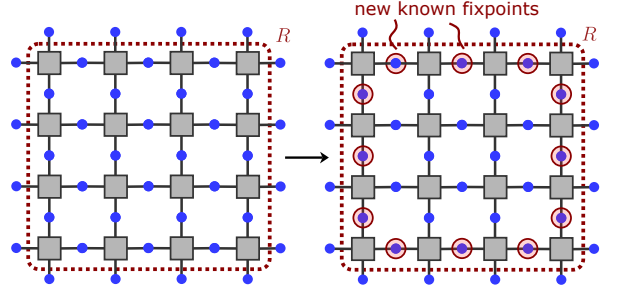
$$\phi_i|_{U_i^C} = \text{id}_{U_i^C}. \quad (\text{B18})$$

*Proof.* By Lemma 2 we can restrict  $\phi$  to an automorphism on the induced subgraph  $\tilde{G}$ , which has all vertices in  $R$  and the link-vertices directly connected to them as its vertex set. We denote this automorphism again by  $\phi$ . The link-vertices that form the boundary of  $\tilde{G}$  (i.e, link-vertices that are only connected to one site-structure) are by construction fixpoints of  $\phi$ . Let  $U_1, \dots, U_n$  be the site-structures that are directly connected to the link-vertices on the boundary of  $\tilde{G}$ .

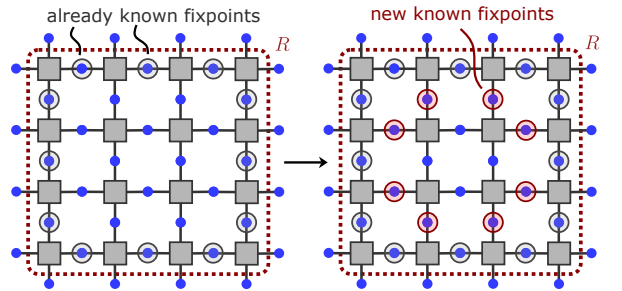
We demonstrate this result by mathematical Induction. If  $R$  contains no site-structure, then there is nothing to show. If  $R$  contains exactly one site-structure  $U_1$ , then  $\phi|_{U_1^C} = \text{id}_{U_1^C}$ , thus  $\phi$  is of the desired form.

For larger  $R$ , we proceed as follows.

1. We apply Lemma 4 repeatedly to the site-structures  $U_i$ , we find that the link-vertices between the site-structures  $U_i$  site-structures, are fixpoints of  $\phi$ .



2. Now, for the site-structures  $U_1, \dots, U_n$ , three link-vertices are known to be fixpoints. Then Lemma 5 implies that also the fourth link-vertex of these site-structures is a fixpoint.



3. We apply Lemma 6 successively to the site-structures  $U_1, \dots, U_n$ . For the first site-structure  $U_1$  we obtain the factorization

$$\phi = \phi_{U_1} \phi_1, \quad (\text{B19})$$

where  $\phi_{U_1}|_{U_1^C} = \text{id}_{U_1^C}$  and  $\phi_1|_{U_1} = \text{id}_{U_1}$ . As every vertex that is a fixpoint of  $\phi$  is also a fixpoint of  $\phi_1$ , we can apply Lemma 6 to  $\phi_1$  and the next site-structure  $U_2$  to obtain

$$\phi = \phi_{U_1} \phi_{U_2} \phi_2, \quad (\text{B20})$$

with the properties

$$\phi_{U_i}|_{U_i^c} = \text{id}_{U_i^c}, \phi_2|_{U_i} = \text{id}_{U_i} \quad (\text{B21})$$

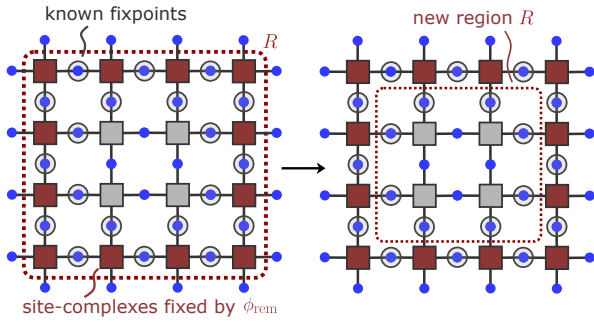
for  $i \in \{1, 2\}$ . Repeating this argument for all site-structures  $U_1, \dots, U_n$ , we obtain

$$\phi = \phi_{\text{rem}} \prod_{i=1}^n \phi_{U_i} \quad (\text{B22})$$

with

$$\phi_i|_{U_i^c} = \text{id}_{U_i^c}, \phi_{\text{rem}}|_{U_i} = \text{id}_{U_i}. \quad (\text{B23})$$

4. All site-structures  $U_1, \dots, U_n$  and their link-vertices are fixpoints of the automorphism  $\phi_{\text{rem}}$ . Thus the boundary of the rectangular region  $R$  can be advanced inwards by one site-structure.



Hence, by induction the automorphism  $\phi$  factorizes as desired. In particular, we have shown that  $\phi$  can only act trivially on the link-vertices. ■

We complete the proof of Theorem 2 by applying Lemma 7 to a vertex-weighted single-link tessellated graph.

**Corollary 1.** *Let  $\Delta$  be a weight function, that turns  $G$  into a vertex-weighted graph, such that the link-vertices are the ports of  $G$  in the sense of Section III. In addition let  $\phi \in \text{Aut}(G)$ , i.e.,  $\Delta$  is invariant under  $\phi$ , such that  $\phi|_R = \text{id}_R$  for some rectangular region  $R$ . Then  $\phi$  acts trivially on all maximum-weight independent sets  $I$ , i.e.,  $\phi(I) = I$ .*

*Proof.* The set  $\phi(I)$  is an independent set, as  $I$  itself is an independent set (cf. Appendix B1). As the weights  $\Delta$  are invariant under  $\phi$ ,  $\phi(I)$  is a maximum-weight independent set. However by Lemma 7,  $\phi(I)$  contains the same ports as  $I$ , hence  $\phi(I) = I$ . ■

## Appendix C: Automorphism groups of various tessellated structures

### 1. Verresen model

In this section we discuss the model proposed by Verresen *et al.* [33] to realize a  $\mathbb{Z}_2$  topological spin liquid by

Rydberg atoms placed on a Ruby lattice. In the PXP approximation, this arrangement can be interpreted as a blockade structure  $\mathcal{C}_{\text{VER}}$  with blockade graph  $G_{\text{VER}}$ , shown in Fig. 12. We explicitly characterize the automorphism group of this structure and show, that it is not fully-symmetric.

For each vertex  $v \in V_{\text{VER}}$ , there is exactly one induced subgraph  $S_v$ , such that  $v \in S_v$  and  $S_v \simeq C_6$ , where  $C_6$  denotes the cycle graph with six vertices. The existence is clear by inspection of the graph, one example is shown in Fig. 12 (a) as red vertices.

We will now argue that this cycle graph is unique for each vertex.  $v$ . It is clear, that we only have to consider vertices in  $B_6(v)$ , in Fig. 12 (b) such a neighborhood is shown. Furthermore we can disregard all vertices  $w \in B_6(v)$ , where  $B_1(w)$  is fully connected. Suppose that such a vertex  $w$  is part of an induced subgraph  $C_6$ . Then there are two adjacent vertices  $x_1, x_2 \in B_1(w)$ , such that  $x_1 \approx x_2$ . However, then  $B_1(w)$  cannot be fully connected. These deleted vertices are colored gray in Fig. 12 (b). In this step we assumed, that the graph is large enough, such that, all gray colored vertices are actually pendant vertices. The uniqueness of this cycle graph in the remaining vertices can now easily be seen, by systematically checking all remaining possibilities.

Now let  $\phi \in \text{Aut}(G_{\text{VER}})$ , and  $u, v \in V_{\text{VER}}$ . Then if  $\phi(u) = v$ , we know that  $\phi(S_u) = S_v$ . This leaves two possibilities, let  $u_1, u_2 \in S_u$  with  $u_1 \approx u_2$  and  $v_1, v_2 \in S_v$  with  $v_1 \approx v_2$ . The two possibilities are

$$\phi(u_1) = v_1, \phi(u_2) = v_2 \quad (\text{C1a})$$

$$\phi(u_1) = v_2, \phi(u_2) = v_1. \quad (\text{C1b})$$

In each case, Lemma 9 implies that the image of each vertex in  $S_u$  is uniquely determined.

From this information, the image of every vertex in  $V_{\text{VER}}$  can be determined, i.e., this information uniquely characterizes the automorphism. For two adjacent vertices  $u, v \in S_u$ , there is exactly one subset  $W_{u,v} \subseteq V_{\text{VER}}$ , such that the induced subgraph corresponding to this subset is isomorphic to the fully connected graph with four vertices denoted  $K_4$  (cf. Fig. 12 (c)). The image of  $W_{u,v}$  under an automorphism  $\phi \in \text{Aut}(G_{\text{VER}})$  must again be isomorphic to  $K_4$ .

If the images  $\phi(u), \phi(v)$  are known, then we know that  $W_{\phi(u), \phi(v)} = \phi(W_{u,v})$ . Thus, the remaining vertices in  $W_{u,v}$  are either invariant under  $\phi$  or get swapped. The structure of the graph  $G_{\text{VER}}$  (cf. Fig. 12 (c)) shows, that there is a vertex  $w_1 \in W_{u,v}$  such that

$$(B_1(u) \cap B_1(w_1)) \setminus W_{u,v} = \{a\} \text{ with } a \in V_{\text{VER}}. \quad (\text{C2})$$

For the remaining vertex  $w_2 \in W_{u,v}$ , we find that

$$(B_1(u) \cap B_1(w_2)) \setminus W_{u,v} = \{\}. \quad (\text{C3})$$

Thus, under the action of the automorphism  $\phi$  we obtain

$$(B_1(\phi(u)) \cap B_1(\phi(w_1))) \setminus W_{\phi(u), \phi(v)} = \{\phi(a)\} \quad (\text{C4a})$$

$$(B_1(\phi(u)) \cap B_1(\phi(w_2))) \setminus W_{\phi(u), \phi(v)} = \{\}. \quad (\text{C4b})$$

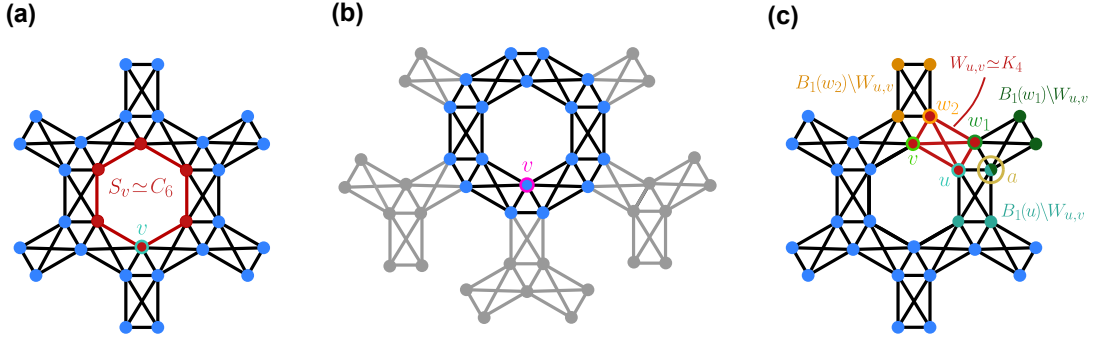


Figure 12. *Automorphisms of the Verresen model.* (a) Shown is one plaquette of the blockade graph  $G_{\text{VER}}$  that encodes the arrangement of Rydberg atoms proposed by Verresen *et al.* [33], to realize a  $\mathbb{Z}_2$  topological spin liquid. The induced subgraph formed by the red colored vertices is isomorphic to  $C_6$ . For each vertex  $v \in V_{\text{VER}}$  there exists exactly one set  $S_v$ , such that  $v \in S_v$  and its induced subgraph is isomorphic to  $C_6$ . (b) Shown is the neighborhood  $B_6(v)$  for some Vertex  $v \in V_{\text{VER}}$ . From this neighborhood, we remove every vertex  $w \in B_6(v)$ , such that  $\partial B_1(w)$  is fully connected. These removed vertices are colored in gray. The remaining vertices show, that  $S_v$  is indeed unique. (c) For any adjacent vertices  $u, v \in S_u$ , there exists exactly one set  $W_{u,v}$  (red colored vertices and edges) that contains  $u$  and  $v$  and its induces subgraph is isomorphic to  $K_4$ . The name of the vertices is indicated by the edge color of the red vertices. The remaining vertices  $w_1, w_2$  in  $W_{u,v}$  are uniquely characterized by the properties  $(B_1(u) \cap B_1(w_1)) \setminus W_{u,v} = \{a\}$  and  $(B_1(u) \cap B_1(w_2)) \setminus W_{u,v} = \{\}$ . The sets  $B_1(\cdot) \setminus W_{u,v}$  are shown in orange, dark green, dark cyan for vertices  $w_2, w_1$  and  $u$ . The overlap of the two sets is indicated by the split colored vertex, which is named  $a$ . This implies, that the images of  $w_1$  and  $w_2$  under an automorphism are uniquely determined by the images of  $u$  and  $v$ .

Therefore  $\phi(w_1)$  and  $\phi(w_2)$  can be uniquely identified in  $W_{\phi(u), \phi(v)}$ .

This argument can be repeated for every pair of adjacent vertices in the set  $S_x$  for some  $x \in V_{\text{VER}}$ , i.e., the automorphism is determined by its action on a single set  $S_u$  for some  $u \in V_{\text{VER}}$ . Hence the automorphism group consists of lattice translations, rotations and reflections.

We will now explicitly determine the size of this automorphism group. One unit cell of this tessellated graph contains 7 vertices, therefore the whole graph contains  $7N_x N_y$  vertices, where  $N_x, N_y$  the number of unit cells in  $x, y$  direction. We assume periodic boundary conditions. Choosing one reference vertex, there are  $7N_x N_y$  possible images. For each of these, two automorphisms are possible. Therefore we find  $|\text{Aut}(G_{\text{VER}})| = 14N_x N_y$ .

## 2. Zeng model

In Ref. [40], Zeng *et al.* introduced a blockade structure  $\mathcal{C}_{\text{ZQDM}}$  (they dubbed it Rydberg gadget), which realizes a quantum dimer model on a square lattice as its low-energy subspace  $\mathcal{H}_{\mathcal{C}_{\text{ZQDM}}}$ . In Fig. 13 (a), the blockade graph  $G_{\text{ZQDM}}$  of  $\mathcal{C}_{\text{ZQDM}}$  is shown. The structure has two different detunings  $\Delta_{\text{green}}$  and  $\Delta_{\text{blue}}$ , they correspond to the blue and green colored atoms respectively. The blue colored atoms are the ports of this structure, whereas the green colored ones are the ancillas (or gadget atoms). The only restriction on the detunings is that  $\Delta_{\text{green}} > \Delta_{\text{blue}}$ . We will see later, that automorphisms cannot map atoms of different colors into each other, so any automorphism leaves the detunings invariant, therefore we can safely ignore the detuning in the following argument. In this section, we rigorously

characterize the automorphism group of this blockade graph and show that  $\mathcal{C}_{\text{ZQDM}}$  is not fully-symmetric.

### a. Reduction of the blockade graph

As a first step to determining the automorphism group we construct a reduced graph with the same automorphism group, i.e, we eliminate vertices that do not contribute any degrees of freedom to the automorphism group.

First observe that the vertices of the Zeng blockade graph  $G_{\text{ZQDM}} = (V_{\text{ZQDM}}, E_{\text{ZQDM}})$  decompose into the two sets

$$M_1 := \{v \in V_{\text{ZQDM}} \mid \partial B_1(v) \text{ is connected}\} \quad (\text{C5a})$$

$$M_2 := \{v \in V_{\text{ZQDM}} \mid \partial B_1(v) \text{ is not connected}\}. \quad (\text{C5b})$$

The vertices in the set  $M_2$  coincide with the green colored vertices, the vertices in the set  $M_1$  coincide with the red colored vertices shown in Fig. 13. By construction of  $G_{\text{ZQDM}}$  the vertex set  $M_2$  decomposes into a disjoint union of connected components  $M_2 = \sqcup_k Q_k$ , the induced subgraph of each  $Q_k$  is isomorphic to  $K_4$ , the complete graph with 4 vertices. We now introduce an equivalence relation on  $G_{\text{ZQDM}}$ ,

$$v \equiv w := v = w \vee \exists k : v, w \in Q_k. \quad (\text{C6})$$

Symmetry and reflexivity of this relation are obvious. For transitivity consider  $v \equiv w$  and  $w \equiv u$ . If  $v = w$  or  $w = u$ , it is obvious that  $v \equiv u$ . In the remaining case, note that  $w$  is only part of exactly one  $Q_k$ . It follows that  $u, v \in Q_k$ , as desired.

This equivalence relation partitions the vertex set  $V_{\text{ZQDM}}$  into equivalence classes  $V_{\text{ZQDM}}^{\text{red}} = \{[v] \mid v \in V_{\text{ZQDM}}\}$ , where

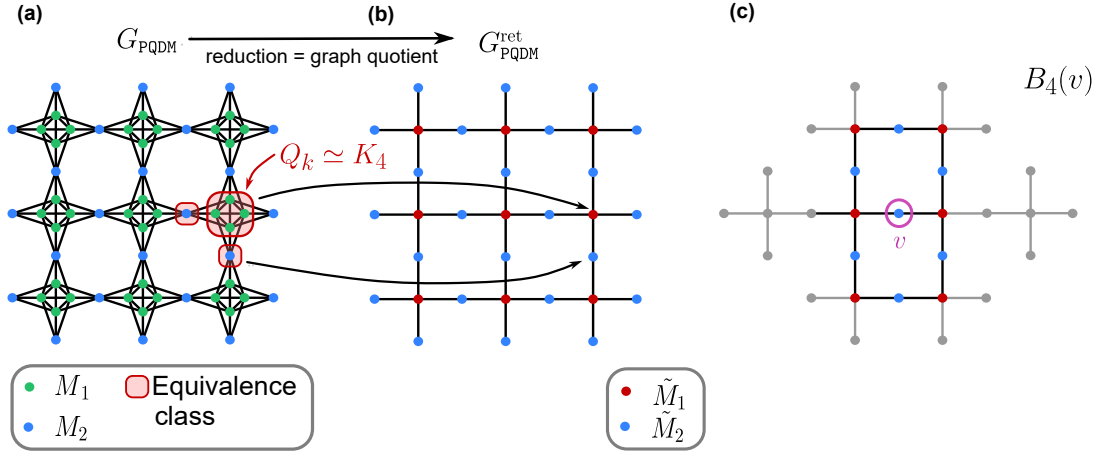


Figure 13. *Reduction of the Zeng model.* (a) Shown is the blockade graph  $G_{\text{PQDM}}$ , proposed by Zeng *et al.* to realize a quantum dimer model with a blockade structure. Vertices in the set  $M_1$  are colored green, those in the set  $M_2$  are colored blue. The set  $M_1$  decomposes into connected components  $Q_k$ , the induced subgraph of every such component is isomorphic to  $K_4$ . By an equivalence relation we identify the vertices that lie in the same component  $Q_k$ . Some of the equivalence classes are shown as red boxes. (b) Shown is the quotient graph of  $G_{\text{PQDM}}$  by the aforementioned equivalence relation, the resulting graph is denoted as  $G_{\text{PQDM}}^{\text{red}}$ . We prove in this section, that the automorphism group of both graphs has the same size. (c) Shown is the neighborhood  $B_4(v)$  of some vertex  $v \in M_2$ . From this neighborhood, all pendant vertices are removed. From the remaining graph, again, all pendant vertices are removed. This process is repeated, until no pendant vertices are left. The removed vertices are colored in gray. This shows, that there are exactly two sets  $S_1, S_2$  with  $v \in S_1, S_2$ , such that their induced subgraph is isomorphic to  $C_8$ .

$[v]$  denotes the equivalence class of  $v$ . We define the reduced graph as  $G_{\text{ZQDM}}^{\text{red}} = (V_{\text{ZQDM}}^{\text{red}}, E_{\text{ZQDM}}^{\text{red}})$  with the edge set,  $E_{\text{ZQDM}}^{\text{red}} = \{[v], [u] \mid \{u, v\} \in E_{\text{ZQDM}}\}$ . This construction is also known as a *quotient graph*. The resulting graph is shown in Fig. 13.

### b. Establishing a bijection

Now we show, that there is a bijection between the automorphism group of the reduced graph and the automorphism group of the original graph.

**Lemma 8.** For  $\phi \in \text{Aut}(G_{\text{ZQDM}})$ , define

$$\mathcal{F}_\phi : V_{\text{ZQDM}}^{\text{red}} \rightarrow V_{\text{ZQDM}}^{\text{red}}, [u] \mapsto [\phi(u)]. \quad (\text{C7})$$

Then the map  $\mathcal{F} : \text{Aut}(G_{\text{ZQDM}}) \rightarrow \text{Aut}(G_{\text{ZQDM}}^{\text{red}})$ ,  $\phi \mapsto \mathcal{F}_\phi$  is a bijection.

*Proof.* First we have to show that  $\mathcal{F}_\phi$  is well-defined. To this end let  $[u] = [v]$ . Then either  $u = v$  or  $u, v \in Q_k$ . Only the latter case is nontrivial. As  $\phi$  preserves connectedness and  $\phi(M_2) = M_2$ , the images of  $u$  and  $v$  lie in the same connected component, i.e.,  $\phi(u), \phi(v) \in Q_{k'}$  for some  $k'$ . This implies that  $[\phi(u)] = [\phi(v)]$ .

Second, we have to show that  $\mathcal{F}_\phi$  defines a graph automorphism. For bijectivity note, that the map  $\mathcal{F}_{\phi^{-1}}$  inverts the map  $\mathcal{F}_\phi$ . For edge transitivity, let  $\{[u], [v]\} \in E_{\text{ZQDM}}^{\text{red}}$ , so *w.l.o.g.* we can assume, that  $\{u, v\} \in E_{\text{ZQDM}}$ . This implies that  $\{\phi(u), \phi(v)\} \in E_{\text{ZQDM}}$ , hence

$$\{\tilde{\phi}([u]), \tilde{\phi}([v])\} = \{[\phi(u)], [\phi(v)]\} \in E_{\text{ZQDM}}^{\text{red}}. \quad (\text{C8})$$

Now we have to show the bijectivity of the map  $\mathcal{F}$ . To this end we will construct an inverse map  $\mathcal{G} : \text{Aut}(G_{\text{ZQDM}}^{\text{red}}) \rightarrow \text{Aut}(G_{\text{ZQDM}})$ , such that  $\mathcal{G}$  inverts  $\mathcal{F}$ .

The key ingredient in this construction is, that an automorphism  $\phi \in \text{Aut}(G_{\text{ZQDM}})$  is uniquely determined, when its action on the set  $M_2$  is known. Let  $u \in M_1$ , note from the structure of the graph, that there exists exactly three vertices  $v_1, v_2, v_3 \in M_2$ , such that

$$\bigcap_{i \in \{1,2,3\}} \partial B_1(v_i) = \{u\}. \quad (\text{C9})$$

The vertex  $u$  does not have any more adjacent vertices in  $M_2$ . The application of the automorphism  $\phi$  on C9 yields

$$\bigcap_{i \in \{1,2,3\}} \partial B_1(\phi(v_i)) = \{\phi(u)\}, \quad (\text{C10})$$

i.e.,  $\phi(u)$  is uniquely determined by the images  $\phi(v_i)$ .

Now let  $\Phi \in \text{Aut}(G_{\text{ZQDM}}^{\text{red}})$ , we shall construct an automorphism  $\mathcal{G}_\Phi \in \text{Aut}(G_{\text{ZQDM}})$ . The vertex set  $V_{\text{ZQDM}}^{\text{red}}$  decomposes into the components

$$\tilde{M}_1 := \{[v] \in V_{\text{ZQDM}}^{\text{red}} \mid \deg([v]) = 2\} \quad (\text{C11a})$$

$$\tilde{M}_2 := \{[v] \in V_{\text{ZQDM}}^{\text{red}} \mid \deg([v]) = 4\}. \quad (\text{C11b})$$

Here  $\deg(\cdot)$  denotes the *degree* of a vertex, i.e. the number of vertices it is connected to. As the degree is invariant under automorphisms, so are the sets  $\tilde{M}_1$  and  $\tilde{M}_2$ . From the construction of  $G_{\text{ZQDM}}^{\text{red}}$  we obtain a different characterization of these sets,

$$\tilde{m}_1 = \{[v] \in V_{\text{ZQDM}}^{\text{red}} \mid |[v]| = 4\} \quad (\text{C12a})$$

$$\tilde{m}_2 = \{[v] \in V_{\text{ZQDM}}^{\text{red}} \mid |[v]| = 1\}. \quad (\text{C12b})$$

Hence, for  $[v] \in \tilde{M}_2$ ,  $\mathcal{G}_\Phi([v])$  is an equivalence class with one element. For  $v \in M_2$ , we also know  $[v] = 1$ , therefore  $[v] \in \tilde{M}_2$  and hence  $\Phi([v])$  only contains one element. So we can define  $\mathcal{G}_\Phi(v)$  such that  $\Phi([v]) = \{\mathcal{G}_\Phi(v)\}$ . For  $u \in M_1$ , we can now define  $\mathcal{G}_\Phi(u)$  as the unique element in the intersection on the left side of Eq. (C10).

We have to show that the map  $\mathcal{G}_\Phi$  defined this way, actually is an automorphism. For edge transitivity, let  $\{v, v'\} \in E_{\text{ZQDM}}$ . The first case is *w.l.o.g.*  $v' \in M_1$  and  $v \in M_2$ . In this case,  $\mathcal{G}_\Phi(v')$  is defined such that  $\{\mathcal{G}_\Phi(v), \mathcal{G}_\Phi(v')\} \in E_{\text{ZQDM}}$ . The other case is  $v, v' \in M_1$ , here we know that  $v, v' \in Q_k$  for some  $k$  so they share two neighbors  $u_1, u_2 \in M_2$ . From the previous case it follows, that  $\mathcal{G}_\Phi(u_1)$  and  $\mathcal{G}_\Phi(u_2)$  are neighbors of both  $\mathcal{G}_\Phi(v)$  and  $\mathcal{G}_\Phi(v')$ . This is only possible, if  $\mathcal{G}_\Phi(v)$  and  $\mathcal{G}_\Phi(v')$  lie in the same connected component  $Q_{k'}$  for some  $k'$ . This implies  $\{\mathcal{G}_\Phi(v), \mathcal{G}_\Phi(v')\} \in E_{\text{ZQDM}}$ .

To show bijectivity we show that for  $\Phi \in \text{Aut}(G_{\text{ZQDM}}^{\text{red}})$ ,  $G_{\Phi^{-1}} = G_\Phi^{-1}$ . To this end consider for  $v \in M_2$

$$\{v\} = [v] = \Phi(\Phi^{-1}([v])) \quad (\text{C13a})$$

$$= \Phi(\{\mathcal{G}_{\Phi^{-1}}(v)\}) \quad (\text{C13b})$$

$$= \Phi([\mathcal{G}_{\Phi^{-1}}(v)]) \quad (\text{C13c})$$

$$= \{\mathcal{G}_\Phi(\mathcal{G}_{\Phi^{-1}}(v))\}, \quad (\text{C13d})$$

where we used that the equivalence classes of  $v$  and  $\mathcal{G}_{\Phi^{-1}}(v)$  only contain one element. As an automorphism in  $\text{Aut}(G_{\text{ZQDM}})$  is uniquely determined by its action on the set  $M_2$  and the action of  $\mathcal{G}_\Phi \circ \mathcal{G}_{\Phi^{-1}}$  on  $M_2$  is the identity, we infer that  $\mathcal{G}_\Phi \circ \mathcal{G}_{\Phi^{-1}}$  acts the identity on  $V_{\text{ZQDM}}$ . The proof for  $\mathcal{G}_{\Phi^{-1}} \circ \mathcal{G}_\Phi$  is analogous.

Now we will prove that  $\mathcal{G}$  is the inverse of  $\mathcal{F}$ . Let  $\phi \in \text{Aut}(G_{\text{ZQDM}})$ , for  $v \in M_2$  we obtain

$$\{\mathcal{G}(\mathcal{F}(\phi))(v)\} = \mathcal{F}(\phi)([v]) = [\phi(v)] = \{\phi(v)\}. \quad (\text{C14})$$

As this uniquely determines the automorphism,  $\phi = \mathcal{G}(\mathcal{F}(\phi))$ .

On the other hand, starting with an automorphism  $\Phi \in \text{Aut}(G_{\text{ZQDM}}^{\text{red}})$ , we obtain for  $v \in M_2$ ,

$$\mathcal{F}(\mathcal{G}(\Phi))([v]) = [\mathcal{G}(\Phi)(v)] = \Phi([v]). \quad (\text{C15})$$

This uniquely determines the action of  $\mathcal{F}(\mathcal{G}(\Phi))$ , because for any vertex  $[u] \in \tilde{M}_1$  we find two neighbors  $[v_1], [v_2] \in \tilde{M}_2$  such that

$$\partial B_1([v_1]) \cap \partial B_1([v_2]) = \{[u]\}. \quad (\text{C16})$$

Therefore, for any automorphism  $\Phi' \in \text{Aut}(G_{\text{ZQDM}}^{\text{red}})$ , we find

$$\partial B_1(\Phi'([v_1])) \cap \partial B_1(\Phi'([v_2])) = \{\Phi'([v])\}. \quad (\text{C17})$$

Therefore we conclude that  $\mathcal{F}(\mathcal{G}(\Phi)) = \Phi$ .  $\blacksquare$

### c. Characterization of the automorphism group

We will now characterize the automorphism group  $\text{Aut}(G_{\text{ZQDM}}^{\text{ret}})$ . Suppose we have a square lattice with periodic boundary conditions and side lengths  $N_x, N_y > 2$ .

As we will only deal with one graph in this section, we write  $u \sim v$  whenever  $\{u, v\} \in E_{\text{ZQDM}}^{\text{ret}}$ .

Pick any vertex  $v \in V_{\text{ZQDM}}^{\text{ret}}$  with degree 2. Then for this vertex there exist exactly two subsets  $S_1, S_2 \subset V_{\text{ZQDM}}^{\text{ret}}$  such that  $v \in S_1, S_2$  and the induced subgraph of  $S_1$  and  $S_2$  is isomorphic to the cycle graph  $C_8$ . To prove this, we note that a set  $S$  with these properties must be contained in the neighborhood  $B_4(v)$ . This neighborhood is shown in Fig. 13 (here we used the assumption  $N_x, N_y > 2$ ). Also  $S$  cannot contain any pendant vertices (i.e. vertices with only one neighbor) in  $B_4(v)$ , so we remove them. From the resulting set, we again remove all pendant vertices and repeat until we reach a set with no pendant vertices. These removed vertices are colored gray in Fig. 13. In the resulting graph it is clear, that there exist exactly two subsets with the desired property.

In the following argument, we make use of the next lemma.

**Lemma 9.** *Let  $G_1, G_2 \simeq C_k$  for some  $k \geq 3$ , and  $x_1, x_2 \in G_1$  such that  $x_1 \sim x_2$ . Then any graph isomorphism  $\phi : G_1 \rightarrow G_2$  is uniquely determined by  $\phi(x_1)$  and  $\phi(x_2)$ .*

*Proof.* We write  $G_1 = \{x_1, \dots, x_k\}$  and  $G_2 = \{y_1, \dots, y_k\}$ , such that for all  $l \leq k$ ,  $x_l \sim x_{l+1}$  and  $y_l \sim y_{l+1}$ , with the boundary condition  $k+1 = 0$ .

Suppose we already determined the images  $\phi(x_1), \dots, \phi(x_l)$  for  $l \geq 2$ . We know that  $x_{l-1} \sim x_l \sim x_{l+1}$ , therefore  $\phi(x_{l-1}) \sim \phi(x_l) \sim \phi(x_{l+1})$ . As  $G_2$  is a cycle graph, each vertex has exactly two neighbors. Therefore  $\phi(x_{l+1})$  is the unique neighbor of  $\phi(x_l)$ , that is not  $\phi(x_{l-1})$ . By induction, this shows that all images  $\phi(x_l)$  for  $l \geq 2$  can be determined.  $\blacksquare$

Let  $\Phi \in \text{Aut}(G_{\text{ZQDM}}^{\text{ret}})$  and consider the image  $\Phi(v)$ . For this vertex also exactly two vertex sets  $S'_1, S'_2$  exist, such that  $\Phi(v) \in S'_1, S'_2$  and the induced subgraph of both sets is isomorphic to  $C_8$ . The sets  $\Phi(S_1)$  and  $\Phi(S_2)$  are also isomorphic to  $C_8$ , as  $\Phi$  is an automorphism. Furthermore  $\Phi(v) \in \Phi(S_1), \Phi(S_2)$ . Thus, there are two possibilities

$$S'_1 = \Phi(S_1) \text{ and } S'_2 = \Phi(S_2) \quad (\text{C18a})$$

$$S'_1 = \Phi(S_2) \text{ and } S'_2 = \Phi(S_1). \quad (\text{C18b})$$

Let  $v_1, v_2$  be the two adjacent vertices of  $v$ , they lie in  $S_1$  and  $S_2$ . Let  $w_1, w_2$  be the two adjacent vertices of  $\Phi(v)$ , then there are again two possibilities,

$$w_1 = \Phi(v_1), w_2 = \Phi(v_2) \quad (\text{C19a})$$

$$w_1 = \Phi(v_2), w_2 = \Phi(v_1). \quad (\text{C19b})$$

So overall there are four possibilities. For each of these, Lemma 9 implies, that the images of all vertices in  $S_1$  and  $S_2$  are uniquely determined.

Now we show that this completely determines the automorphism  $\Phi$ . Take some vertex  $u \in S_1$  with  $u \neq v$ . Then there exists another set of vertices  $S_3$ , such that its induced subgraph is isomorphic to  $C_8$  and  $S_3 \neq S_1$ . Likewise, there exists such a set of vertices  $S'_3$ , such that  $\Phi(u) \in S'_3, S'_3 \neq S'_1$  and the induced subgraph of  $S'_3$  is

isomorphic to  $K_{12}$ . So we know that  $\Phi(S_3) \neq S'_1$ , as  $\Phi$  is bijective. Therefore the only possibility is  $\Phi(S_3) = S'_3$ . As  $u$  has only two adjacent vertices, they also lie in  $S_1$  and  $S_3$ . Because they lie in  $S_1$ , their image under  $\Phi$  is already determined. Because they lie in  $S_3$ , it follows from Lemma 9, that the image of every vertex in  $S_3$  is uniquely determined. This argument can be repeated for every degree two vertex, whose image is already determined.

Now we can count the possible automorphisms. For  $v \in V_{\text{ZQDM}}^{\text{ret}}$ , there are  $2N_x N_y$  possibilities for  $\Phi(v)$ . After that, there are 4 additional possibilities which lead to  $8N_x N_y$  possible automorphisms, so  $|\text{Aut}(G_{\text{ZQDM}})| = |\text{Aut}(G_{\text{ZQDM}}^{\text{ret}})| = 8N_x N_y$ . This size of this automorphism group is actually as small as possible. For a tessellated square lattice of lengths  $N_x, N_y$ , there are  $N_x N_y$  distinct translation automorphisms. Furthermore global reflections and rotations form a dihedral group  $D_8$ , combinations lead to at least  $8N_x N_y$  distinct automorphisms. Via the bound in Appendix A 4, this result implies, that, in this structure, the number of orbits  $|L_C/\mathcal{A}_C|$  grows exponentially with the system size.

The requirement that  $N_x, N_y > 2$  is actually important. If this is to the case, additional automorphisms appear. The action of these can be pictured in the following way. Take two adjacent unit cells in the direction with length 2. Then these unit cells actually share two vertices instead of one. The map that exchanges these two vertices is a graph automorphism.

Even with these additional automorphisms, the automorphism group is in general not large enough such that there is only one orbit. We checked this explicitly for a system size of  $N_x = 3, N_y = 2$  (this was one of the systems diagonalized in [40]), there the ground state space  $L_C$  decomposes into two distinct orbits.

### 3. Stastny model

In Ref. [81], Stastny *et al.* proposed a blockade structure  $C_{\text{STC}}$  to realize the toric code. This structure is shown in Fig. 14. In this section we characterize the automorphism group of its blockade graph  $G_{\text{STC}}$  and show that it is not fully-symmetric. We use the same methods as developed in Appendix C 2. As all arguments are quite similar, we will not give them in full detail.

We decompose  $V_{\text{STC}}$  into the subsets,

$$M_1 := \{v \in V_{\text{STC}} \mid \partial B_1(v) \text{ is connected}\} \quad (\text{C20a})$$

$$M_2 := \{v \in V_{\text{STC}} \mid \partial B_1(v) \text{ is not connected}\}. \quad (\text{C20b})$$

The vertices in  $M_1$  are colored blue in Fig. 14, the vertices in  $M_2$  are colored green. We observe, that the set  $M_1$  decomposes into connected components  $M_2 = \sqcup_k Q_k$ , where  $Q_k \simeq K_3$ . By introducing the equivalence relation

$$v \sim w \Leftrightarrow v = w \vee \exists k : v, w \in Q_k. \quad (\text{C21})$$

We obtain the reduced graph  $G_{\text{STC}}^{\text{red}} = (V_{\text{STC}}^{\text{red}}, E_{\text{STC}}^{\text{red}})$  as the quotient graph of  $G_{\text{STC}}$  under Eq. (C21).

The reduced graph is shown in Fig. 14. Via analogous arguments as in Appendix C 2 the automorphism group of  $G_{\text{STC}}^{\text{red}}$  has the same size as the automorphisms group of  $G_{\text{STC}}$ .

To explicitly characterize this automorphism group, we will assume that we assume, that  $N_x, N_y \geq 3$ . Notice that for every vertex  $v \in \tilde{M}_2$ , there are exactly two sets of vertices  $S_1, S_2$  with  $v \in S_1, S_2$ , such that their induced subgraph is isomorphic to  $K_{12}$ . To see this, we only have to consider the neighborhood  $B_6(v)$ . From this neighborhood, all pendant vertices (vertices with only one neighbor) can be removed. The resulting graph is shown in Fig. 14, it contains the two cycles graphs that contain  $v$ .

Let  $\Phi \in \text{Aut}(G_{\text{STC}}^{\text{red}})$ , then also for  $\Phi(v)$ , there are exactly two sets of vertices  $S'_1, S'_2$  with  $v \in S'_1, S'_2$ , such that their induced subgraph is isomorphic to  $K_{12}$ . Also  $\Phi(S_1)$  and  $\Phi(S_2)$  have the same property, as  $\Phi$  is an automorphism. Therefore there are the possibilities

$$S'_1 = \Phi(S_1), S'_2 = \Phi(S_2) \quad (\text{C22a})$$

$$S'_1 = \Phi(S_2), S'_2 = \Phi(S_1). \quad (\text{C22b})$$

Let  $v_1, v_2$  be the two adjacent vertices of  $v$ , they lie in  $S_1$  and  $S_2$ . Let  $w_1, w_2$  be the two adjacent vertices of  $\Phi(v)$ , then there are again two possibilities,

$$w_1 = \Phi(v_1), w_2 = \Phi(v_2) \quad (\text{C23a})$$

$$w_1 = \Phi(v_2), w_2 = \Phi(v_1). \quad (\text{C23b})$$

So overall there are four possibilities. For each of these Lemma 9 implies, that the images of all vertices in  $S_1$  and  $S_2$  are uniquely determined.

Now we show that this completely determines the automorphism  $\Phi$ . Take some vertex  $u \in S_1$  with  $u \neq v$ . Then there exists another set of vertices  $S_3$ , such that its induced subgraph is isomorphic to  $C_{12}$  and  $S_3 \neq S_1$ . Likewise, there exists such a set of vertices  $S'_3$ , such that  $\Phi(u) \in S'_3, S'_3 \neq S'_1$  and the induced subgraph of  $S'_3$  is isomorphic to  $K_{12}$ . So we know that  $\Phi(S_3) \neq S'_1$ , as  $\Phi$  is bijective. Therefore the only possibility is  $\Phi(S_3) = S'_3$ . As  $u$  has only two adjacent vertices, they also lie in  $S_1$  and  $S_3$ . Because they lie in  $S_1$ , their image under  $\Phi$  is already determined. Because they lie in  $S_3$ , it follows from Lemma 9, that the image of every vertex in  $S_3$  is uniquely determined. This argument can be repeated for every degree two vertex, whose image is already determined.

We can now count the automorphisms of this graph. Choosing an arbitrary reference vertex  $v \in V_{\text{STC}}^{\text{red}}$ , there are  $3N_x N_y$  possibilities for  $\Phi(v)$ , each leading to four possible automorphisms (every possibility described above is actually a valid automorphism but this is not crucial). Therefore  $|\text{Aut}(V_{\text{STC}})| = |\text{Aut}(V_{\text{STC}}^{\text{red}})| = 12N_x N_y$ .

### Appendix D: Ground state of $H_{\text{Loop}}$ for $\Omega \neq 0$

In this section, we prove rigorously that by switching on  $\Omega$ , the gap in the spectrum of  $\tilde{H}_{\text{Loop}}(0, \omega)$  does not close.

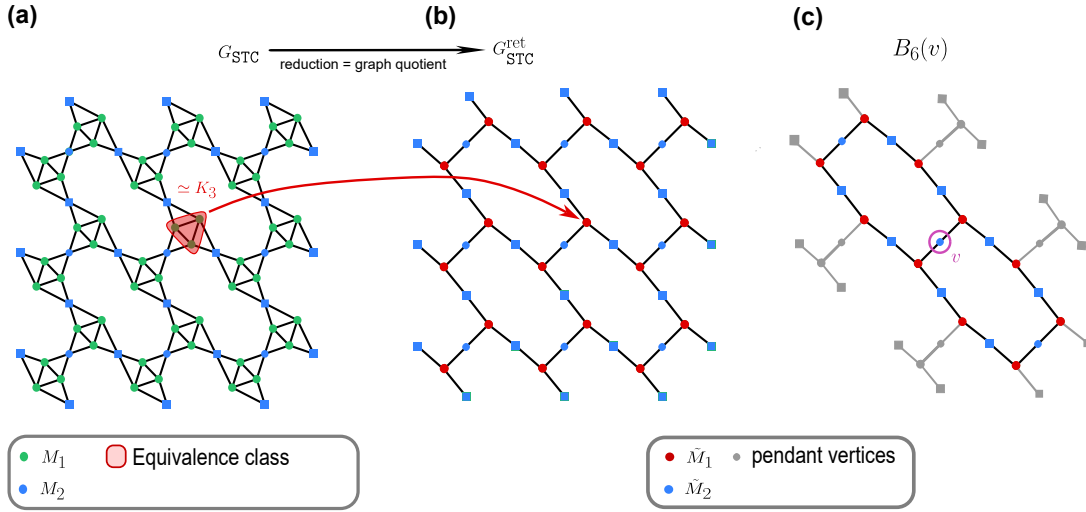


Figure 14. *Reduction of the Stastny model.* (a) Shown is the blockade graph proposed by Stastny *et al.*  $G_{\text{STC}}$  to realize the Toric Code with a blockade structure. Vertices in the set  $M_1$  are colored blue, those in the set  $M_2$  are colored green. The set  $M_2$  decomposes into connected components  $Q_k$ , the induced subgraph of every such component is isomorphic to  $K_3$ . By an equivalence relation we identify the vertices that lie in the same component  $Q_k$ . Some of the equivalence classes are shown as red boxes. (b) Shown is the quotient graph of  $G_{\text{STC}}$  by the aforementioned equivalence relation, the resulting graph is denoted as  $G_{\text{STC}}^{\text{red}}$ . We prove in this section, that the automorphism group of both graphs has the same size. (c) Shown is the neighborhood  $B_6(v)$  of some vertex  $v \in M_1$ . From this neighborhood, all pendant vertices are removed. From the remaining graph, again, all pendant vertices are removed. This process is repeated, until no pendant vertices are left. The removed vertices are colored in gray. This shows, that there are exactly two sets  $S_1, S_2$  with  $v \in S_1, S_2$ , such that their induced subgraph is isomorphic to  $C_{12}$ .

To this end, we apply a result by Michalakis *et al.* [114] that provides sufficient conditions for the stability of a spectral gap under perturbations.

### 1. Conditions for gap stability

We will shortly summarize the conditions for gap stability given by Michalakis. The system considered, is defined on the lattice  $\Lambda_L := [0, L]^2 \subseteq \mathbb{Z}^2$ , which is endowed with the usual graph metric (= the  $\ell^1$  metric). We refer to  $L$  as the system size. To each site  $I \in \Lambda_L$ , a Hilbert space  $\mathcal{H}_I$  is associated, the system Hilbert space is given by  $\mathcal{H}_{\Lambda_L} := \bigotimes_{I \in \Lambda_L} \mathcal{H}_I$ . The unperturbed system Hamiltonian  $H_0$  is assumed to satisfy the following properties.

1.  $H_0$  can be written as a sum of local operators

$$H_0 := \sum_{I \in \Lambda} Q_I, \quad (\text{D1})$$

where each operator  $Q_I$  has a constant range of support.

2. The Hamiltonian  $H_0$  satisfies periodic boundary conditions.
3. The projection  $P_0$  onto the ground state subspace of  $H_0$  satisfies  $P_0 Q_I = q_{0,I} Q_I$ , where  $q_{0,I}$  denotes the minimal eigenvalue of  $Q_I$ .

4. For all  $L \geq 2$ ,  $H_0$  has a spectral gap  $\gamma > 0$ , which is independent of the system size.

We denote the support of an operator as  $\text{supp}(Q_I)$ .

The perturbation  $V$  is assumed to have the form

$$V = \sum_{I \in \Lambda_L} \sum_{r=0}^L V_I(r) \quad (\text{D2})$$

such that  $\text{supp}(V_I) \subseteq B_l(I)$  for some  $l > 0$ . Moreover for allowed perturbations there exists a rapidly decaying function  $f(r)$ , such that  $\|V_I(r)\| \leq Jf(r)$  for some constant  $J > 0$ . Such a perturbation is called a  $(J, f)$ -perturbation. This conditions are trivially satisfied, if Eq. (D2) only contains terms up to a finite range. I.e., there is a constant  $R > 0$  independent of the system size, such that  $V_I(r) = 0$  for all  $r \geq R$ . The perturbation we consider in the following sections has this property.

There are two more conditions for gap stability, these are the *local-gap* condition and *local TQO* (topological quantum order). For any set  $A \subseteq \Lambda$ , we define

$$H_A = \sum_{\text{supp}(Q_I) \subseteq A} Q_I. \quad (\text{D3})$$

Furthermore for  $\epsilon > 0$ , let  $P_B(\epsilon)$  be the projection onto the eigenstates of  $H_A$  with energy less than or equal  $\epsilon$ .

A Hamiltonian  $H$  satisfies the *local-gap condition*, iff there exists an at most polynomial decaying function  $\gamma(r) > 0$ , such that for all  $I_0 \in \Lambda$ ,  $P_{B_r(I_0)}(\gamma(r)) =$

$P_{B_r(I_0)}(0)$ . Here  $B_r(I_0)$  denotes the ball with radius  $r$ .

Lastly we define the condition *local TQO*. Let  $I_0 \in \Lambda$  and  $A = B_r(I_0)$ ,  $A(l) = B_{r+l}(I_0)$  for some  $r \leq L^* < L$  and  $l \leq L - r$ , where  $L$  denotes the system size. The cut-off parameter  $L^*$  has to scale with the system size  $L$ . Let  $|\psi_1\rangle, |\psi_2\rangle$  be two ground states of  $H_{\omega, A(l)}$  and  $\rho_i(A) := \text{Tr}_{A(l) \setminus A} [|\psi_i\rangle \langle \psi_i|]$  for  $i = 1, 2$  their corresponding reduced density matrices. Then a system satisfies local TQO iff

$$\|\rho_1(A) - \rho_2(A)\|_1 \leq 2F(l), \quad (\text{D4})$$

where  $F$  is a decaying function and  $\|\cdot\|_1$  is the Schatten-1 norm.

These conditions are sufficient, to guarantee the stability of the spectral gap of  $H_0$ .

**Theorem 3** (Michalakis [114]). *Let  $H_0$  be a Hamiltonian satisfying conditions 1.-4., local TQO and local-gap. Let  $V$  be a  $(J, f)$ -perturbation, then there exists constants  $J_0 > 0$  And  $L_0 \geq 2$ , such that for  $J \leq J_0$  and  $L \geq L_0$ , the spectral gap of  $H_0 + V$  is bounded from below by  $\gamma/2$ .*

## 2. Locality and frustration-freeness

In the following sections, we show that the conditions stated in Appendix D 1 are satisfied for our setup. Our first task is to define suitable local Hilbert spaces and a suitable local decomposition of  $\tilde{H}_0 := \tilde{H}_{\text{Loop}}(0, \omega)$  and then verify frustration-freeness and the local-gap condition.

We partition our Hamiltonian  $\tilde{H}_0$  as follows,

$$\begin{aligned} \tilde{H}_0 = & - \underbrace{\sum_{i \in V_{\text{Loop}}} \Delta_i n_i + U \sum_{\{i, j\} \in E_{\text{Loop}}} n_i n_j}_{:= H_0^{\text{R}}} \\ & + \underbrace{\frac{\omega}{2} \sum_{\text{Faces } p} (\mathbb{1} - U_p)}_{:= H_0^{\text{p}}}. \end{aligned} \quad (\text{D5})$$

We want to note, that Eq. (D5) already contains a local decomposition of  $\tilde{H}_0$ . However, this form does not satisfy frustration-freeness, as the blockade competes with the detuning. We solve this problem, by partitioning the individual atoms into larger blocks, such that the frustration-freeness is recovered in this ‘‘coarse-grained’’ picture.

### a. Hilbert space

As we are working with a finite blockade strength, the system Hilbert space is given by the tensor product  $\mathcal{H} = \bigotimes_{i \in V_{\text{Loop}}} \mathcal{H}_i$ , where  $\mathcal{H}_i \simeq \mathbb{C}^2$ , is the Hilbert space of one atom.

As shown in Fig. 15 (a), we partition  $\mathcal{C}_{\text{Loop}}$  into unit cells, consisting of two tetrahedrons and the ‘‘wings’’ attached to one of the tetrahedrons. Furthermore Fig. 15 (a)

shows, that we can view these unit cells as attached to the vertices of a square lattice. We denote this square lattice as  $\Lambda$ . To avoid confusion with the vertices of  $\mathcal{C}_{\text{Loop}}$ , we refer to the vertices of  $\Lambda$  as *sites*. We refer to the collection of atoms contained in the unit cell attached to the site  $I \in \Lambda$  as  $V_I$ . We endow this square lattice with the usual graph metric (cf. Appendix B 1) and write  $I \sim J$  for neighboring sites. The square lattice is natural to this construction, as for two vertices  $i \in V_I$  and  $j \in V_J$ ,  $i \sim j$  is only possible if  $I = J$  or  $I \sim J$ . This means, the coarse graining is compatible with the local structure of the graph. This construction can immediately be generalized to the extended tessellations  $\mathcal{C}_{\text{Loop}}^{\text{ext}}$ , described in Section VIII E.

The Hilbert space describing one unit cell  $V_I$  is given by the tensor product

$$\mathcal{H}_I := \bigotimes_{i \in V_I} \mathcal{H}_i \simeq \mathbb{C}^{2^8}. \quad (\text{D6})$$

The last equality follows, as one unit cell contains 14 atoms. For  $\mathcal{C}_{\text{Loop}}^{\text{ext}}$  (cf. Section VIII E), this number is modified to  $6K + 8$ , where  $K$  denotes the length of the links. By associativity of the tensor product, the Hilbert space  $\mathcal{H}$  has the form

$$\mathcal{H} = \bigotimes_{I \in \Lambda} \mathcal{H}_I. \quad (\text{D7})$$

### b. Frustration-freeness of the blockade Hamiltonian

The next step is to construct a frustration-free decomposition of  $\tilde{H}_0$ . We first focus on the part  $H_0^{\text{R}}$ , that describes the blockade. The structure  $\mathcal{C}_{\text{Loop}}$  is constructed as an amalgamation of FSU-structures. The amalgamation has the nice property, that the resulting structure is frustration-free, thus the idea underlying the following constructions is to ‘‘reverse’’ the amalgamation and fit the emerging pieces into a square lattice.

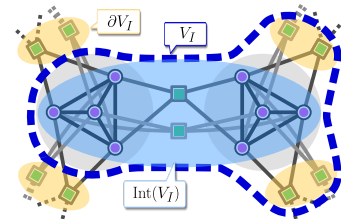
Formally, for a site  $I$  we define the interior of  $V_I$ , as the set of atoms that are not in blockade with atoms in other sites, i.e.,

$$\text{Int}(V_I) := \{i \in V_I \mid i \sim j \Rightarrow j \in V_I\}. \quad (\text{D8})$$

Furthermore we define the boundary of  $V_I$ , as the set of atoms that have a blockade with  $\text{Int}(V_I)$ , i.e.,

$$\partial V_I := \{i \in \mathcal{C}_{\text{Loop}} \mid \exists j \in \text{Int}(V_I) : i \sim j\}. \quad (\text{D9})$$

We want to note, that  $\partial V_I$  is not a subset of  $V_I$ .



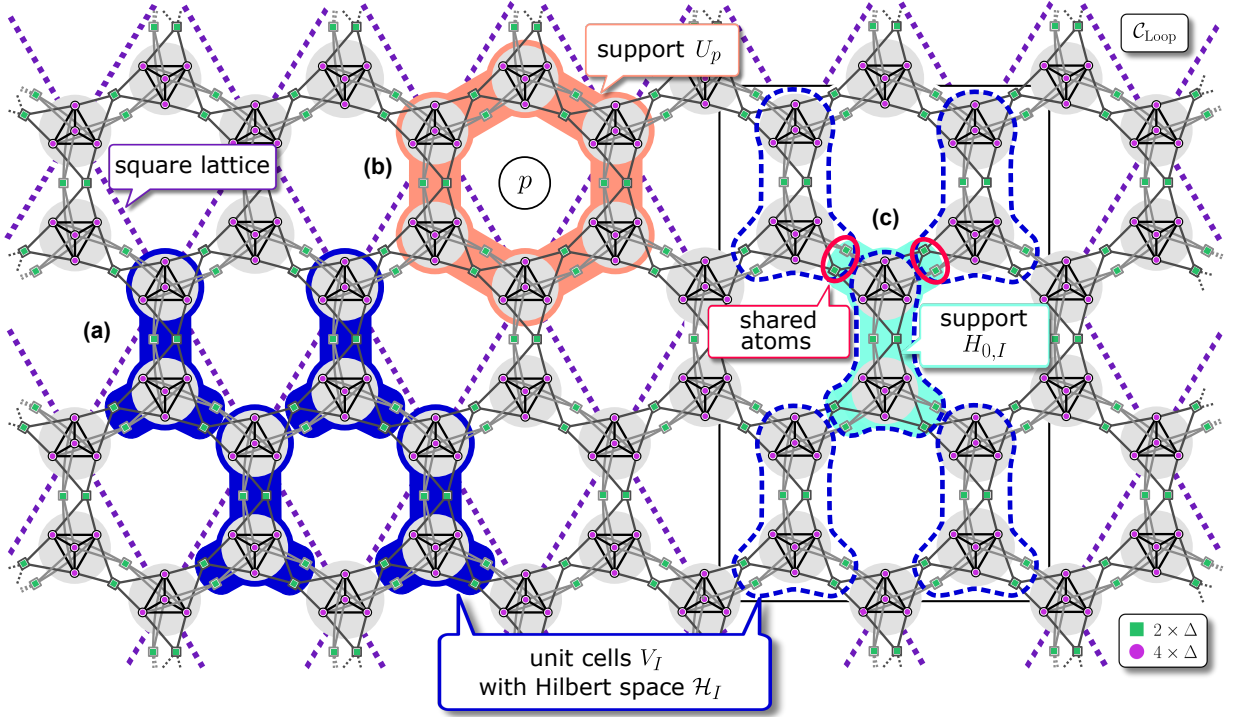


Figure 15. *Coarse graining of  $\mathcal{C}_{\text{Loop}}$* . This figure summarizes the constructions in Appendix D 2, to show that the Hamiltonian  $H_{\text{Loop}}$  can be viewed as frustration-free. The fill color of the atoms denotes their detuning in  $\mathcal{C}_{\text{Loop}}$  (green:  $2\Delta$ , pink:  $4\Delta$ ). (a) The vertex set  $V_{\text{Loop}}$  is partitioned into unit cells  $V_I$ , these are highlighted in dark blue.  $\mathcal{C}_{\text{Loop}}$  can equivalently be described by “contracting” these unit cells into a single Hilbert spaces  $\mathcal{H}_I$ , that are attached to sites in a square lattice. This square lattice is shown as dashed violet lines. (b) The support of a plaquette operator  $U_p$  is highlighted in orange. This support contains part of three unit cells. (c) The Hamiltonian  $H_0^R$  is partitioned into local terms  $H_{0,I}$ . The support of such an operator is highlighted in cyan. The dashed dark blue lines hint the surrounding unit cells. The red ellipses highlight the atoms where  $H_{0,I}$  acts on its neighboring unit cells.

We define local Hamiltonians associated to the site  $I \in \Lambda$ , whose support is contained in  $B_1(I)$ , by

$$H_{0,I} := - \sum_{i \in \text{Int}(V_I)} \Delta_i n_i - \sum_{i \in \partial V_I} \frac{\Delta_i}{2} n_i + U \sum_{\substack{i,j \in V_I \\ i \sim j}} n_i n_j. \quad (\text{D10})$$

The support of these Hamiltonians is visualized in Fig. 15 (b).

Any atom  $i \in V_I$  is either contained in the interior of exactly one site or the boundary of exactly two sites. Moreover, there are no blockades between atoms in  $\partial V_I$ , thus these local Hamiltonians form a decomposition of  $H_0$ , as

$$H_0^R = \sum_{I \in \Lambda} H_{0,I}. \quad (\text{D11})$$

We now show the frustration-freeness of Eq. (D11), i.e., a ground state  $|E_0^R\rangle$  of  $H_0^R$  satisfies  $H_{0,I}|E_0^R\rangle = E_{0,I}|E_0^R\rangle$ , where  $E_{0,I}$  denotes the minimal eigenvalue of  $H_{0,I}$ .

All operators  $H_{0,I}$  and  $H_0^R$  are diagonal in the configuration basis. Hence, the ground state energy of  $H_0^R$  is

lower bounded by the sum of the ground state energies of  $H_{0,I}$ . We show, that this lower bound is actually attained. This then implies, that every ground state of  $H_0^R$  is a ground state of  $H_{0,I}$  for all  $I \in \Lambda$ .

The operator  $H_{0,I}$  is supported on the set  $\bar{V}_I := \text{Int}(V_I) \cup \partial V_I$ . Thus the requirement, that a configuration is a ground state of  $H_{0,I}$ , only constrains the state of the atoms in  $\bar{V}_I$ .

Let  $\mathcal{C}_{2\text{FSU}}$  be the structure arising as the amalgamation of an FSU-structure and its mirror image, such that equivalent atoms on two pairs of edges are identified (cf. Section VIII C). Thus we know the configurations on  $\bar{V}_I$ , that are ground states of  $H_{0,I}$ . One such configuration is shown in Fig. 16. It is possible to extend this to all of  $V_{\text{Loop},2}$  by assigning this configuration to  $\bar{V}_I$  for all  $I \in \Lambda$ . As  $\bar{V}_I$  and  $\bar{V}_J$  have nonempty intersection if  $I \sim J$ , it is not immediately clear that this is possible. Luckily, whenever  $I \sim J$ , assigning this configuration to  $\bar{V}_I$  or  $\bar{V}_J$ , results in the same configuration of the atoms in  $\bar{V}_I \cap \bar{V}_J$ , as shown in Fig. 16.

This configuration on  $V_{\text{Loop}}$  realizes the lower bound for the ground state energy described above and thus is a ground state of  $H_0^R$ .

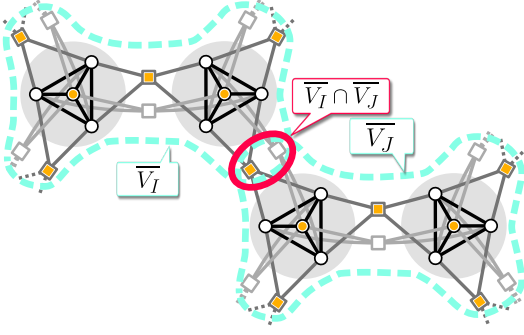


Figure 16. *Ground state configuration on  $V_{\text{Loop}}$ .* Shown is a section of  $\mathcal{C}_{\text{Loop}}$ , consisting of two sets  $\bar{V}_I$  and  $\bar{V}_J$  (marked with cyan dashed lines). The fill colors of the atoms denotes their state (white: unexcited, orange: excited). The shown configuration realizes a ground state of  $H_{0,I}$  and  $H_{0,J}$ . Focusing on only  $V_I$ , the configuration assigns the pair of edge atoms on the top left and the pair of edge atoms on the bottom right the same configuration (dark gray: excited, light gray: unexcited). The same is true for the edges on the top right and the bottom left. Thus it is possible to assign the identical configuration to  $\bar{V}_J$  with  $J \sim I$ , as both assignments assign the same state to the atoms in  $\bar{V}_I \cap \bar{V}_J$  (red ellipse).

### c. Frustration-freeness of the full Hamiltonian

Lastly we focus on the term  $H_0^p$ , which introduces new local operators  $\mathbb{1} - U_p$ . To be consistent with the conventions in [114], we want to attach these operators to Hilbert spaces in our square lattice. To this end, we extend our square lattice  $\Lambda$ , by introducing additional sites on the plaquettes of  $\Lambda$  and the edges of  $\Lambda$ . We refer to the former set of sites as  $\Lambda_e$  and the latter as  $\Lambda_p$ . We refer to this extended lattice as  $\Lambda^{\text{ext}}$ .

To the sites  $I \in \Lambda_e$  and  $I \in \Lambda_p$ , we attach the trivial Hilbert spaces  $\mathcal{H}_I \simeq \{0\}$ . This is just a formality, to be consistent with [114], the Hilbert space is unchanged,

$$\mathcal{H} \simeq \bigotimes_{I \in \Lambda^{\text{ext}}} \mathcal{H}_I. \quad (\text{D12})$$

Note that the support of the operators  $H_{0,I}$ , defined in Eq. (D10), is now contained in  $B_2(I)$  in the extended lattice  $\Lambda^{\text{ext}}$ . In the extended lattice, it is natural to attach the operator  $\mathbb{1} - U_p$  to the sites in  $\Lambda_p$ . Then the support of these operators is contained in  $B_2(p)$ , as shown in Fig. 15 (b). We subsequently define the local operators  $Q_I$ , by

$$Q_I := \begin{cases} \frac{\omega}{2}(\mathbb{1} - U_p), & I = p \in \Lambda_p \\ H_{0,I}, & I \in \Lambda \\ 0, & I \in \Lambda_e. \end{cases} \quad (\text{D13})$$

Then the Hamiltonian (D5) can be written as

$$\tilde{H}_0 = H_0^{\text{R}} + H_0^{\text{p}} = \sum_{I \in \Lambda} Q_I. \quad (\text{D14})$$

We proceed to show the frustration-freeness of Eq. (D14). By construction (cf. Section VIII D) the loop automorphisms  $\phi_p$ , that induce the operators  $U_p$ , are compositions of edge permutations and vertex permutations (permutations of vertices in a tetrahedron). Thus, it is easily verified, that  $i \in \partial V_I$  implies that  $\phi_p(i) \in \partial V_I$  and likewise for  $i \in \text{Int}(V_I)$ . This implies, that the operators  $H_{0,I}$  are invariant under  $U_p$ , i.e.,  $[H_{0,I}, U_p] = 0$ . Moreover, we know that  $[H_{0,I}, H_{0,J}] = 0$ , as the operators  $H_{0,I}$  are diagonal in the same basis and  $[U_p, U_q] = 0$ , as discussed in Section VIII D. Hence, all operators  $Q_I$  are simultaneously diagonalizable. It follows, that the ground state energy of  $\tilde{H}_0$  is lower bounded by the sum of the ground state energies  $E_0[Q_I]$  of the operators  $Q_I$ .

As  $U_p^2 = \mathbb{1}$ , the operator  $\mathbb{1} - U_p$  is a projector. Thus the smallest eigenvalue of this operator is 0. An eigenstate  $|\psi\rangle$  with this eigenvalue must satisfy  $U_p|\psi\rangle = |\psi\rangle$ . It is easily verified, that the state

$$|\omega\rangle := \frac{1}{\sqrt{|L_{\text{Loop}}|}} \sum_{\mathbf{n} \in L_{\text{Loop}}} |\mathbf{n}\rangle \quad (\text{D15})$$

satisfies  $U_p|\omega\rangle = |\omega\rangle$  and thus  $Q_I|\omega\rangle = 0$  for  $I \in \Lambda_p$ . Here  $|L_{\text{Loop}}|$  denotes the number of elements in  $L_{\text{Loop}}$ . All states  $|\mathbf{n}\rangle \in \mathcal{H}_{L_{\text{Loop}}}$  are by definition ground states of  $H_0^{\text{R}}$ . It follows, that  $|\omega\rangle$  is also a ground state of  $H_0^{\text{R}}$ . Then the previous discussion implies, that  $|\omega\rangle$  is a ground state of all operators  $Q_I = H_{0,I}$  for  $I \in \Lambda$ . Hence we have shown the frustration-freeness of Eq. (D14).

In addition to frustration-freeness, the Hamiltonian (D14) has a spectral gap independent of the system size. An excited state must either fail to be a ground state of an operator  $H_{0,I}$ , leading to a spectral gap of  $\Delta$ , or fail to be a ground state of  $\omega/2(\mathbb{1} - U_p)$ , leading to a spectral gap of  $\omega/2$ . Hence  $\tilde{H}_0$  has a spectral gap of  $\min(\Delta, \omega/2)$ , independent of the system size.

### 3. Local-gap condition

The argument for the local-gap condition is analogous to that for the spectral gap in Appendix D 2 c. Analogous as in Eq. (D5), we split the localized Hamiltonian  $H_{0,A}$ , defined by Eq. (D3), into  $\tilde{H}_{0,A} = \tilde{H}_{0,A}^{\text{R}} + \tilde{H}_{0,A}^{\text{p}}$ . The operators  $\tilde{H}_{0,A}^{\text{R}}$  ( $\tilde{H}_{0,A}^{\text{p}}$ ) contain all terms associated to sites in  $\Lambda$  ( $\Lambda_p$ ).

Let  $L_{\text{Loop},A}$  denote the ground state configurations of  $H_{0,A}^{\text{R}}$ , as defined by Eq. (D3). Further define the multiplicative group  $\mathcal{U}$  generated by the operators  $U_p$  with support inside  $A$ , i.e.  $\mathcal{U} := \langle U_p | p \in A \rangle$ . Pick an arbitrary  $\mathbf{n} \in L_{\text{Loop},A}$  and define the set  $\mathcal{U}|\mathbf{n}\rangle := \{U|\mathbf{n}\rangle | U \in \mathcal{U}\}$ . Then the state

$$|\omega, \mathbf{n}\rangle_A := \frac{1}{\sqrt{|\mathcal{U}|\mathbf{n}\rangle|}} \sum_{|\mathbf{m}\rangle \in \mathcal{U}|\mathbf{n}\rangle} |\mathbf{m}\rangle \quad (\text{D16})$$

satisfies  $U_p|\omega, \mathbf{n}\rangle_A = |\omega, \mathbf{n}\rangle_A$ , because by construction  $U_p$  acts as a bijection on the set  $\mathcal{U}|\mathbf{n}\rangle$ . Thus  $Q_I|\omega, \mathbf{n}\rangle_A = 0$

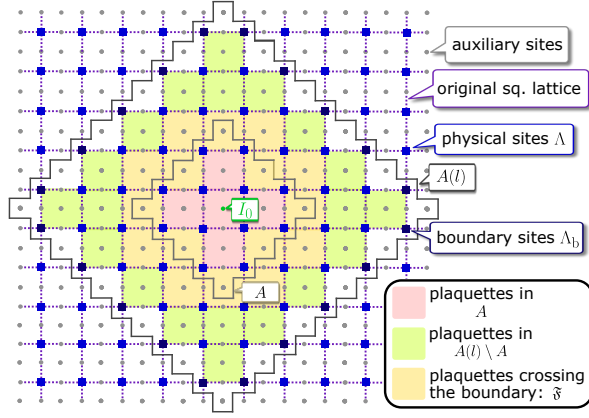


Figure 17. *Setup for local TQO.* Shown is the setup for the proof of the local TQO condition. The blue squares and gray circles represent sites of the square lattice  $\Lambda^{\text{ext}}$ , constructed to describe the structure  $\mathcal{C}_{\text{Loop}}$ . The blue squares represent the physical sites, where the Hilbert spaces  $H_I$  are attached. The gray circles represent the auxiliary sites only used to attach the plaquette operators. The square lattice  $\Lambda$ , that only contains the physical sites, is depicted as dashed violet lines. The physical sites on the boundary of  $A(l)$ , denoted as  $\Lambda_b$ , are highlighted in a darker blue color. The green vertex  $I_0$  is the midpoint of the region  $A = B_r(I_0)$ , in the depicted configuration  $r = 3$ . The boundary of the region  $A$  is shown as a light gray line. The boundary of  $A(l)$  is shown as a dark gray line, in the depicted configuration  $l = 5$ . The plaquette operators  $U_p$  with support lying in  $A(l)$ , are partitioned into three classes, in the figure this is shown by the color of the corresponding plaquette of the lattice  $\Lambda$  (Plaquettes fully in  $A$ : red, Plaquettes fully in  $A(l) \setminus A$ : green, Plaquettes crossing the boundary: orange). The distance  $l$  is chosen sufficiently large, such that all plaquettes that intersect  $A$ , are fully contained in  $A(l)$ .

for  $I \in \Lambda_p$ . Furthermore  $|\omega, \mathbf{n}\rangle_A$  is a ground state of  $\tilde{H}_{0,A}^R$ . By the discussion in Appendix D 2 b,  $|\omega, \mathbf{n}\rangle_A$  is a ground state of every operator  $Q_I$  for  $I \in \Lambda$ .

Analogous as in Appendix D 2 c, it follows that  $H_{0,A}$  has a spectral gap of at least  $\gamma = \min(\Delta, \omega/2)$ , independent of the system size  $L$ . Hence, the local-gap condition is satisfied for a constant function  $\gamma(L)$ .

#### 4. Local TQO

In this section we verify the local TQO condition, in fact we will show, that for sufficiently large  $l$ , the reduced density matrices as defined in Appendix D 1 are equal for all ground states. To this end, we need to explicitly characterize the ground states of the local Hamiltonians  $\tilde{H}_{0,A(l)}$ . The calculation is in some parts very similar to the calculation the leads to the entanglement entropy for the toric code model, for reference see [134]. However there are some differences, due to our model having "internal degrees of freedom".

The local Hamiltonians  $\tilde{H}_{0,A(l)}$  have a peculiar structure. For any two sites  $I \sim J$  in  $\Lambda$ , with  $I \in A$  and  $J \notin A$ , the Hamiltonian  $H_{0,I}$  is not part of  $\tilde{H}_{0,A(l)}$ . In this case in  $V_I$ , there are neither detunings nor blockades. However it can happen, that  $\tilde{H}_{0,A(l)}$  contains an operator  $U_p$ , that acts nontrivially on  $I$ . We refer to these sites as  $\Lambda_b$ , they are shown in Fig. 17. We define  $\Lambda_i := \Lambda \setminus \Lambda_b$ .

By construction, the ground state configurations of the sites in  $\Lambda_i$  can naturally be identified with loop configurations on the (unextended) square lattice. In this picture, the symmetry operators  $U_p$  behave in the same way, as the operators  $B_p$  in the toric code model.

Let  $H_{\text{Loop},A}$  denote the ground state subspace of  $H_0^R$  (cf. Eq. (D5)). We note, that the group  $\mathcal{U}$ , introduced in Appendix D 3, acts freely. I.e., for any nonempty product  $U_{p_1} \cdots U_{p_n}$  holds that  $U_{p_1} \cdots U_{p_n} |\mathbf{n}\rangle \neq |\mathbf{n}\rangle$  for all  $|\mathbf{n}\rangle \in H_{\text{Loop},A}$ . This follows as any collection of plaquettes in  $A(l)$  must have a boundary (as there are no "half" plaquette operators). For two neighboring vertices  $I, J \in \mathcal{P}$ , this product swaps the atoms on the edge between  $I$  and  $J$ , thus the action of the product acts nontrivially.

It immediately follows, that for every state  $|\mathbf{n}\rangle \in H_{\text{Loop},A}$ , the states  $\prod_{p \subseteq A(l)} U_p^{s_p} |\mathbf{n}\rangle$  are mutually orthonormal, for all combinations of  $s_p \in \{0, 1\}$ . Here the notation  $p \subseteq A(l)$  denotes that all physical sites of the support of  $U_p$  are contained in  $A(l)$ . Thus, the local ground state D16 has the form

$$|\omega, \mathbf{n}\rangle_{A(l)} := \mathcal{N} \sum_{|\mathbf{m}\rangle \in \mathcal{U}|\mathbf{n}\rangle} |\mathbf{m}\rangle \quad (\text{D17a})$$

$$= \mathcal{N} \sum_{s_p=0,1} \prod_{p \subseteq A(l)} U_p^{s_p} |\mathbf{n}\rangle \quad (\text{D17b})$$

$$= \mathcal{N} \prod_{p \subseteq A(l)} (1 + U_p) |\mathbf{n}\rangle. \quad (\text{D17c})$$

The constant  $\mathcal{N}$  denotes the normalization of the state. It is easy to see, that  $\mathcal{N} = (\sqrt{2})^{-c_{A(l)}}$ , where  $c_{A(l)}$  denotes this number of plaquettes that are part of  $A(l)$ . In the following, we suppress the index  $A(l)$  from the state Eq. (D17c).

For any ground state of  $H_{0,A(l)}^R$ , a ground state of  $H_{0,A(l)}$  can be generated by Eq. (D17c). However, if  $|\mathbf{m}\rangle \in \mathcal{U}|\mathbf{n}\rangle$ , then both states generate the same ground state, i.e.,  $|\omega, \mathbf{n}\rangle = |\omega, \mathbf{m}\rangle$ .

For convenience, we define  $B := A(l) \setminus A$ . As  $|\mathbf{n}\rangle$  is a product state, we can write it as a tensor product  $|\mathbf{n}\rangle = |\mathbf{n}\rangle_A |\mathbf{n}\rangle_B$ , where  $|\mathbf{n}\rangle_A$  ( $|\mathbf{n}\rangle_B$ ) denote the configuration of atoms in A (B). It is possible to find a product of operators  $U_p$ , such that

$$U_{p_1} \cdots U_{p_n} |\mathbf{n}\rangle = |\mathbf{0}\rangle_A |\mathbf{n}'\rangle_B. \quad (\text{D18})$$

This is due to the trivial Homology group of  $A$  with open boundary conditions. We define the operator  $X$  as a product of  $\sigma_i^x$  on every atom in  $B$ , where  $|\mathbf{n}'\rangle_B$  differs from the state  $|\mathbf{0}\rangle_B$ . The support of this operator is contained in  $B$ . This implies, that the states  $|\mathbf{n}\rangle$  and

$X|\mathbf{0}\rangle$ , generate the same ground state, hence

$$|\omega, \mathbf{n}\rangle = \mathcal{N} \prod_{p \subseteq A(l)} (\mathbb{1} + U_p) X |\mathbf{0}\rangle. \quad (\text{D19})$$

We partition the plaquettes contained in  $A(l)$  into three sets, plaquettes contained in  $A$ , plaquettes contained in  $B$  and plaquettes that cross the boundary of  $A$  and  $B$ . We refer to the latter set as  $\mathfrak{F}$ . These three sets of plaquettes are shown in Fig. 17. In the following we assume that  $l$  and thus  $L_0$  are sufficiently large, such that all plaquettes that intersect  $A$  are contained in  $A(l)$ . This is the case in Fig. 17. In this spirit, we define the states

$$|\omega, \mathbf{0}\rangle_A := \mathcal{N}_A \prod_{p \subseteq A} (\mathbb{1} + U_p) |\mathbf{0}\rangle_A \quad (\text{D20a})$$

$$|\omega, \mathbf{n}\rangle_B := \mathcal{N}_B \prod_{p \subseteq B} (\mathbb{1} + U_p) X |\mathbf{0}\rangle_B. \quad (\text{D20b})$$

The normalizations are given by  $\mathcal{N}_A = (\sqrt{2})^{-c_A}$  and  $\mathcal{N}_B = (\sqrt{2})^{-c_B}$ , where  $c_A$  and  $c_B$  denote the number of plaquettes contained in  $A$  and  $B$  respectively. Using these definitions, Eq. (D19) becomes

$$|\omega, \mathbf{n}\rangle = \tilde{\mathcal{N}} \prod_{p \in \mathfrak{F}} (\mathbb{1} + U_p) |\omega, \mathbf{0}\rangle_A |\omega, \mathbf{n}\rangle_B \quad (\text{D21a})$$

$$= \tilde{\mathcal{N}} \sum_{s_p=0,1} \prod_{p \in \mathfrak{F}} U_p^{s_p} |\omega, \mathbf{0}\rangle_A |\omega, \mathbf{n}\rangle_B. \quad (\text{D21b})$$

Here the normalization is given by  $\tilde{\mathcal{N}} = (\sqrt{2})^{c_A+c_B-c_{A(l)}} = (\sqrt{2})^{-c_{AB}}$ , where  $c_{AB} = |\mathfrak{F}|$  denotes the number of plaquettes in  $\mathfrak{F}$ .

We define the vector  $\mathbf{s} := (s_p)_{p \in \mathfrak{F}} \in \mathbb{Z}_2^{c_{AB}}$  and the shorthand notation  $U_{\mathbf{s}} := \prod_{p \in \mathfrak{F}} U_p^{s_p}$ . By construction, all products  $U^{\mathbf{s}}$  are induced by an automorphism  $\phi \in \mathcal{A}_{\text{Loop}}$ . By Section VIII D, these automorphisms are compositions of edge permutations and vertex permutations (cf. Eq. (26)). As the support of these permutations is either contained in  $A$  or  $B$  and all these permutations commute, we can partition them as  $\phi = \phi_A \circ \phi_B$ , where  $\phi_A$  ( $\phi_B$ ) only acts on atoms in  $A$  ( $B$ ). The permutation  $\phi_A$  defines an operator  $U_{\mathbf{s}}^A := U_{\phi_A}$  (cf. Section V) with support in  $A$ , the permutation  $\phi_B$  defines an operator  $U_{\mathbf{s}}^B := U_{\phi_B}$  with support in  $B$ . We want to emphasize, that the permutations  $\phi_A$  and  $\phi_B$  themselves are not automorphisms of  $\mathcal{C}_{\text{Loop}}$ , and thus  $U_{\mathbf{s}}^A$  and  $U_{\mathbf{s}}^B$  are not symmetries of the Hamiltonian. However, because all permutations defining  $\phi_A$  and  $\phi_B$  square to the identity, the same is true for the operators  $U_{\mathbf{s}}^A$  and  $U_{\mathbf{s}}^B$ , i.e.,  $(U_{\mathbf{s}}^A)^2 = 1$  and  $(U_{\mathbf{s}}^B)^2 = 1$ . Furthermore,  $U_{\mathbf{s}}^A$  and  $U_{\mathbf{s}}^B$  are unitary, as they act as permutations on the Hilbert space  $\mathcal{H}$ . We obtain the decomposition

$$U_{\mathbf{s}}^A \otimes U_{\mathbf{s}}^B = U_{\mathbf{s}} = \prod_{p \in \mathfrak{F}} U_p^{s_p}. \quad (\text{D22})$$

Applying this to Eq. (D21b) yields

$$|\omega, \mathbf{n}\rangle = \tilde{\mathcal{N}} \sum_{\mathbf{s} \in \mathbb{Z}_2^{c_{AB}}} U_{\mathbf{s}}^A |\omega, \mathbf{0}\rangle_A U_{\mathbf{s}}^B |\omega, \mathbf{n}\rangle_B. \quad (\text{D23})$$

To reach the desired result, we have to compute the partial trace of Eq. (D23). To this end, we show that the states  $U_{\mathbf{s}}^B |\omega, \mathbf{n}\rangle_B$  are orthonormal. As a preliminary step we consider the product  $U_{\mathbf{s}'}^B U_{\mathbf{s}}^B$  for  $\mathbf{s}, \mathbf{s}' \in \mathbb{Z}_2^{c_{AB}}$ . The fact that  $U_p^2 = \mathbb{1}$  for all plaquettes  $p$ , implies that  $U_{\mathbf{s}} U_{\mathbf{s}'} = U_{\mathbf{s} \oplus \mathbf{s}'}$ , where the operation  $\mathbf{s} \oplus \mathbf{s}'$  denotes addition (modulo 2) in  $\mathbb{Z}_2^{c_{AB}}$ . Decomposing these operators as in Eq. (D22) yields

$$U_{\mathbf{s}}^A U_{\mathbf{s}'}^A \otimes U_{\mathbf{s}}^B U_{\mathbf{s}'}^B = U_{\mathbf{s}} U_{\mathbf{s}'} \quad (\text{D24a})$$

$$= U_{\mathbf{s} \oplus \mathbf{s}'} \quad (\text{D24b})$$

$$= U_{\mathbf{s} \oplus \mathbf{s}'}^A \otimes U_{\mathbf{s} \oplus \mathbf{s}'}^B. \quad (\text{D24c})$$

From this equality, it follows that  $U_{\mathbf{s}}^A U_{\mathbf{s}'}^A = \lambda U_{\mathbf{s} \oplus \mathbf{s}'}^A$  and  $U_{\mathbf{s}}^B U_{\mathbf{s}'}^B = \lambda^{-1} U_{\mathbf{s} \oplus \mathbf{s}'}^B$ , for  $\lambda \in \mathbb{C}$ . The operators acting as permutations on  $\mathcal{H}$ , further implies that  $\lambda = 1$ , which shows that

$$U_{\mathbf{s}}^A U_{\mathbf{s}'}^A = U_{\mathbf{s} \oplus \mathbf{s}'}^A \quad (\text{D25a})$$

$$U_{\mathbf{s}}^B U_{\mathbf{s}'}^B = U_{\mathbf{s} \oplus \mathbf{s}'}^B. \quad (\text{D25b})$$

Now we consider the scalar product

$$S_{\mathbf{s}, \mathbf{s}'} := \langle \omega, \mathbf{n} |_B U_{\mathbf{s}'}^B U_{\mathbf{s}}^B | \omega, \mathbf{n} \rangle_B \quad (\text{D26a})$$

$$= \langle \omega, \mathbf{n} |_B U_{\mathbf{s}' \oplus \mathbf{s}}^B | \omega, \mathbf{n} \rangle_B. \quad (\text{D26b})$$

We show that  $S_{\mathbf{s}, \mathbf{s}'} = 0$  for  $\mathbf{s} \neq \mathbf{s}'$ . For notational convenience, define the multiplicative group of plaquette operators in  $B$ ,  $\mathcal{U}^B := \langle U_p | p \subseteq B \rangle$ . Analogous to  $\mathcal{U}^B$  this group acts freely on states  $|\mathbf{n}\rangle$ , thus Eq. (D20b) can also be written as

$$|\omega, \mathbf{n}\rangle_B = \mathcal{N}_B \sum_{\mathbf{m} \in \mathcal{U}^B |\mathbf{n}'\rangle} |\mathbf{m}\rangle. \quad (\text{D27})$$

Hence, if  $U_{\mathbf{s} \oplus \mathbf{s}'}^B |\mathbf{n}'\rangle \notin \mathcal{U}^B |\mathbf{n}'\rangle$  for all  $\mathbf{s}, \mathbf{s}'$ , it follows that  $S_{\mathbf{s}, \mathbf{s}'} = 0$ . The remainder of this section is dedicated to proving this fact.

Consider a site  $I \in B$  with an adjacent site  $J \in A$ , then there are two plaquette operators  $U_{p_1}, U_{p_2}$ , whose support contains  $I$  and  $J$ . In particular this implies that  $p_1, p_2 \in \mathfrak{F}$ . The vertices in  $V_I$  that are adjacent to vertices in  $V_J$  are either a pair of edge vertices or a tetrahedron. We refer to the set of these vertices as  $\partial_J V_I$ .

Suppose that  $\partial_J V_I$  is the pair of edge vertices on edge  $e$ . Then  $U_{p_1}$  and  $U_{p_2}$  both contain the edge permutation  $\varphi_e$ . If the product  $U_{\mathbf{s}}$  contains one of these plaquette operators, then also  $U_{\mathbf{s}}^B$  contains this edge permutation once. On the other hand,  $U_{p_1}$  and  $U_{p_2}$  are the only plaquette operators containing the edge permutation  $\varphi_e$ . Thus no product of plaquette operators  $U_p$  with  $p \subseteq B$  contains this edge permutation, which implies  $U_{\mathbf{s}}^B |\mathbf{n}\rangle \notin \mathcal{U}^B |\mathbf{n}\rangle$ .

Suppose that  $\partial_J V_I$  consists of the vertices in one tetrahedron  $s$ . Then the operators  $U_{p_1} U_{p_2}$  contain two different vertex permutations  $\varphi_s^{\alpha_1}$  and  $\varphi_s^{\alpha_2}$ . No other plaquette operators contain these two vertex permutations. If a product  $U_{\mathbf{s}}$  were to contain only one of the plaquette operators

$U_{p_1}$  or  $U_{p_2}$ , then  $U_s^B$  would contain only one of the aforementioned vertex permutations, *w.l.o.g.* let this be  $\varphi_s^{\alpha_1}$ . A product of plaquette operators  $U_p$  with  $p \subseteq B$  can either contain  $\varphi_s^{\alpha_3}$  ( $\alpha_3 \neq \alpha_1, \alpha_2$ ) or the identity on the tetrahedron  $s$ . Thus  $U_s^B |\mathbf{n}\rangle \notin \mathcal{U}^B |\mathbf{n}\rangle$ . As  $\varphi_s^{\alpha_1} \circ \varphi_s^{\alpha_2} = \varphi_s^{\alpha_3}$ , it follows that in this case  $U_s^B |\mathbf{n}\rangle \in \mathcal{U}^B |\mathbf{n}\rangle$  is possible.

This argument shows, that  $U_s^B |\mathbf{n}\rangle \in \mathcal{U}^B |\mathbf{n}\rangle$  implies that for any site  $I \in B$  with an adjacent site  $J \in A$ , both or none of the plaquette operators, whose support contains  $I$  and  $J$ , must be part of the product  $U_s$ . In other words  $\mathbf{s} = (0, \dots, 0)$  or  $\mathbf{s} = (1, \dots, 1)$ .

We examine the case  $\mathbf{s} = (1, \dots, 1)$  separately. The product  $U_s$  acts as edge permutations in a closed loop that encompasses the region  $A$ . Thus this loop is not the boundary of a collection of plaquettes (this loop is not homologically trivial) and thus  $U_{(1, \dots, 1)}^B |\mathbf{n}\rangle \notin \mathcal{U}^B |\mathbf{n}\rangle$ .

In summary we have shown that

$$\langle \omega, \mathbf{n} |_B U_{\mathbf{s}' \oplus \mathbf{s}}^B | \omega, \mathbf{n} \rangle_B = 0, \quad (\text{D28})$$

iff  $\mathbf{s}' \oplus \mathbf{s} \neq 0$ , which is equivalent to  $\mathbf{s}' \neq \mathbf{s}$ . In the other case the scalar product is 1, due to  $U_{\mathbf{s}' \oplus \mathbf{s}}^B$  being unitary.

Thus we can complete the family  $U_s^B |\omega, \mathbf{0}\rangle_B$  to an orthonormal basis of  $\mathcal{H}_B = \bigotimes_{I \in B} \mathcal{H}_I$ . We use this basis to compute the partial trace of the density matrix corresponding to Eq. (D23) with respect to  $B$ . This results in

$$\rho(\omega, \mathbf{n})_A = \tilde{\mathcal{N}}^2 \sum_{\mathbf{s}, \mathbf{s}' \in \mathbb{Z}_2^{c_{AB}}} U_s^A |\omega, \mathbf{0}\rangle_A \langle \omega, \mathbf{0} |_A U_{\mathbf{s}'}^A \quad (\text{D29})$$

Notice that after taking the partial trace, Eq. (D29) does not depend on the state  $|\mathbf{n}\rangle$  any more. As all ground states can be generated from some state  $|\mathbf{n}\rangle$  by Eq. (D17c), all these ground states have the same reduced density matrix (D29), if  $l \geq l_0$  is sufficiently large. Thus Eq. (D4) is satisfied, where  $F$  can be taken as a step function.

## Appendix E: Derivation of the effective Hamiltonian

In this section, we derive the properties of the low-energy effective Hamiltonian given in Eq. (40). We use the method described by Datta *et al.* [135], which yields a well-defined effective Hamiltonian even for extensive system sizes. However, we want to note that the results of this section also hold for other approaches to perturbatively derive an effective Hamiltonian (e.g., [119, Section 3]).

Let  $V_{\text{Loop}}$  and  $E_{\text{Loop}}$  be the vertex set and edge set, of the blockade structure  $\mathcal{C}_{\text{Loop}}$ . Then the system Hamiltonian  $H_{\text{Loop}}$  is given by (cf. Eq. (2))

$$\begin{aligned} H_{\text{Loop}}(\Omega) := & - \underbrace{\sum_{i \in V_{\text{Loop}}} \Delta_i n_i + U \sum_{\{i, j\} \in E_{\text{Loop}}} n_i n_j}_{:= H_0} \\ & + \Omega \underbrace{\sum_{i \in V_{\text{Loop}}} \sigma_i^x}_{:= V}. \end{aligned} \quad (\text{E1})$$

This Hamiltonian describes a blockade interaction with a finite (but arbitrarily large) blockade strength  $U$ . This is necessary, to keep the tensor product structure of the Hilbert space.

For the perturbation theory,  $H_0$  assumes the role of the classical unperturbed Hamiltonian, whereas  $V$  is the perturbation.

### 1. Unitary block-diagonalization by Datta

The method of Datta provides a method to perturbatively *block-diagonalize* a Hamiltonian of the form  $H = H_0 + \lambda V$ . Here  $H_0$  is the unperturbed Hamiltonian with exactly known spectrum,  $V$  the perturbation and  $\lambda$  the perturbation strength.

The blocks are defined with respect to the unperturbed Hamiltonian  $H_0$ . Let  $P_0$  be the projection onto the ground state manifold of  $H_0$  and  $Q_0 := \mathbb{1} - P_0$ . Then the goal is to find a unitary transformation  $e^S$ , with anti-Hermitian generator  $S$ , such that  $H' := e^S H e^{-S}$  is block-diagonal in the sense that,  $P_0 H' Q_0 = Q_0 H' P_0 = 0$ . The restriction of this transformed Hamiltonian onto the ground state manifold, i.e.,  $P_0 H' P_0$  is the *low-energy effective Hamiltonian* for  $H$ . The method of Datta yields a series expansion of  $S$  and  $H'$ , in powers of  $\lambda$ , such that  $H'$  is block-diagonal up to some order  $n$ .

In this section we shortly describe the setup and conditions for the method of Datta to be applicable. The system is defined on a finite subset of a square lattice  $\Lambda \subseteq \mathbb{Z}^2$ . To each vertex  $I \in \Lambda$ , a copy of some finite-dimensional Hilbert space  $\mathcal{H}_I \simeq \mathcal{H}$ , is attached. The Hilbert space describing the whole system, is the tensor product  $\mathcal{H}_\Lambda = \bigotimes_{I \in \Lambda} \mathcal{H}_I$ .

The unperturbed Hamiltonian is required to have the form

$$H_0 = \sum_{X \subset \Lambda} H_{0, X}, \quad (\text{E2})$$

where  $H_{0, X}$  acts trivially on the Hilbert spaces attached outside of  $X$ . In addition, it is required, that there is a tensor product basis of  $\mathcal{H}_\Lambda$ , such that every term  $H_{0, X}$  is diagonal in this basis and the ground state of  $H_0$  is a ground state for every term  $H_{0, X}$ . We refer to the latter condition as *frustration-freeness*. That our Hamiltonian (E1) satisfies these conditions (after the Hilbert space is properly partitioned) is already covered by the proof of the frustration-freeness in Appendix D 2. The desired tensor product basis is the basis of excitation patterns.

The perturbation is required to have the form

$$V = \sum_{X \subset \Lambda} V_X, \quad (\text{E3})$$

where the local terms  $V_X$  act trivially on Hilbert spaces attached outside of  $X$ . Additionally  $\|V_X\|$  has to decay requirement sufficiently fast with the size of  $X$ .

For our perturbation (cf. Eq. (E1)), we set

$$V_I := \Omega \sum_{i \in I} \sigma_i^x \quad (\text{E4})$$

and  $V_X = 0$  otherwise. As the perturbation only acts on individual sites, it trivially satisfies the decay requirements. Hence, we can apply the block-diagonalization methods of Datta *et al.* to our system.

In the remainder of this section, we shortly sketch the construction of the effective Hamiltonian. We start with some preliminary definitions.

For any set  $X \subseteq \Lambda$ , we define  $B_X := \cup_{I \in X} B_1(I)$ , here  $B_1(I)$  denotes the ball with radius 1 in the graph metric on  $\Lambda$  (cf. Appendix B1). Furthermore, define the projector  $P_{B_X}^0$  as the projection onto the subspace of states, that are ground states of  $H_{0,Y}$ , for all  $Y \subseteq X$ . Moreover, define

$$P_{B_X}^1 := P_{B_X \setminus X}^0 - P_{B_X}^0, \quad (\text{E5})$$

the projector onto the states that are ground states in  $B_X \setminus X$  but fail to be ground states in  $X$ . For any local operator  $A_X$  whose support is contained in  $X$ , define its

off-diagonal part as

$$A_{B_X}^{01} := P_{B_X}^1 A_X P_{B_X}^0 + P_{B_X}^0 A_X P_{B_X}^1. \quad (\text{E6})$$

For the generator, Datta *et al.* make the ansatz

$$S := \sum_{j=1}^n \lambda^j S_j, \quad (\text{E7})$$

where  $n$  is arbitrary but finite. They further require the terms  $S_j$  to be a sum of local operators  $S_j = \sum_{X \subset \Lambda} S_{j,X}$ . The transformed Hamiltonian  $H'$  then has the form

$$H' = H_0 + \underbrace{\sum_{j=1}^n \lambda^j ([S_j, H_0] + V_j)}_{\text{block-diagonal}} + \underbrace{\sum_{j \geq n+1} \lambda^j V_j}_{\text{higher-order remainder}}. \quad (\text{E8})$$

The operators  $V_j$  are a sum of local operators  $V_j = \sum_{Y \subset \Lambda} V_{j,Y}$ , the local terms are given by  $V_{0,B_X} := V_{B_X}$  for  $j = 0$  and for  $j \geq 1$ , by

$$\begin{aligned} V_{j,Y} := & - \sum_{\substack{p \geq 2 \\ 1 \leq k_1, \dots, k_p \leq n \\ k_1 + \dots + k_p = j}} \frac{1}{p!} \sum_{\substack{\{X_1, \dots, X_p\}_c \\ Y = B_{X_1} \cup \dots \cup B_{X_p}}} [S_{k_p, B_{X_p}}, \dots, [S_{k_2, B_{X_2}}, V_{k_1, B_{X_1}}^{01}]] \\ & + \sum_{\substack{p \geq 1 \\ 1 \leq k_1, \dots, k_p \leq n \\ k_1 + \dots + k_p = j-1}} \frac{1}{p!} \sum_{\substack{\{X, X_1, \dots, X_p\}_c \\ Y = B_X \cup B_{X_1} \cup \dots \cup B_{X_p}}} [S_{k_p, B_{X_p}}, \dots, [S_{k_1, B_{X_1}}, V_{B_X}]]. \end{aligned} \quad (\text{E9})$$

The notation  $\{X_1, \dots, X_p\}_c$  denotes that the summation is performed over subsets of  $\Lambda$  satisfying the conditions

$$\begin{aligned} X_2 \cap B_{X_1} &\neq \emptyset, \\ X_3 \cap B_{X_1 \cup X_2} &\neq \emptyset, \\ &\vdots \\ X_p \cap B_{X_1 \cup \dots \cup X_p} &\neq \emptyset. \end{aligned} \quad (\text{E10})$$

This condition results from the commutators in Eq. (E9) vanishing otherwise.

Requiring that the off-diagonal part in the first  $n$  summands of Eq. (E8) vanishes yields a formula for  $S$ ,

$$S_{j,B_X} := \sum_{\substack{E,k,E',k' \\ E \neq E'}} \frac{\langle E, k | V_{j,B_X}^{01} | E', k' \rangle}{E - E'} |E, k\rangle \langle E', k'|. \quad (\text{E11})$$

The states  $|E, k\rangle$  form an eigenbasis of the Hamiltonian

$$\bar{H}_{0,X} = \sum_{Y: Y \cap X \neq \emptyset} H_{0,Y}. \quad (\text{E12})$$

By construction, keeping only the first  $n$  orders in Eq. (E8), yields a block-diagonal operator. The projection of this operator onto the ground state manifold of  $H_0$  is our low-energy effective Hamiltonian. It has the form

$$H_{\text{eff}} := P_0 \sum_{j \geq 0} \lambda^j \sum_{X \subset \Lambda} V_{j,B_X} P_0. \quad (\text{E13})$$

We want to note, that it is a priori unclear if neglecting the higher-order off-diagonal terms and the diagonal terms in the high energy manifold is a good approximation. In particular it is unclear if the spectral properties of  $H_{\text{eff}}$  carry over to  $H$ .

## 2. Invariance of the effective Hamiltonian

A local symmetry of  $H_0$  ( $V$ ) is a unitary operator  $U$ , that satisfies  $U^\dagger H_{0,X} U = H_{0,X}$  ( $U^\dagger V_X U = V_X$ ) for all  $X \subset \Lambda$ . In this section we show, that any (local) symmetry of  $H_0$  and  $V$ , is also a local symmetry of the constructed effective Hamiltonian.

The local symmetry immediately implies that  $[P_{B_X}^0, U] = 0$  and  $[P_{B_X}^1, U] = 0$ , thus if  $U^\dagger A U = A$ , then also  $U^\dagger A^{01} U = A^{01}$ . Furthermore it implies that  $\bar{H}_{0,X}$  is invariant under  $U$ . Thus  $U|E, k\rangle$  is an eigenstate of  $H_{0,X}$  with the same energy  $E$  but different index, we denote it as  $U(k)$ . As  $U$  is a unitary operator, this constitutes a permutation of the indices.

Because of the recursive definition of the operators  $V_j$  it is natural to proof their invariance under  $U$  by induction. The base case is given by  $V_0 = V$ , which is invariant under  $U$  by definition. Thus assume that the invariance of  $S_{k,B_X}$  and  $V_{k,B_X}$  under  $U$  is already proven for  $k < j$ . Note that the expression (E9) only involves operators  $V_k$  and  $S_k$  with  $k < j$ . To calculate  $U^\dagger V_{j,B_X} U$ , we repeatedly use the identity  $U^\dagger [A, B] U = [U^\dagger A U, U^\dagger B U]$ , that holds for arbitrary operators  $A, B$ . As all operators inside the commutators are invariant under  $U$ , it follows that  $V_{j,B_X}$  is invariant under  $U$ .

Using that  $U$  only permutes the eigenstates  $|E, k\rangle$  of  $\bar{H}_{0,X}$ , this implies the invariance of  $S_{j,B_X}$ , as

$$U^\dagger S_{j,B_X} U = \sum_{\substack{E,k,E',k' \\ E \neq E'}} \frac{\langle E, k | V_{j,B_X}^{01} | E', k' \rangle}{E - E'} U^\dagger |E, k\rangle \langle E', k' | U \quad (\text{E14a})$$

$$= \sum_{\substack{E,k,E',k' \\ E \neq E'}} \frac{\langle E, k | U^\dagger V_{j,B_X}^{01} U | E', k' \rangle}{E - E'} |E, k\rangle \langle E', k' | \quad (\text{E14b})$$

$$= \sum_{\substack{E,k,E',k' \\ E \neq E'}} \frac{\langle E, k | V_{j,B_X}^{01} | E', k' \rangle}{E - E'} |E, k\rangle \langle E', k' | = S_{j,B_X}. \quad (\text{E14c})$$

This completes the induction. It follows immediately, that Eq. (E13) is invariant under  $U$ , as desired.

## 3. Diagonal elements

For a fully-symmetric blockade structure, the symmetries heavily constrain the form of the effective Hamiltonian. We first consider the diagonal elements. Let  $\mathbf{n}, \mathbf{m} \in L_{\text{Loop}}$ . As  $\mathcal{C}_{\text{Loop}}$  is fully-symmetric, there exists an automorphism  $\phi \in \mathcal{A}_{\text{Loop}}$ , such that  $\mathbf{n} = \phi \cdot \mathbf{m}$ . Using the invariance of the effective Hamiltonian under the symmetry operators  $U_\phi$  yields

$$\langle \mathbf{n} | H_{\text{eff}} | \mathbf{n} \rangle = \langle \phi \cdot \mathbf{m} | H_{\text{eff}} | \phi \cdot \mathbf{m} \rangle \quad (\text{E15a})$$

$$= \langle \mathbf{m} | U_\phi^\dagger H_{\text{eff}} U_\phi | \mathbf{m} \rangle \quad (\text{E15b})$$

$$= \langle \mathbf{m} | H_{\text{eff}} | \mathbf{m} \rangle, \quad (\text{E15c})$$

i.e. all diagonal elements are equal. Hence by addition of a constant to the effective Hamiltonian (a shift in the energy scale) the diagonal elements can be set to 0. This is consistent, with our result in Appendix A 2, where we showed, that all states from  $\mathcal{H}_{\text{Loop}}$  enter with equal weight into the ground state.

## 4. Off-diagonal elements

In this section, we will derive the off-diagonal part of the effective Hamiltonian in leading order, i.e., we consider the smallest  $n$  such that  $H_{\text{eff}}$  has nonzero off-diagonal terms.

As our perturbation  $V$  is a sum of operators  $\sigma^x$ , it can flip the state of *exactly one* atom. More precisely, this means that the matrix element satisfies  $\langle \mathbf{n}' | V | \mathbf{n} \rangle \neq 0$ , only if  $\mathbf{n}$  and  $\mathbf{n}'$  differ in at most one component.

We claim, that  $\langle \mathbf{n}' | V_j | \mathbf{n} \rangle \neq 0$  only if  $\mathbf{n}$  and  $\mathbf{n}'$  differ in at most  $j$  components. As it is straightforward, we only sketch the proof by induction. The previous paragraph contains the base case, assume this is true for  $V_k$  and  $S_k$  for  $k < j$ . In Eq. (E9), expand all the commutators and insert identities of the form  $\sum_{\mathbf{n}} |\mathbf{n}\rangle \langle \mathbf{n}|$  between all products. Then the matrix element  $\langle \mathbf{n}' | V_j | \mathbf{n} \rangle$  can only be nonzero, if the matrix elements the sum contains at least one product of matrix elements that is nonzero. Each of the operators  $S_{k_l}$  can change at most  $k_l$  components of the vector  $\mathbf{n}$ . As  $k_1 + \dots + k_p = j$  in the first sum and  $k_1 + \dots + k_p + 1 = j$  in the second sum, it follows that  $V_j$  can change maximally  $j$  components in the vector  $\mathbf{n}$ . As the matrix elements of  $S_j$ , are only rescaled matrix elements of  $V_j$ , the same is true for  $S_j$ .

The number of components that have to be changed to transform the configuration  $\mathbf{n}$  into the configuration  $\mathbf{n}'$ , is known as the Hamming distance. The previous section shows, that  $\langle \mathbf{n}' | H_{\text{eff}} | \mathbf{n} \rangle \neq 0$  requires that the order of perturbation theory  $n$  is at least the Hamming distance between  $\mathbf{n}$  and  $\mathbf{n}'$ .

By construction, two configurations  $\mathbf{n}, \mathbf{n}' \in L_{\text{Loop}}$ , differ in edges along a closed loop. The smallest closed loop consists of a single plaquette in  $\mathcal{C}_{\text{Loop}}$  (assuming the lattice is sufficiently large). Thus, if  $\mathbf{n}$  and  $\mathbf{n}'$  have the smallest possible Hamming distance, they satisfy  $|\mathbf{n}'\rangle = U_p |\mathbf{n}\rangle$ . We conclude, that in leading order, the only nonzero matrix elements of  $H_{\text{eff}}$  are  $\langle \mathbf{n} | H_{\text{eff}} U_p | \mathbf{n} \rangle$  for  $\mathbf{n} \in L_{\text{Loop}}$ .

The structure  $\mathcal{C}_{\text{Loop}}$  being fully-symmetric implies that for  $\mathbf{n}, \mathbf{m} \in L_{\text{Loop}}$ , there exists an automorphism  $\phi \in \mathcal{A}_{\text{Loop}}$ , such that  $\mathbf{n} = \phi \cdot \mathbf{m}$ . As  $\mathcal{A}_{\text{Loop}}$  is abelian, we obtain

$$\langle \mathbf{n} | H_{\text{eff}} U_p | \mathbf{n} \rangle = \langle \phi \cdot \mathbf{m} | H_{\text{eff}} U_p | \phi \cdot \mathbf{m} \rangle \quad (\text{E16a})$$

$$= \langle \mathbf{m} | U_\phi^\dagger H_{\text{eff}} U_p U_\phi | \mathbf{m} \rangle \quad (\text{E16b})$$

$$= \langle \mathbf{m} | H_{\text{eff}} U_p | \mathbf{m} \rangle. \quad (\text{E16c})$$

Thus, the leading order off-diagonal matrix elements of the effective Hamiltonian are equal to some constant  $C_p \equiv \langle \mathbf{m} | H_{\text{eff}} U_p | \mathbf{m} \rangle$ , that can only depend on the plaquette  $p$ . However, for periodic boundary conditions, the Hamiltonian  $H_{\text{Loop}}$  is invariant under translations. Thus implies that  $C \equiv C_p$  for all plaquettes  $p$ . Therefore the leading order part of the effective Hamiltonian has the form

$$H_{\text{eff,lo}} = \sum_{\mathbf{n}, \mathbf{m} \in L_{\mathbb{Z}_2}} \langle \mathbf{n} | H_{\text{eff}} | \mathbf{m} \rangle |\mathbf{n}\rangle \langle \mathbf{m}| \quad (\text{E17a})$$

$$= \sum_{\mathbf{n} \in L_{\mathbb{Z}_2}} \sum_{\text{Faces } p} \langle \mathbf{n} | H_{\text{eff}} U_p | \mathbf{n} \rangle |\mathbf{n}\rangle \langle \mathbf{n}| U_p \quad (\text{E17b})$$

$$= C \sum_{\mathbf{n} \in L_{\mathbb{Z}_2}} \sum_{\text{Faces } p} |\mathbf{n}\rangle \langle \mathbf{n}| U_p \quad (\text{E17c})$$

$$= C \sum_{\text{Faces } p} U_p. \quad (\text{E17d})$$

Lastly we comment on the properties of  $C$ . Let  $K$  denote the Hamming distance between the states  $U_p |\mathbf{n}\rangle$  and  $U_p |\mathbf{n}'\rangle$ , i.e., the leading order. By the definition (E13) we obtain  $C = \mathcal{O}(\Omega^K)$ . The dependence of  $C$  on  $\Delta E$ ,  $C = \mathcal{O}(1/\Delta E^{K-1})$  is less trivial. It can be proven by induction, as by the definition (E11), the matrix elements of  $S$  are the matrix elements of  $V$ , rescaled by constants of order  $\mathcal{O}(1/\Delta E)$ . Counting orders of  $S$  yields the exponent  $K - 1$ .

We were unable to derive the sign of  $C$ , as this would involve explicitly calculating the effective Hamiltonian up to order 24. However, we have two reasons to believe that  $C < 0$ . First, this is consistent with the fact that the finite volume ground states are in the zero flux sector. Second, using another method to derive the effective Hamiltonian (that is unfortunately not valid in the thermodynamic limit), we were able to show that  $C < 0$  [107].

From the leading order onwards, nonzero matrix elements are possible in every even order. Thus the next term in  $H_{\text{eff}}$  has a coefficient of order  $\mathcal{O}(\Omega^{K+2}/\Delta E^{K+1})$ .

## Appendix F: Unit ball embeddings

Here we provide exact coordinates for the unit ball embeddings of the FSU-structure and its extension by links depicted in Fig. 8 (b) and (d) of the main text. The units are given in blockade radii so that  $r_B = 1$ .

Positions of the vertices in the unit ball embedding of the FSU-structure shown in Fig. 8 (b):

Vertex label	Vertex position
Tetrahedron 1	( -0.45455 -0.26243 0.0 )
Tetrahedron 2	( 0.45455 -0.26243 0.0 )
Tetrahedron 3	( 0.0 0.52486 0.0 )
Tetrahedron 4	( 0.0 0.0 -0.74227 )
$A$	( 0.0 -0.7873 0.37113 )
$B$	( 0.68182 0.39365 0.37113 )
$C$	( -0.68182 0.39365 0.37113 )
$\bar{B}$	( -0.68182 -0.39365 -0.74227 )
$\bar{C}$	( 0.68182 -0.39365 -0.74227 )
$\bar{A}$	( 0.0 0.7873 -0.74227 )

Positions of the vertices in the unit ball embedding of the extended FSU-structure shown in Fig. 8 (d):

Vertex label	Vertex position
Tetrahedron 1	( -0.45455 -0.26243 0.0 )
Tetrahedron 2	( 0.45455 -0.26243 0.0 )
Tetrahedron 3	( 0.0 0.52486 0.0 )
Tetrahedron 4	( 0.0 0.0 -0.74227 )
Wing $\bar{A}$	( 0.0 -0.7873 0.37113 )
Wing $\bar{B}$	( 0.68182 0.39365 0.37113 )
Wing $\bar{C}$	( -0.68182 0.39365 0.37113 )
Wing $B$	( -0.68182 -0.39365 -0.74227 )
Wing $C$	( 0.68182 -0.39365 -0.74227 )
Wing $A$	( 0.0 0.7873 -0.74227 )
Bridge $\bar{A}$	( 0.72727 -1.1547 0.63093 )
Bridge $A$	( 0.72727 1.1547 -1.00206 )
$A$	( 1.45455 -1.1547 0.63093 )
$\bar{A}$	( 1.45455 1.1547 -1.00206 )
Bridge $\bar{B}$	( 0.63636 1.20719 0.63093 )
Bridge $B$	( -1.36364 0.05249 -1.00206 )
$\bar{B}$	( 0.27273 1.83702 0.63093 )
$B$	( -1.72727 0.68232 -1.00206 )
Bridge $\bar{C}$	( -1.36364 -0.05249 0.63093 )
Bridge $C$	( 0.63636 -1.20719 -1.00206 )
$\bar{C}$	( -1.72727 -0.68232 0.63093 )
$C$	( 0.27273 -1.83702 -1.00206 )